# SYN-OROGENIC MAGMATISM, MID-CRUST EXHUMATION, AND PLACER GOLD DEPOSITION: THE ANACONDA METAMORPHIC CORE COMPLEX OF WESTERN MONTANA

by

Caden James Howlett

A thesis submitted in partial fulfillment
of the requirements for the degree

of

Master of Science

in

Earth Sciences

MONTANA STATE UNIVERSITY
Bozeman, Montana

April 2020

~In memory of my friend Bryce W. Astle~

1995-2015


“Challenge yourself.”

# ACKNOWLEDGEMENTS

I would first like to express my deepest gratitude to my advisor Dr. Andrew Laskowski, whose academic guidance was invaluable and generosity unmatched. Thank you for teaching me to avoid getting "caught in the weeds", providing me with unceasing intellectual stimulation and, most importantly, for genuine friendship. Thank you to Dr. David Lageson for six years of continuous inspiration and for infecting me with a profound enthusiasm for field geology and the history of the geological sciences. I am grateful for Dr. Devon Orme's guidance, friendship, and ability to articulate complex ideas. I am appreciative for Dr. Colleen Elliott at MBMG for sharing her extensive knowledge of western Montana and geologic mapping techniques.

Thank you to my wonderful office-mate and field partner Aislin Reynolds, who kept me level-headed during eight weeks of fieldwork in the mosquito-infested drainages of the Anaconda Range and for a month on the oxygen-depleted Tibetan Plateau. Thank you to Erica Duncan for being the closest and most supportive friend I've ever had. I also thank one of my best friends, Chance Ronemus, for providing thought-provoking conversations on topics ranging from zircon fertility to the origin on consciousness.

I express love and appreciation for my mother and father, whose positive impact on my life cannot be described with words. Thank you for the never-ending support and encouragement.

Finally, this project would not have been possible without support from the MSU Dept. of Earth Sciences, the Geological Society of America, the Tobacco Root Geological Society, and the USGS EDMAP program.

TABLE OF CONTENTS

TABLE OF CONTENTS CONTINUED

TABLE OF CONTENTS CONTINUED

# LIST OF TABLES

Table Page

# LIST OF FIGURES

Figure Page

LIST OF FIGURES CONTINUED

Figure Page

# ABSTRACT

Since their initial discovery in the late 1960's, metamorphic core complexes have remained of high interest in tectonics research. Early uncertainty regarding the mechanics of slip along low-angle normal (detachment) faults is now accompanied by controversy surrounding the relationship between magmatism and large-magnitude extension. As deeply exhumed geologic structures that record lithospheric thermomechanical processes, investigating core complex formation is crucial to understanding how the mid-crust behaves in extensional tectonic settings. In some regions, the exhumation of these structures is also linked to the formation of economically valuable mineral deposits, making them of notable societal importance. This thesis is a two-part investigation of core complex evolution that addresses the concepts above, formatted with introductory and concluding chapters that bound two main chapters prepared for publication. Chapter two consists of a study that tests the utility of using detrital zircon (DZ) U-Pb geochronology and DZ unmixing models to determine the source of placer gold. New zircon U-Pb (n=1,058) and Lu-Hf (n=61) isotopic data are presented from four placer deposit samples extracted from the Pioneer District of western Montana. Geochronology and DZ unmixing modeling suggest that gold from the placer deposits was derived from vein and skarn lode sources in northern footwall of the Anaconda metamorphic core complex (AMCC). Our data offers the first DZ-based support for previous interpretations that the Late Cretaceous Royal Stock pluton precipitated gold along its contact with overlying Proterozoic through Mesozoic supracrustal rock, and was subsequently weathered, transported, and deposited in the AMCC supradetachment basin during the Late Oligocene-Early Miocene. Chapter three consists of an integrated geologic, geochronologic, thermochronologic, and isotopic investigation of the AMCC footwall. Results suggest that the AMCC is an example of a core complex that was primed for large-magnitude extension through crustal thickening and voluminous magmatism. It is proposed that buckling of the Farallon slab, marked by the onset of "ignimbrite flare up" volcanism, was responsible for the initiation of AMCC extension. Furthermore, a compilation of MCC cooling ages and ages of Cenozoic volcanics across the western USA suggest that removal of the Farallon Plate was a primary driver of Cordilleran core complex formation.

# CHAPTER ONE

## INTRODUCTION TO THESIS

Metamorphic core complexes (MCCs) are domal geologic structures that exhume mid-crustal rocks through extensional tectonic processes. First described in the western USA, MCCs generally consist of ductilely deformed metamorphic-plutonic rocks separated from an unmetamorphosed, brittlely deformed upper plate by a low-angle normal (detachment) fault (e.g. Anderson, 1972; Crittenden, 1980; Wernicke, 1981; Coney and Harms, 1984). MCC footwalls serve as windows into the thermomechanical properties of the lithosphere (e.g. Platt et al., 2015) and, in some cases, exhume elements and minerals of economic significance (e.g. Marchev et al., 2005; Howlett and Laskowski, in review). Despite their global occurrence and tectonic and economic importance, the mechanisms responsible for initiating and facilitating core complex formation remain controversial. In addition, the exhumation, erosion, transportation, and deposition of economically valuable minerals from MCC footwalls into supradetachment basins is sparsely mentioned in modern literature. In this thesis I address both questions, with two manuscripts that focus on the Anaconda metamorphic core complex (AMCC) of western Montana.

The first manuscript presented here (chapter two) is a provenance analysis of gold placer deposits in the northern AMCC supradetachment basin (the Pioneer District). We apply detrital zircon U-Pb geochronology and DZ unmixing modeling to four placer deposit samples to test previously proposed hypotheses regarding gold source and, more broadly, the plausibility of using these techniques on similar deposits elsewhere. This

work is timely in that it confirms the utility of using detrital zircon geochronology to determine the source of economically valuable minerals; it is innovative in that it applies cutting-edge detrital zircon U-Pb geochronology interpretation techniques (inverse Monte Carlo unmixing modeling); it is provocative because it explores the genesis of an economic mineral deposit that is likely linked to the formation of a metamorphic core complex; and it is of broad interest because it describes how placer gold deposits evolve from genesis to eventual exposure, erosion, transport, and deposition. Broadly speaking, our conclusion that these techniques can be used to accurately determine the source of placer gold may facilitate more localized and less environmentally impactful mining operations.

The second manuscript (chapter three) contributes to the long-lasting debate surrounding the driving mechanisms of metamorphic core complex formation in the western USA. A topic of extensive discussion in continental core complex literature is the importance of magmatism in core complex evolution (Whitney et al., 2013); there is little consensus as to whether magmatism is a result of large-magnitude extension or if it is the cause of core complex formation (e.g. Gans et al., 1989; Armstrong and Ward, 1991; Stevens et al., 2016; and many others). Variability in the relationship between main phase plutonism and footwall exhumation across core complexes has been noted (e.g. Hill et al., 1995; Foster and Fanning, 1997; Stevens et al., 2016), suggesting that the influence of magmatism on exhumation is variable.

There are also long-standing questions regarding the role that sublithospheric processes (like slab rollback and upper mantle dynamics) play in MCC formation. It has

been proposed by some researchers that mantle-derived magmatism and deep lithospheric processes are essential for the magmatism and flow of crust in the extensional tectonic settings that create core complexes (Gans et al., 1989; Amato and Miller, 2004; Konstantinou et al., 2013). Others have argued that the localization of MCCs in some regions discount the idea that the upper plate is sensitive to slab dynamics at depth (e.g. Stevens et al., 2017). Chapter three of this thesis investigates the relationship between magmatism and extension in the Anaconda MCC of western Montana through an integrated geologic, geochronologic, thermochronologic, and isotopic study. In addition, geochronology and thermochronology data from MCCs spanning southern Canada to southern Arizona is compiled and analyzed to investigate the relationship between Cenozoic volcanism and core complex formation in the NA Cordillera. This latter portion of chapter three gives new insights into how dynamics of the subducted Farallon slab may have initiated extension in the northern Cordillera and addresses sublithospheric controls on MCC development generally.

Literature Cited

Amato, J. M., & Miller, E. L. (2004). Geologic map and summary of the evolution of the Kigluaik Mountains gneiss dome, Seward Peninsula, Alaska. In Donna L. Whitney, C. Teyssier, & C. S. Siddoway, *Gneiss Domes in Orogeny*. Geological Society of America.

Armstrong, R. L. (1972). Low-Angle (Denudation) Faults, Hinterland of the Sevier Orogenic Belt, Eastern Nevada and Western Utah. *Geological Society of America Bulletin*, *83*(6), 1729.

Coney, P. J., & Harms, T. A. (1984). Cordilleran metamorphic core complexes: Cenozoic extensional relics of Mesozoic compression. *Geology*, *12*(9), 550–554.

Crittenden, M. D., Coney, P. J., & Davis, G. H. (Eds.). (1980). *Cordilleran metamorphic core complexes*. Boulder, Colo: Geological Society of America.

Foster, D. A., & Fanning, C. M. (1997). Geochronology of the northern Idaho batholith and the Bitterroot metamorphic core complex: Magmatism preceding and contemporaneous with extension. *Geological Society of America Bulletin*, 16.

Gans, P. B., Mahood, G. A., & Schermer, E. (1989). Synextensional magmatism in the Basin and Range Province; A case study from the eastern Great Basin. In *Geological Society of America Special Papers* (Vol. 233, pp. 1–53). Geological Society of America.

Hill, E. J., Baldwin, S. L., & Lister, G. S. (1995). Magmatism as an essential driving force for formation of active metamorphic core complexes in eastern Papua New Guinea. *Journal of Geophysical Research: Solid Earth*, *100*(B6), 10441–10451.

Konstantinou, A., Strickland, A., Miller, E., Vervoort, J., Fisher, C. M., Wooden, J., & Valley, J. (2013). Synextensional magmatism leading to crustal flow in the Albion-Raft River-Grouse Creek metamorphic core complex, northeastern Basin and Range: *Tectonics*, *32*(5), 1384–1403.

Lee Armstrong, R., & Ward, P. (1991). Evolving geographic patterns of Cenozoic magmatism in the North American Cordillera: The temporal and spatial association of magmatism and metamorphic core complexes. *Journal of Geophysical Research: Solid Earth*, *96*(B8), 13201–13224.

Marchev, P., Kaiser-Rohrmeier, M., Heinrich, C., Ovtcharova, M., von Quadt, A., & Raicheva, R. (2005). Hydrothermal ore deposits related to post-orogenic extensional magmatism and core complex formation: The Rhodope Massif of Bulgaria and Greece. *Ore Geology Reviews*, *27*(1–4), 53–89.

Platt, J. P., Behr, W. M., & Cooper, F. J. (2015). Metamorphic core complexes: windows into the mechanics and rheology of the crust. *Journal of the Geological Society*, *172*(1), 9–27.

Stevens, Liane M., Bendick, R., & Baldwin, J. A. (2017). Synconvergent exhumation of metamorphic core complexes in the northern North American Cordillera. *Geology*, *45*(6), 495–498.

Stevens, L.M., Baldwin, J. A., Crowley, J. L., Fisher, C. M., & Vervoort, J. D. (2016). Magmatism as a response to exhumation of the Priest River complex, northern Idaho: Constraints from zircon U–Pb geochronology and Hf isotopes. *Lithos*, *262*, 285–297.

Wernicke, B. (1981). Low-angle normal faults in the Basin and Range Province: nappe tectonics in an extending orogen. *Nature*, *291*(5817), 645–648.

Whitney, D. L., Teyssier, C., Rey, P., & Buck, W. R. (2013). Continental and oceanic core complexes. *Geological Society of America Bulletin*, *125*(3–4), 273–298.

# CHAPTER TWO

# DETERMINING THE SOURCE OF PLACER GOLD IN THE ANACONDA METAMORPHIC CORE COMPLEX SUPRADETACHMENT BASIN USING DETRITAL ZIRCON U-PB GEOCHRONOLOGY, PIONEER DISTRICT, WESTERN MONTANA

## Contribution of Authors and Co-Authors

Manuscript in Chapter 2

Author: Caden J. Howlett

Contributions: Conceived the study, performed fieldwork and analyses, interpreted results, created figures, and wrote the manuscript.

Co-Author: Andrew K. Laskowski

Contributions: Conceived the study, performed fieldwork and analyses, discussed implications, and edited earlier manuscripts.

Manuscript Information Page

Caden J. Howlett, Andrew K. Laskowski

*Geosphere*

Status of Manuscript:
____ Prepared for submission to a peer-reviewed journal
**_X_** Officially submitted to a peer-review journal *(submitted December 22, 2019)*
____ Accepted by a peer-reviewed journal
____ Published in a peer-reviewed journal

## ABSTRACT

Despite the widespread occurrence and economic significance of gold placer deposits, modern provenance studies of placer sediments are scarce and remain largely qualitative. This study is an attempt to test the plausibility—and better refine the current approach—of using detrital zircon (DZ) geochronology to trace the source of economically valuable minerals in placer deposits. The Pioneer District placer deposits were the site of the first gold discovery in Montana in 1852, and their hypothesized proximity to the lode source and complex surrounding structural framework makes them an ideal candidate to test the utility of DZ geochronology in placer provenance analysis. We present a new set of DZ U-Pb (n=1,058) and Lu-Hf (n=61) isotopic data from four Pioneer District placer deposit samples. Each of the four samples yielded similar age spectra with a range of U-Pb ages between 2200 and 25 Ma. We interpret that ≥250 Ma zircons were recycled from Mesoproterozoic Belt Supergroup, Paleozoic-Mesozoic passive margin sedimentary rocks, and the synorogenic Beaverhead Conglomerate. 237 DZ U-Pb ages ≤250 Ma reveal two prominent age-probability peaks centered at ~69 Ma and ~26 Ma, which we interpret record first-cycle derivation from the Royal Stock pluton and nearby Dillon Volcanics, respectively. We evaluate these data using an inverse Monte Carlo DZ unmixing model that, by comparing the mixed placer age spectra to the DZ spectra of potential sources, calculates probable relative contributions from each input source. Relative contribution calculations determine a 12% contribution from the Royal Stock and a disproportionately large 43% contribution from the Beaverhead

conglomerate. Absence of the Beaverhead Fm. in the hypothesized source region suggests complete erosion of unit into the placer-bearing basin.

DZ geochronology and the unmixing modeling results suggest that gold in the Pioneer District placer deposits was derived from vein and skarn lode sources in northern footwall of the Anaconda metamorphic core complex. Our data offers the first detrital zircon based support for previous interpretations that the Late Cretaceous Royal Stock pluton precipitated gold along its contact with overlying Proterozoic through Mesozoic supracrustal rock, and was subsequently exhumed, transported, and deposited in the AMCC supradetachment basin during the Late Oligocene. These results serve as confirmation of the utility of using DZ geochronology and emerging modeling techniques to determine the source history of economically valuable minerals. The worldwide occurrence of gold placer deposits with unknown source areas provides abundant opportunity to apply these techniques.

## INTRODUCTION

Placer deposits are broadly defined as any deposits of sand, gravel, and other detritus that contain accumulations of economically valuable minerals (Yeend & Shawe, 1989). Gold placer deposits are notably important deposits that result from weathering and release of gold from a bedrock source, gold transportation, and mechanical concentration of gold in streams and river gravels (e.g. Boyle, 1979; Loen, 1986; McCulloch et al., 2003). It is estimated that approximately two-thirds of the total world gold supply—and roughly half of the gold mined in California, Alaska, Idaho, and Montana—has been produced by placer deposits (Figure 2.1; Boyle, 1979; Yeend &

Shawe, 1989). These deposits therefore play an essential role in the discovery and production of gold worldwide.

Since placer deposits are formed by normal surficial processes that act on gold-bearing bedrock of varying richness, their geographic distribution is wide, and their sizes and concentrations vary greatly (Figure 2.1). These deposits occur predominately in Tertiary and Quaternary rocks largely due to the destruction of older placers by erosion (Edwards & Atkinson, 1986). Additionally, the preservation of placer deposits in relatively young rock units may reflect the role that tectonic events play in their

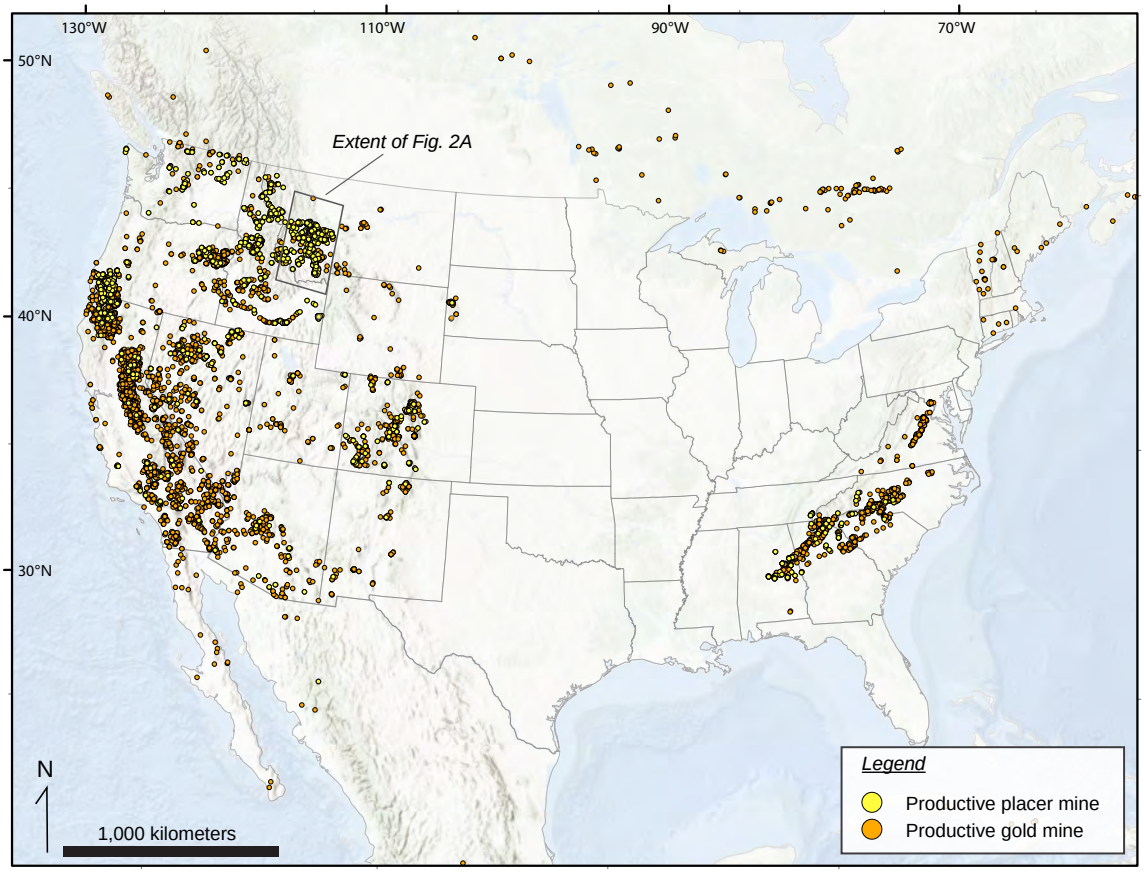


Figure 2.1. Overview map showing the location of previously and currently productive gold mines in North America. Yellow circles are representative of placer mines and orange circles are locations that include both placer and lode deposits. Data sourced from USGS Mineral Resources Data System (MRDS). Terrain base map sourced from Esri/NOAA.

formation. For example, the relatively young depositional ages of many gold placers in Montana and Idaho can be attributed to the shedding of detrital gold from the recently exposed gold-bearing magmatic core of the northern Cordillera hinterland (Figure 2.1).

The concentration and size of gold placer deposits depend almost entirely on the supply of source materials (Yeend & Shawe, 1989). Conducting provenance studies on the gold-bearing sediments within placer deposits can give insight into the original bedrock source and/or rock units that hosted vein or skarn gold. Placer gold source regions that are actively shedding gold are of particular interest, as their identification could allow extraction of gold directly from the lode source. Additionally, it has been established that an effective technique to discover new placer deposits is through the identification of potential source areas (Edwards & Atkinson, 1986). When DZ signatures from a mixed placer sample can be correlated with a specific source unit, additional placer deposits may be located by determining other sinks that may have had a contribution from the source.

Provenance studies of the gold-bearing placer sediments are scarce and remain largely qualitative. Most studies interested in gold placer provenance have investigated gold nugget morphology, surface texture, and bulk chemistry to determine an approximate transport distance from the source (e.g. Loen, 1986; Loen, 1995). Knight et al. (1999) conducted a study of gold particle shape and rim characteristics to determine the distance of fluvial transport of placer deposits in the Klondike District of Canada, concluding that gold morphology "shows a smooth, well-defined relationship to distance of transport from the lode source" (p. 635).

Other techniques that have been used to determine placer gold source include the analysis of clast type and measurement of heavy mineral concentrations from within placer deposits (e.g. Loen, 1994). Although these techniques may give adequate preliminary insight into placer source characteristics, the development of more quantitative techniques to investigate provenance—specifically detrital zircon geochronology—provides the opportunity to conduct a more rigorous investigation of placer gold source.

Detrital zircon geochronology has become an essential tool in the study of sediment provenance because of the ubiquity of zircon in most depositional systems and the increasing ability to determine U-Pb ages with reasonable efficiency, accuracy, and precision (e.g. Gehrels, 2014). Formed primarily in felsic igneous rocks, zircon is a heavy and resistant mineral that does not commonly break down when weathered into sedimentary systems; thus, zircon can be recycled multiple times in a system and be sourced from sedimentary strata that are not its initial depositional unit. It is for this reason that many detrital zircons may give insight into an ultimate source, but not necessarily a proximal one. Conversely, the weathering of metamorphic and igneous rocks can provide first-cycle grains that can allow direct interpretation of provenance. Although interpreting the origin of detrital zircons with U-Pb geochronology is an established technique for constraining the source rocks of sediments, it is not routinely applied to gold placer deposits. Davis et al. (1994) first proposed that geochronologic analysis of detrital zircons within placer deposits provides U-Pb ages that can be correlated to ages of surrounding igneous and sedimentary rocks, giving insight into

potential source areas of the gold-bearing sediments. Three studies in the Witwatersrand basin of South Africa used U-Pb geochronology of detrital zircons to gain insight into the controversial origin of gold deposited in quartzite reefs (Ruiz et al., 2006; Koglin et al., 2010; Zeh & Gerdes, 2012). The technique has also been applied to fingerprint to source of gem and gold placers in the Mamfe Basin of southwest Cameroon (Kanouo et al., 2012; Kanouo et al., 2018). More recently, researchers have also begun pairing the U-Pb ages of detrital zircons with corresponding geochemical signatures (such as Lu-Hf), which serve as separate provenance tracers for the mixed sediments (Zeh & Gerdes, 2012; Kanouo et al., 2018).

The use of DZ geochronology to determine the source of gold placers works under the assumption that the gold and the zircon grains were sourced from the same region and were transported and deposited together. This assumption is supported by the fact that placer deposits are commonly enriched in denser minerals like zircon, monazite, and garnet (Reid and Frostick, 1985).

The increasing efficiency of U-Pb geochronology and the abundance of new detrital zircon provenance studies have resulted in the development of new detrital zircon modeling techniques to determine source areas. A model developed by Sundell and Saylor ("DZmix", 2017) attempts to determine the mixing of source samples through inverse Monte Carlo modeling by comparing mixed detrital samples to randomly generated combinations of source distributions. These models enable a more robust, quantitative provenance analysis that allow one to go as far as estimating the relative contributions of different potential source units (Sundell & Saylor, 2017).

**Test Case**

This study is an attempt to further test the plausibility—and better refine the current approach—of using detrital zircon geochronology to trace the source of economically valuable minerals in placer deposits.

The Pioneer District placer deposits were the site of the first gold discovery in Montana in 1852 (Pardee, 1951), and their hypothesized proximity to their lode source and complex surrounding structural framework make them an ideal candidate to test the utility of this technique. There is debate surrounding whether the gold originated from a vein or skarn lode source, and the source location remains unknown (Pardee, 1951; Loen, 1986; McCulloch, 2003). It is possible that the placer gold was sourced from the nearby Late Cretaceous Royal Stock, initially concentrated in Oligocene Cabbage Patch and Miocene Squaw Gulch conglomerate beds, and reworked during Pleistocene glaciation. We test this hypothesis by comparing new detrital zircon U-Pb ages (n=1,058) from the Pioneer District placer deposits with the age spectra of plausible source units that may have been in contact with the Royal Stock. We also present new detrital zircon Lu-Hf (n=61) isotopic data, which serve as an independent provenance indicator, from four samples within the Pioneer District placer deposits. Additionally, results from the application of Sundell & Saylor's (2017) detrital zircon unmixing model are incorporated to better understand the provenance of the deposits and the utility of the technique.

## GEOLOGIC SETTING

The Pioneer District, straddling the northern Flint Creek Range and the Deer Lodge Valley, is a site of rich placer deposits from which ~300,000 ounces of gold were

recovered between 1870 and 1986 (Figure 2.2; Loen, 1986). Located along the eastern edge of the Cordilleran hinterland of western Montana (Figure 2.2a), the Flint Creek Range represents the northern footwall of the Anaconda metamorphic core complex (AMCC) (O'Neill et al., 2004; Foster et al., 2010). The AMCC exhumes metamorphosed Cretaceous-Tertiary plutonic rocks and Mesoproterozoic-Phanerozoic sedimentary rocks

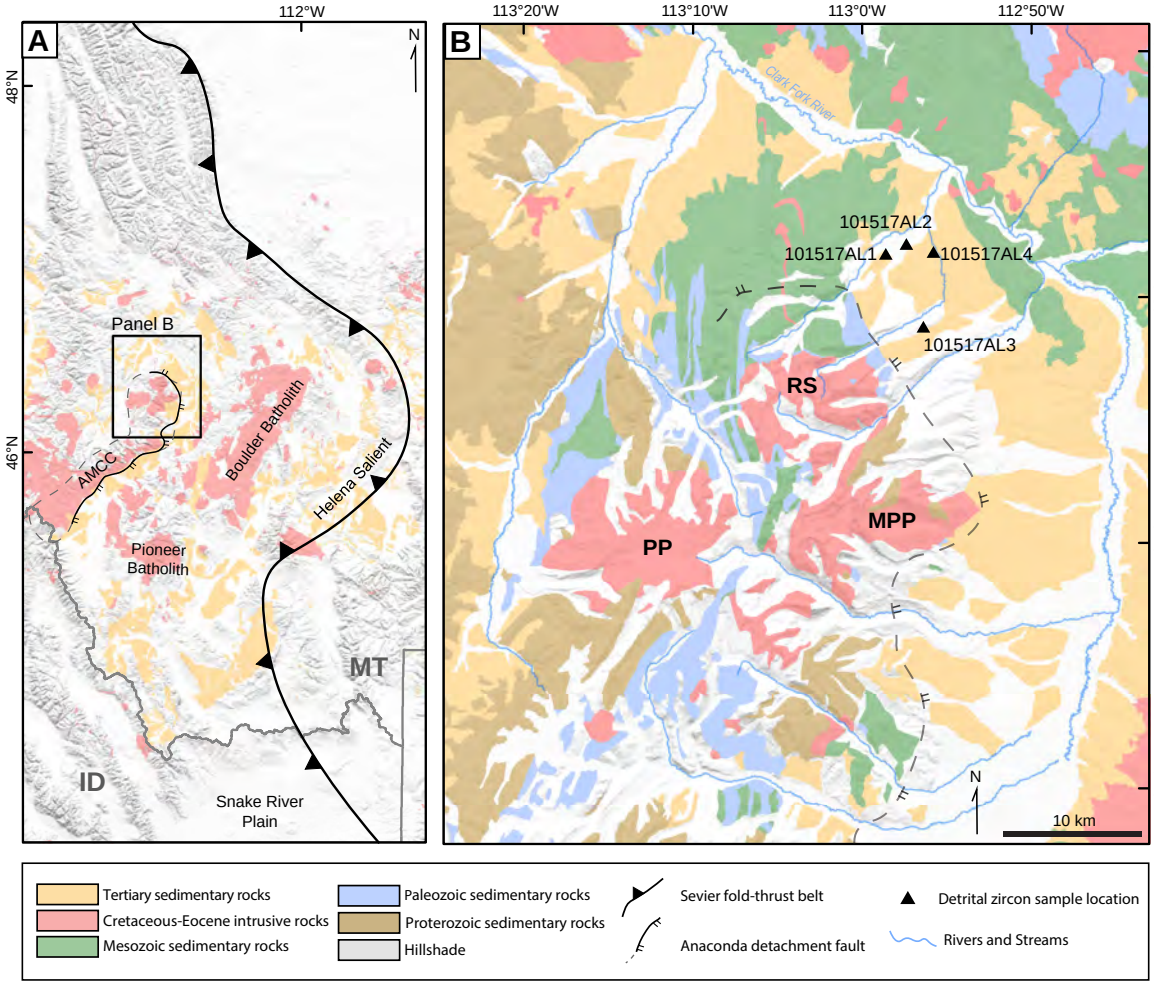


Figure 2.2. Tectonic overview maps showing (a) the field area in the context of the western Montana segment of the North American Cordillera, showing the distribution of Cretaceous-Eocene plutons and tertiary sedimentary rocks in relation to the Anaconda metamorphic core complex (AMCC) (Foster et al., 2010). Map (b) is a simplified geologic map of the region surrounding the Pioneer District, displaying undivided Proterozoic-Tertiary sedimentary rocks and major plutons. RS--Royal Stock; PP--Philipsburg Batholith; MPP--Mount Powell Pluton.

from depths of ~12 km, based on thermobarometry data (Grice et al., 2006). The metamorphic-plutonic footwall of the AMCC is separated from largely unconsolidated, synextensional sedimentary rocks of the hanging wall by the low-angle Anaconda detachment fault (O'Neill et al., 2004; Foster et al., 2010).

The northern footwall of the AMCC, proximal to the Pioneer District placers, is composed of folded Mesoproterozoic through Mesozoic metasedimentary and sedimentary rocks that have been intruded by several granite and granodiorite plutons (Figure 2.2b; Emmons & Calkins, 1913; Grice, 2006; Portner et al., 2011). The dominant plutons include the 69–60 Ma Royal Stock and the two-mica (muscovite and biotite) Mount Powell batholith (Figure 2.2b; Marvin et al., 1989; Grice, 2006), which are both exposed near the Anaconda detachment. Today, the Royal Stock is exposed approximately one vertical km above and eight km south of the Pioneer District placer deposits (Figure 2.2b). Much of the strata now exposed in the hanging wall of the AMCC is interpreted to have been deposited in an Eocene-Oligocene supradetachment basin (Janecke et al., 2005; Stroup et al., 2008). Of particular interest in this study are the late-Oligocene Cabbage Patch Formation and mid-Miocene Squaw Gulch conglomerate beds, which were deposited in the proximal hanging wall of the Anaconda detachment, commonly referred to as the Flint Creek Basin (Loen, 1986; Stroup et al., 2008; Portner et al., 2011). It has been hypothesized that the Cabbage Patch Fm. and Squaw Gulch beds were the original depositional units of the Pioneer District placer deposits prior to subsequent glacial transport and redeposition in the Pleistocene (Loen, 1986).

No researchers have evaluated the Pioneer District gold placers since the discovery of the AMCC by O'Neill et al. (2004), which adds an interesting tectonic element to the provenance study and a potential mechanism for exhumation of the gold-bearing unit(s). Foster et al. (2010) used $^{40}Ar/^{39}Ar$ thermochronology to determine that slip on the Anaconda detachment initiated ~53 Ma and lasted until at least 38 Ma. Zircon fission track ages of ~27 Ma (Foster et al., 2010) and mapped field relationships (Elliott and Lonn, in review; Howlett et al., 2019) suggest that slip could have lasted much longer than previously thought, into the Oligocene. This raises the possibility that the Pioneer District gold placers, if initially concentrated in Oligocene-Miocene Flint Creek Basin conglomerates, were shed from the AMCC footwall during active extension. Our new detrital zircon data provide insight into the maximum depositional age (MDA) of the placer deposits. Our new geochronological data and recent insights into the tectonic setting of the Pioneer District placer deposits justify revisiting their provenance history.

**Previous Investigations**

Investigation of the Pioneer District gold placers is confined to only a few studies. Pardee (1951) conducted the first detailed analysis of the placer deposits. He concluded that after uplift of the Flint Creek Range, ancestral rivers excavated gold from its lode source and deposited it in "river gravels", later to be destroyed by Pleistocene glaciations and redeposited further down slope (Pardee, 1951). Loen (1986, 1994) expanded on the work of Pardee (1951) and concluded that the placer gold initially underwent weathering in the late-Oligocene but was mostly concentrated in the Miocene Squaw Gulch beds. After Miocene deposition, placer gold was re-transported by Pliocene rivers and

Pleistocene glaciation (Loen, 1986). Loen (1994) used gold morphology and gold composition to include that the placer gold was likely sourced from mineralized veins, skarn, or replacement deposits associated with the Royal Stock pluton of the northern Flint Creek range. Although no bedrock evidence of the source has been discovered, the most detailed geologic map of the region produced by Mutch & McGill (1962) presents a mapped contact between the Royal Stock and Mesoproterozoic-Mesozoic supracrustal rocks, which supports the hypothesis of Loen (1994). McCulloch et al. (2003) concluded that the Pioneer District placer gold originated from skarn deposits by analyzing gold fineness, which is a measure of the proportion of gold in a gold-silver alloy expressed in parts per thousand (e.g. Loen, 1986). Fineness is commonly used in the determination of placer gold source because different lode types (e.g. skarn vs. vein) have characteristic fineness determined by their formation conditions (McCulloch et al., 2003). Several studies interested in the extensional basin sedimentation histories of western Montana conducted provenance analysis of the Eocene-Tertiary rocks exposed in the Flint Creek Basin (Stroup et al., 2008; Portner et al., 2011). These studies were focused specifically on basin development and did not consider the history of gold placer deposition. Regardless, they provide valuable detrital zircon and sedimentological data from the Cabbage Patch Formation.

## METHODS

To better constrain provenance and test the utility of the method applied to placer deposits, four detrital zircon geochronology samples were collected from the reworked placer deposits of the Pioneer District. Analysis of published maps from the Pioneer

District (Pardee, 1951; Loen, 1986) and satellite imagery allowed for previously mined placer deposits to be located and targeting for sampling. Bulk samples were collected from placer deposits located in different modern drainages over a lateral swath of ~6 km to ensure representative age spectra (Figure 2.2b).

**Detrital Zircon Uranium-Lead Geochronology**

Four detrital zircon samples were collected from the Pioneer District and were prepared and analyzed using consistent protocols at the Arizona Laserchron Center (http://www.laserchron.org) (Gehrels et al., 2008).

Zircons were separated from ~2.0 L bulk samples by pulverization in a jaw crusher, sieving, magnetic separation, density separation, and hand-picking. Zircons were mounted in epoxy, polished to a depth of ~30 μm, and backscattered-electron images were obtained using a scanning electron microscope (SEM) for targeting during analysis by laser-ablation inductively-coupled-plasma mass spectrometry (LA-ICPMS).

Zircon U-Pb ages were obtained for ~300 zircon grains per sample using a Photon Machines Analyte G2 Excimer laser (30 μm beam diameter) attached to a Thermo Element2 HR single-collector ICP-MS. The laser ablation process excavates pits that are approximately 15 μm in depth, and the ablated material is subsequently transported in helium to the plasma source of the Element2 ICP-MS. U, Th, and Pb isotopes are measured simultaneously using Faraday detectors with $3 \times 10^{11}$ ohm resistors for $^{238}U$, $^{232}Th$, $^{208}Pb$-$^{206}Pb$, and discrete dynode ion counters for $^{204}$(Pb + Hg) and $^{202}Hg$. Each analysis consists of one 15 s integration on peaks with the laser off, 15 one-second integrations with the laser firing, and a 30 s delay to purge for the next analysis.

All new analytical data and a detailed list of concordance filters are reported in Supplemental Item 1 (Appendix A). KDE plots were generated using the Python-based detritalPy (Sharman, 2018).

**Detrital Zircon Provenance Analysis**

The zircon crystal is ubiquitous in siliciclastic sedimentary systems, has a relatively high density (4.65 g/cm$^3$), and is physically and chemically resistant (e.g. Gehrels, 2014). These characteristics make it the ideal mineral for investigating the erosional and depositional evolution of Earth's surface, as zircon age spectra from a selected sink sample can be compared to the known ages of surrounding possible source rocks, giving insight into the provenance (source history) of the sediments (e.g. Sircombe, 1999). However, the high resistivity of the zircon can have unfavorable consequences in that in enables zircon grains to be recycled through weathering of older sedimentary rocks (e.g. Dickinson et al., 2009). As a result, sedimentary rocks can contain grains from very old sources that were stored and put back into the system one or more times. This recycling of zircons can complicate the interpretations of source history and transport evolution as second-cycle zircons cannot certainly give insight into the proximal source, but only the ultimate one (e.g. Dickinson et al., 2009; Stroup et al., 2008). Direct conclusions into zircon source can, however, be obtained through the dating of first-cycle zircons derived from the weathering of igneous and metamorphic rocks.

The North American Cordilleran hinterland consists of a shortened, thickened, metamorphosed, and magmatically-infiltrated package of sedimentary rocks that contains

an extremely diverse and wide-range of zircon ages (DeCelles, 2004; Dickinson & Gehrels, 2008; Laskowski et al., 2013). The resulting detrital zircon age spectra obtained from syn- and post-orogenic sedimentary deposits are very complex. Despite the complexities and implications of zircon recycling, U-Pb age spectra are still a powerful tool for determining provenance, and new modeling techniques and a number of first-cycle source areas with unique ages allow for direct interpretation of provenance. A list of potential source rocks for the Pioneer District placer deposits for which there are available data are listed in Table 2.1.

**Detrital Zircon Lutetium-Hafnium Geochronology**

Following U-Pb isotopic analysis, Hf isotope measurements were made for 61 grains <250 Ma using an identical laser ablation system attached to a Nu Plasma multicollector ICP-MS at the Arizona Laserchron Center. An average of 15 analyses were conducted for each sample (101517AL1-101517AL4), with measurements made from the same sample spots as LA-ICPMS U-Pb analysis to ensure that Hf isotopic data were determined from the same domain as the U-Pb age. Hf analyses are reported alongside detrital zircon U-Pb data in Supplementary Item 1 (see footnote 1).

Analysis of Lutetium-Hafnium isotopic ratios in zircon crystals provides information into the how isotopically evolved a melt was at the time of crystallization (e.g. Vervoort, 2015). In the Lu-Hf system, the daughter prefers to partition into the melt, which results in crustal rocks having relatively depleted Hf values. Crustal rocks with these characteristics are evolved (low Lu/Hf ratio), while rocks that are depleted in Hf that have recently been derived from the mantle are juvenile (e.g. Chapman et al.,

TABLE 1. POTENTIAL DETRITAL ZIRCON SOURCE ROCKS FOR PIONEER DISTRICT PLACER DEPOSITS

| Source Region | Name | Zircon ages (Ma) | References |
|---|---|---|---|
| Northern Cordillera volcanic centers | Dillon Volcanics | 17-52 | Fritz et al. (2007) |
| | Absaroka Volcanics | 43-55 | Harlan et al. (1996); Hiza (1999); Feeley et al. (2002); Feeley and Cosca (2003) |
| | Challis Volcanics | 43-53 | Chadwick (1981); Gaschnig et al. (2010, 2011) |
| | Lowland Creek Volcanics | 48-53 | Dudás et al. (2010) |
| | Elkhorn Mountain Volcanics | 80-83 | Tilling (1974) |
| Northern Cordilleran plutonic rocks | Pioneer batholith | 50-58; 70-78 | Zen (1996); Murphy et al. (2002); Foster et al. (2012) |
| | Idaho batholith | 53-98 | Foster et al. (2007); Gaschnig et al. (2010, 2011, 2013) |
| | Mount Powell Pluton | 60-65 | Baty (1973); Marvin et al. (1989) |
| | Royal Stock | 60-69 | Baty (1973) |
| | Philipsburg batholith (?) | 75 | Naibert et al. (2010) |
| | Boulder batholith | 73-81 | Lund et al. (2002); Wooden et al. (2008) |
| Sevier fold-thrust belt | Beaverhead Formation | | |
| | Blackleaf Formation | 90-110; 1700-1900; 2500 | Zartman et al. (1995) |
| | Colorado Group (Thermopoilis Shale equivalent) | 90-110; 1000-1200;1700-1900 | Dickinson and Gehrels (2008); Fuentes et al., (2009,2012) |
| | Kootenai Formation | 100-120; 150-175; 1700-1900 | Fuentes et al., (2009,2012) |
| | Ellis Formation | 90-110; 150-170; 1700-1900; 2500 | Fuentes et al., (2009); Laskowski et al. (2013) |
| | Phosphoria Formation | 300-500; 1000-1200; 1600-1800 | Link et al. (2014) |
| | Quadrant | 400-500; 1000-1200; 1400-1900; 2500-3000 | Chapman and Laskowski (2019) |
| | Amsden | 400-500; 1400-1900; 2200-2900 | Chapman and Laskowski (2019) |
| | Mississippian strata | 400-600; 900-1500; 1600-1800; 2300-2900 | Laskowski et al., (2013); Chapman and Laskowski (2019) |
| | Belt Supergroup | 1450–1600; 1700–1860; 2600; 3000–3600 | Ross and Villeneuve (2003); Balgord et al. (2009); Mueller et al. (2016) |

Table 2.1. Potential detrital zircon source rocks for Pioneer District placer deposits

2017). Analysis of hafnium isotopes in detrital zircons of a known age has emerged as a powerful tool for provenance analysis, as it serves as an independent source indicator when paired with detrital U-Pb geochronology ages (Goodge and Vervoort, 2006; Stroup et al., 2008).

Lu-Hf isotopic ratios can be used to gain insight into the magmatic evolution of a region that has experienced multiple episodes of igneous activity (e.g. Gaschnig et al., 2011). Located in the Idaho-Montana segment of the Cordilleran arc, the detrital zircons from the Pioneer District placers provide Lu-Hf signatures that may give further insight into the magmatic evolution of western Montana. Pairing of U-Pb and Lu-Hf (as well as with Sr-Rb, Sm-Nd, etc.) has been applied to now-exposed arc-magmatic rocks in Cordilleran-style margins around the world (Ducea & Barton, 2007; Chapman et al., 2017).

**Detrital Zircon Unmixing Modeling**

An unmixing algorithm developed by Sundell and Saylor (2017) attempts to determine the mixing of source samples through inverse Monte Carlo modeling by comparing mixed detrital samples to randomly generated combinations of source distributions. As a forward modeling technique, detrital and igneous zircon age data for potential source units were input into the model and randomly combined to create a model age spectrum in the form of a kernel density estimate (KDE) (Figure 2.3a). Subsequently, a cross-correlation coefficient was calculated for the model and mixed detrital zircon sample pair (Figure 2.3b). This process was repeated 10,000 times to increase the likelihood that all possible combinations of possible source proportions are

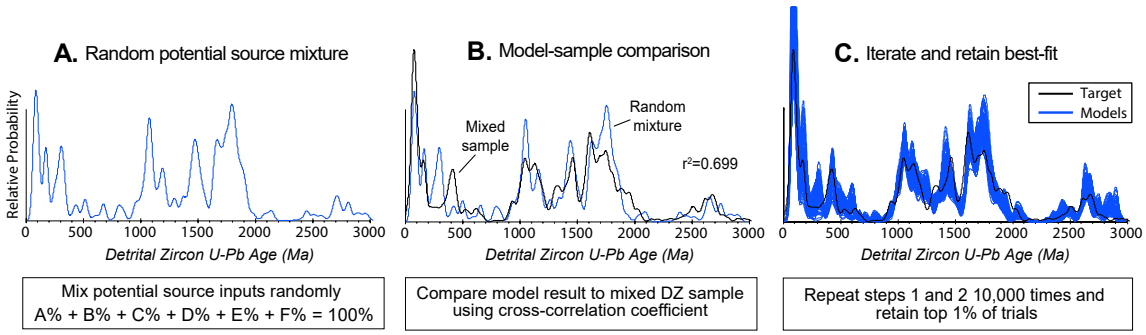


Figure 2.3. Detrital zircon unmixing model schematic. Modified from Bartschi et al., 2018.

tested. The mean relative contributions and 1σ uncertainty of each provenance group are reported from the top 1% of trials ranked by cross-correlation coefficient (Figure 2.3c). In addition to the cross-correlation coefficient comparison, the random mixtures of potential sources are compared by calculating a Kuiper test "V-value" and Kolmogorov-Smirnov (K-S) "D-value" (Sundell and Saylor, 2017). This allows for a side-by-side comparison of relative source contributions calculated using different statistical algorithms. After running the inverse Monte Carlo model, it is possible to run an iterative optimization that determines a single best fit between the model and the mixed sample.

Potential source units that are hypothesized to have contributed sediment to the placer deposits were identified through a combination of fieldwork around the margins of the Royal Stock and analysis of previously published regional geologic maps (this study; Mutch and McGill, 1962; Loen, 1986; Lewis, 1998). Nine distinct units were identified, including (from oldest to youngest): the Missoula Group (Belt Supergroup), the Amsden, Quadrant, Phosphoria, and Kootenai Formations, the Colorado Group (Thermopolis

shale), the Blackleaf and Beaverhead Formations, and the Pioneer Batholith (Royal Stock age-equivalent). Additionally, a Cordilleran passive margin compilation from Laskowski et al. (2013) was included as a model input due to the mapped presence of the Mississippian Madison Formation (Mutch and McGill, 1962) and the high likelihood that previously existing passive margin strata were eroded and deposited in the Flint Creek Basin (e.g. Portner et al., 2011). This compilation of potential sources was narrowed down by hundreds of trials with differing model inputs. By presenting the randomly generated KDEs atop the KDE of the mixed sink sample, the DZMix output allows the user to identify age ranges that were missed by each combination of input sources. A process of trial and error was used to create a randomly generated KDE that most closely approximated the mixed sample.

For the final model run, detrital zircon ages for the Pioneer District placer deposits (samples 101517AL1, 101517AL2, 101517AL3, and 101517AL4) were combined to create a single sink input (n=1,058) that was subsequently compared to random combinations of the potential sources listed above. In order to simplify modeling outputs, the ten potential source units were compiled into respective geologic eras (Proterozoic, Paleozoic, Mesozoic, and Paleocene).

This forward-modeling approach to unmixing detrital zircon samples is superior to a strictly qualitative approach to provenance analysis in that it provides approximate percent contributions from each input source. In a single model run, input sources that are not being incorporated by the model can be generally discounted as a plausible ones.

The relatively fast runtime of the model, even with >10,000 trials, allows for the user to rapidly test different plausible source combinations.

## RESULTS

### Detrital Zircon U-Pb and Lu-Hf Geochronology

#### *101517AL1*

Sample 101517AL1 was collected from processed placer tailings on the west side of the Pioneer Bar, downstream from an inactive dredge. The sample is a poorly sorted, pebble to cobble matrix supported conglomerate, with clasts of quartzite, sandstone, and slate, in order of decreasing abundance.

Zircon U-Pb ages (n=261) range from 24.9 ± 0.3 to 3293.2 ± 8.4 Ma, with 181 of those ages being >250 Ma (Figure 2.4a). U-Pb ages from all major North American crustal provinces are present, with age-probability peaks centered at ~1850, ~1750, ~1640, ~1490, ~1100, and ~430 Ma (Figure 2.4a). This is the case for each of the three remaining samples, all containing abundant grains (n>200) that are older than 250 Ma, with each major North American crustal province represented. Each mixed placer sample contains many grains >2600 Ma. Significant peaks for grains <250 Ma in this sample occur at ~165, ~75, and ~25 Ma. Lu-Hf isotopic ratios were determined for 22 grains ranging in age from 25 to 171 Ma (Figure 2.5). Epsilon values range from -2.8 at 171 Ma to -19.3 at 67 Ma. A subsequent increase with decreasing age in ƐHf bring values up to as high as 13.2 at 26 Ma.

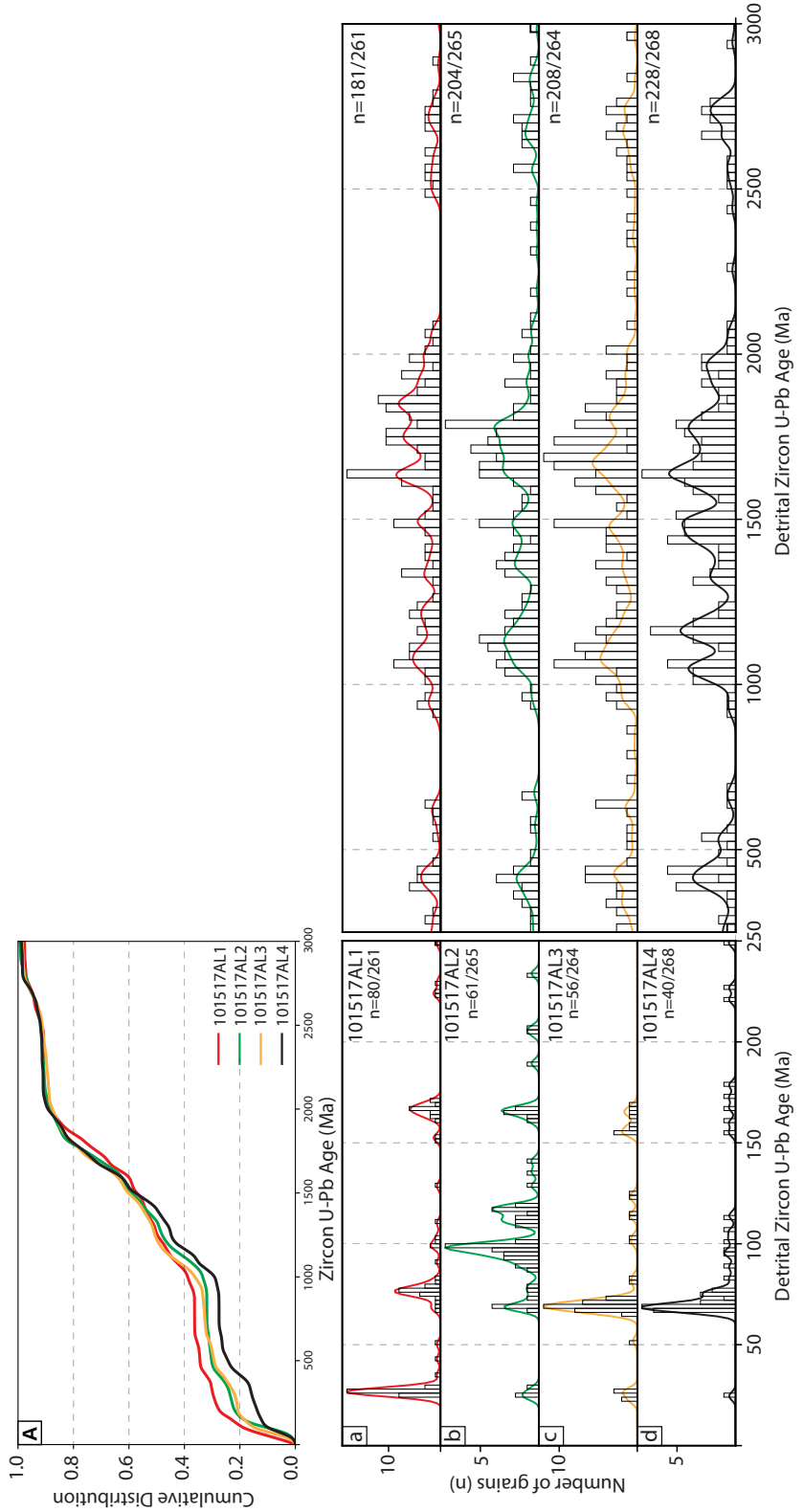


Figure 2.4. (A) Cumulative probability plot and (a-d) kernel density curves with histograms for the four detrital zircon samples collected from the Pioneer District gold placer deposits. Kernel density estimates (KDE) were constructed using a 15 Ma bandwidth and histogram bin widths are 5 Ma for grains <250 Ma and 50 Ma for grains >250 Ma.

***101517AL2***

Sample 101517AL2 was collected from processed placer tailings downstream from an inactive dredge, and is a poorly sorted, pebble to cobble matrix supported conglomerate. In order of decreasing abundance, clasts include granite, sandstone, siltstone, quartzite, and schist with bronze mica.

U-Pb ages (n=265) range from 24.1 ± 0.2 to 3635.5 ± 7.6 Ma, with 204 of those ages >250 Ma (Figure 2.4b). This sample contains the most variability in zircon ages <250 Ma, with significant peaks at ~165, ~115, ~100, ~90, ~69, and ~25 Ma (Figure 2.4b). This is the only sample collected from the placer deposits that contains a prominent age-probability peak at 90-100 Ma (Figure 2.4b). Lu-Hf isotopic ratios were analyzed for zircons (n =13) ranging in age from 24.9 to 167.8 Ma (Figure 2.5). Epsilon Hf values vary from −9.6 calculated at 167.8 Ma to –15.3 at 77 Ma. Like 101517AL1, epsilon Hf values become much more juvenile with corresponding U-Pb ages in the Tertiary, with an epsilon Hf value of 14.0 calculated at 24.9 Ma.

***101517AL3***

Sample 101517AL3 was collected from sandy, reworked tailings immediately down slope from abundant schist and metacarbonate float. Clasts in sample include quartzite, sandstone, biotite schist, metacarbonate, paragneiss, and granite.

U-Pb ages (n=264) range from 22.2 ± 0.2 to 3750.3 ± 7.7 Ma, with 208 of those ages being >250 Ma (Figure 2.4c). Age spectra for grains <250 Ma is similar to 101517AL1, with the exception that this sample contains a greater abundance of ~69 Ma grains (30 grains). Lu-Hf isotopic ratios were collected for 14 grains ranging in age from

22.2 to 168.3 Ma (Figure 2.5). Epsilon values range from -3.3 at 168 Ma to -21.9 at 65 Ma, followed by an increase in epsilon-Hf values up to as high as 9.6 at 27 Ma.

***101517AL4***

Sample 101517AL4 was sampled from a matrix-supported glacial moraine deposit with cobble to boulder-sized granite and quartzite. The sample was collected ~5 km downstream from Pikes Peak Creek placer mine. U-Pb ages (n=268) range from 24.5 ± 0.4 to 3472.5 ± 10.1 Ma, with 228 of those ages being >250 Ma. The only prominent peak determined for grains <250 Ma is at ~69 Ma, and the sample contains only one

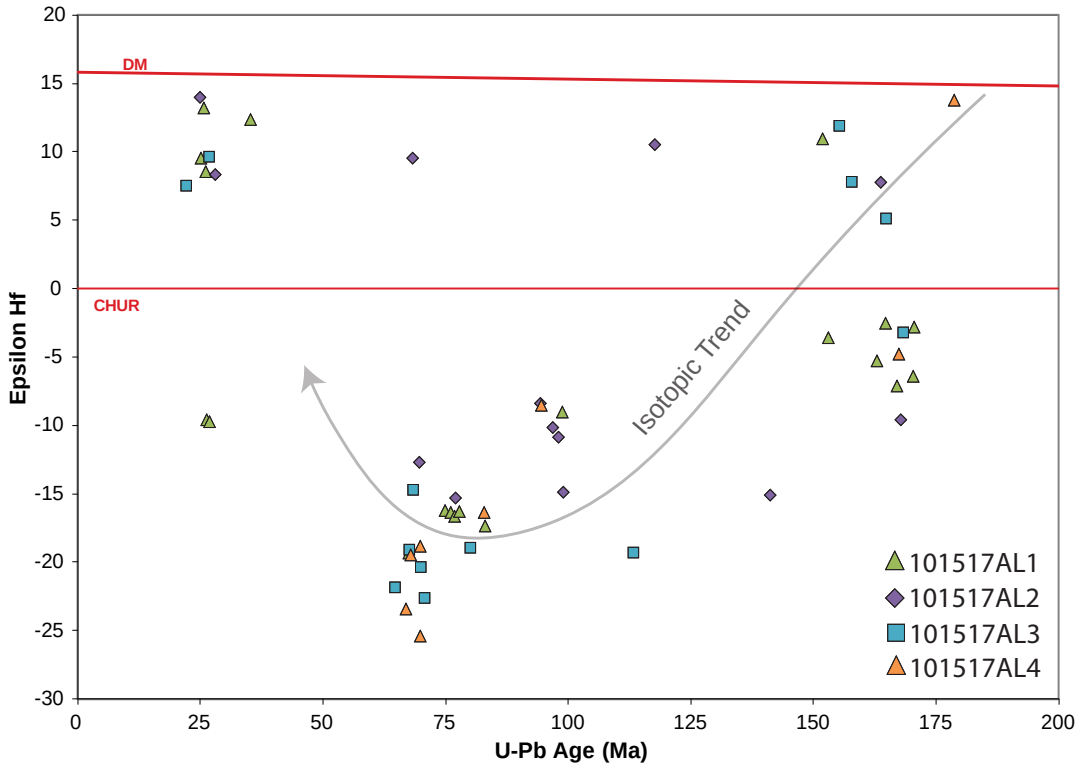


Figure 2.5. εHf values plotted against detrital zircon U-Pb ages from the Pioneer District placer deposits. Shown in relation to the chondritic uniform reservoir (CHUR) and depleted mantle (DM) evolution lines. Grey arrow shows isotopic trend which is interpreted to serve as a proxy for crustal thickening followed by increased mantle input (e.g. Gaschnig et al., 2011).

grain at ~25 Ma (Figure 2.4d). Epsilon Hf values were collected for 8 grains ranging in age from 22.2 to 168.3 Ma (Figure 2.5). Epsilon values range from -4.8 at 167.4 Ma to -23.4 at 66.9 Ma. No tertiary zircon grains in this sample were analyzed for Lu-Hf.

**DZ Unmixing Modeling**

The inverse Monte Carlo modeling results for the Pioneer District placer deposits are shown in Figure 2.6. These results represent the most geologically plausible and statistically robust outputs determined by inputting mapped units in the hypothesized source area that produce a randomly generated KDE with the highest cross-correlation coefficient to the mixed sample.

Figures 2.6a and 2.6b display the top 1% of model fits retained relative to the combined, mixed samples. With a KDE bandwidth of 20 Ma, the source inputs (see methods section) yield a cross-correlation coefficient between model and mixed sample of $0.873 \pm 0.014$.

Figures 2.6c and 2.6d show the relative contributions from each source input calculated by the cross-correlation coefficient and Kuiper test, respectively. The Missoula Group of the Belt Supergroup displays the smallest relative sediment contribution at ~4%. The Paleozoic passive margin and Mesozoic foreland basin rocks have relative contributions of ~16% and 25%, respectively. The Royal Stock pluton of the northern Flint Creek Range has a calculated contribution slightly smaller than that of the passive margin at ~11%. Lastly, the Beaverhead Fm. has the largest relative contribution of approximately 43%.

The only notable difference between the two contribution plots is that the Kuiper test resulted in a slightly larger contribution from the Mesozoic inputs and less from the Royal Stock.

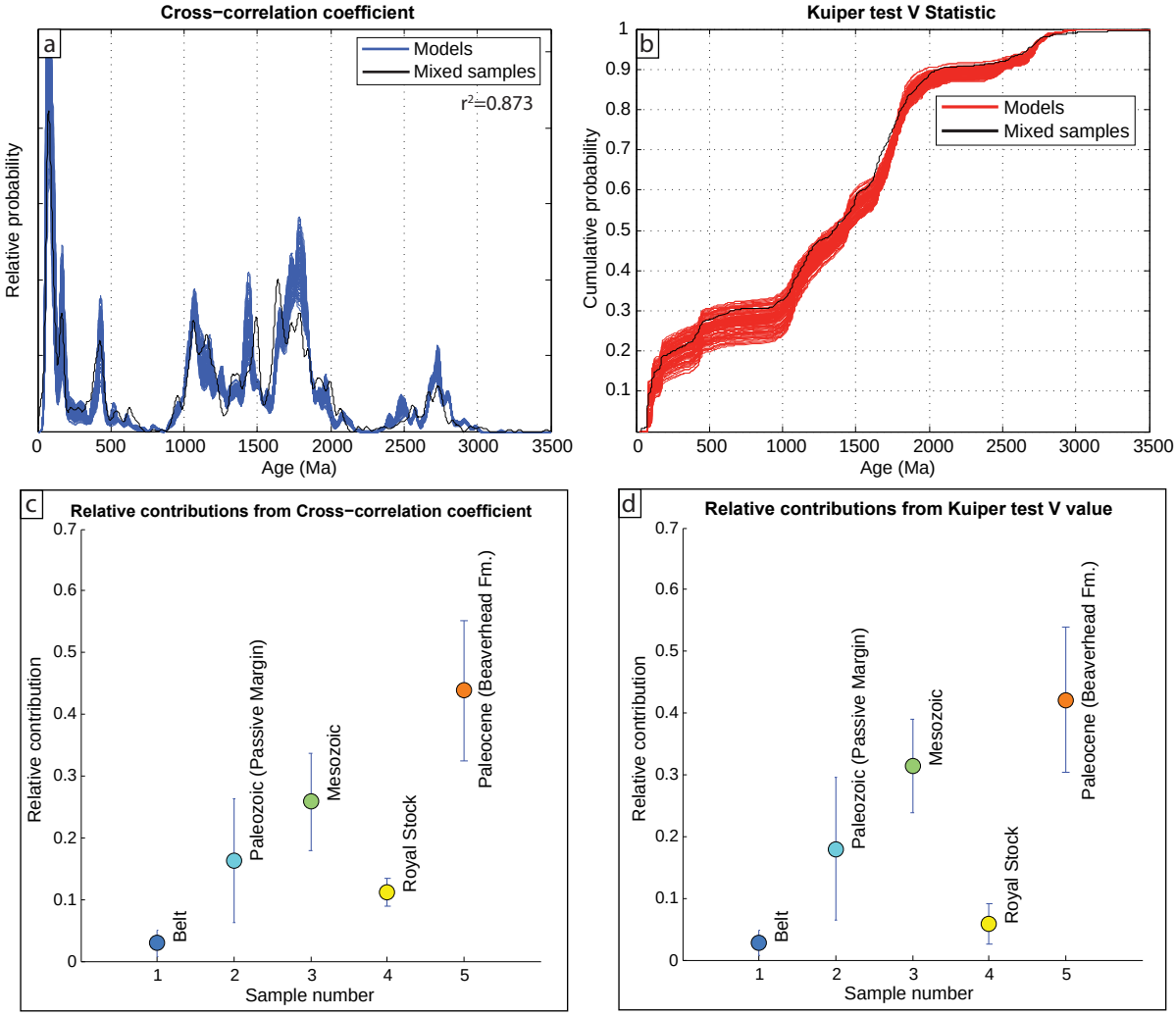


Figure 2.6. Inverse Monte Carlo unmixing model results for the Pioneer District placer deposits. (a) Probability density plots of top 1% of model fits retained relative to combined, mixed placer samples, (b) retained 1% of model runs displayed as cumulative distribution plot, (c) relative contributions from 10 input sources calculated using cross-correlation coefficient, (d) relative contributions calculated from Kuiper test values. Note similarities in the modeled contributions and the high relative contributions from the synorogenic Beaverhead conglomerate, as well as the presence of first-cycle grains from the Royal Stock pluton. Source inputs and data sources can be accessed in Supplementary material.

# DISCUSSION

## Detrital Zircon U-Pb Geochronology

All detrital zircon samples from the Pioneer District placer deposits display strikingly similar age spectra (Figure 2.4a-2.4d). U-Pb ages from all major North American crustal provinces are present in all four detrital zircon samples, with major peaks in age spectra at ~1850, ~1750, ~1640, ~1490, ~1100, and ~430 Ma. This diverse and wide range of zircon ages suggests abundant zircon recycling, and the ages present in these samples are very similar to those found in the synorogenic Beaverhead conglomerate (e.g. Laskowski et al., 2013; Schwartz and Graham, 2017).

The most prominent age spectra peaks for grains less than 250 Ma occur at ~25, 68-80, 90-120, and 160-180 Ma. The ~25 Ma grains present in all samples likely represent ash-fall from the Dillon Volcanics of SW Montana, an interpretation that is supported by their juvenile Lu-Hf values (Figure 2.5). The presence of these grains could possibly represent a maximum depositional age (MDA) for the Pioneer District placers deposits. However, since the samples were obtained from reworked tailings, it is possible that younger zircon grains from overlying units were incorporated into them. The Late Cretaceous grains are interpreted as first-cycle grains shed from the Royal Stock pluton of the northern Anaconda metamorphic core complex. This interpretation is supported by paleoflow and sedimentological observations made by Stroup et al. (2008). The presence of first-cycle grains shed from the Royal Stock supports the conclusion made by Loen (1994) that it was the original source of the Pioneer district placer gold. 90-120 Ma grains have many possible explanations, including first cycle derivation from the nearby

Idaho Batholith (Gaschnig et al., 2011), shedding of recycled grains from the now-eroded Beaverhead Group (Janecke et al., 2000; Schwartz & Graham, 2017), or contribution from the Vaughn Member of Cretaceous Blackleaf Formation, which has been mapped ~10 kilometers north of the placer deposits (Brooks, 2002; Brooks & Sears, 2009). Grains with U-Pb ages between 150 and 250 Ma are interpreted to have been sourced from the Coast Mountains or Sierra Nevada arc segments (Paterson et al., 2011) and are likely recycled.

**Lu-Hf Isotopic Analysis**

Systematic trends that can be observed in Lu-Hf signatures are not well-studied for the complex plutons and dikes that intruded the hinterland of western Montana. However, various isotopic systems have been used to investigate the evolution of the Idaho Batholith and Challis intrusions of eastern Idaho, which lies approximately 100 kilometers west of the Anaconda metamorphic core complex (Foster et al., 2002; Gaschnig et al., 2011). One of the isotopic trends observed in the Idaho Batholith is a steady decrease in epsilon Hf values from –8 εHf at ~90 Ma to approximately –25 εHf at ~50 Ma, which was interpreted as progressive crustal thickening and incorporation of more previously existing crust into rising arc magmatism (Gaschnig et al., 2011). Epsilon Hf values in the almost immediately subsequent Challis Intrusives and equivalent volcanics (~48 Ma; Gaschnig et al., 2011) display much more juvenile εHf values, ranging from –28 to –3 with an average around –11 (Gaschnig et al., 2011). This “pull-up” in epsilon Hf space is interpreted by Gaschnig et al. (2011) to represent crustal thinning by extensional collapse of the Cordilleran arc crust and increased mantle input.

The detrital zircon Lu-Hf results reported here display a nearly identical trend (Figure 2.5), supporting the interpretation that many of the zircons <250 Ma within the placer deposits are first-cycle (non-recycled) grains sourced from surrounding plutons.

The relatively large spread of epsilon Hf values from intermediate to very juvenile for grains at ~160 Ma is consistent with derivation from the Sierra Nevada and Coast Range segments of the Cordilleran magmatic arc (Paterson et al., 2011). The highly evolved epsilon Hf values for Late Cretaceous-Early Paleogene (75-65 Ma) zircons support the hypothesis that many of these grains were sourced from the Royal Stock pluton, as similar values have been seen for temporally overlapping, arc-associated plutons (e.g. Gaschnig et al., 2011). Oligocene grains in three of the four samples are extremely juvenile, which is consistent with the interpretation that they were sourced as ash-fall from the Dillon Volcanics of southwest Montana (Fritz et al., 2007).

**Detrital Zircon Geochronology Unmixing Modeling**

Application of the unmixing model supports the interpretation that the Pioneer District placer gold was ultimately sourced from the gold-bearing Royal Stock as it intruded into overlying supracrustal rocks with complex detrital zircon signatures (Figure 2.6). Modeling results make evident the significant number of zircons that were likely shed into the placer deposits from the Beaverhead Fm. (Figure 2.6). Another possibility is that the Flint Creek basin shared a similar source with the Beaverhead Formation. However, we deem the former interpretation more plausible due to the time gap between Flint Creek basin and Beaverhead deposition, as the Flint Creek basin sedimentation occurred largely during the Mid-Oligocene to Late-Miocene (Loen, 1986; Portner et al.,

2011), while main-phase deposition of the Beaverhead Fm. occurred during the Paleocene (e.g. Schwartz and Graham, 2017). The absence of Beaverhead strata in the hypothesized source area itself (Figure 2.2) is probably due to its complete erosion during exhumation of the Anaconda metamorphic core complex.

Modeling results do not require significant sediment contribution from the Belt supergroup, a result that is supported by the relatively small mapped extent of the unit in the northern Flint Creek range (Mutch & McGill, 1962; Lewis, 1998). Paleozoic and Mesozoic rocks are approximately equally represented in the hypothesized source region, which is reflected in the modeling result percentages. The slightly larger percent contribution from Mesozoic units could be a consequence of differences in the availability of zircon in the source units, as the Paleozoic passive margin units contain less abundant zircon grains. Additionally, some Paleozoic grains were likely recycled into Mesozoic units, which the model does not have the ability to recognize. Taken together, the diverse DZ age spectra and modeling results suggest sediment derivation and recycling from the Mesoproterozoic Belt Supergroup, Paleozoic-Mesozoic passive margin, Mesozoic foreland basin sedimentary rocks, and the synorogenic Beaverhead Conglomerate. These interpretations are consistent with the mapping results presented in Mutch & McGill (1962) of the northern Flint Creek Range. Although more robust constraints are needed to make conclusive interpretations on maximum depositional age relative to the timing of AMCC exhumation, we propose that initial placer weathering occurred during late-stage slip along the Anaconda detachment and deposition occurred in the Flint Creek supradetachment basin (Figure 2.7).

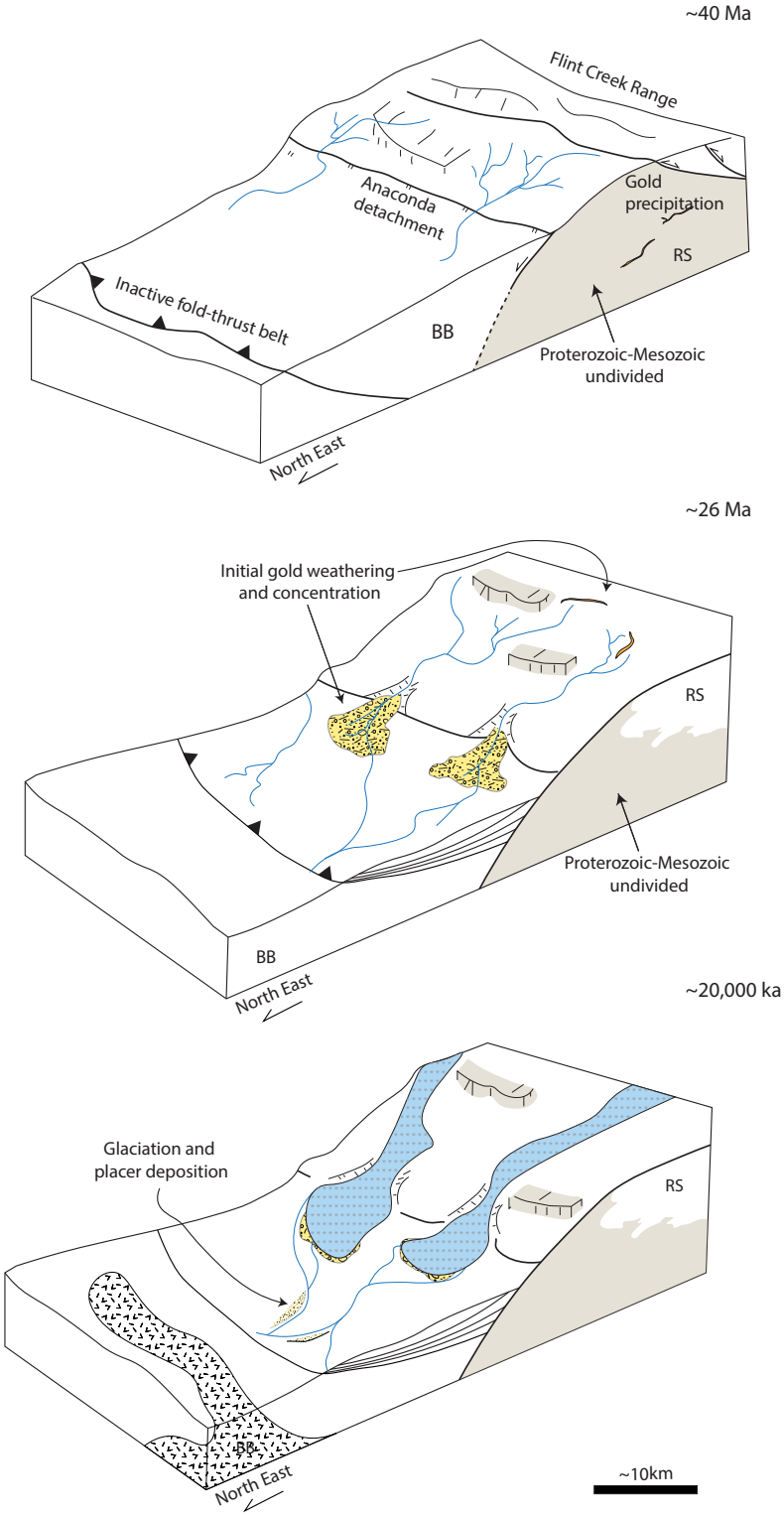


Figure 2.7. Schematic tectonic model for the genesis, erosion, transport, and deposition of the Pioneer District gold placers. RS-Royal Stock; BB-Boulder Batholith. BB is not to scale.

**Limitations**

The use of detrital zircon geochronology to determine to source of gold placers hinges on two main assumptions, the first being that gold and zircon will behave similarly during transport and deposition due to their high densities. It has been demonstrated that sediment samples with identical provenance can display significant intersample variability due to the preferential entrainment of larger and lower-density minerals (e.g. Malusa et al., 2015). Therefore, it is important to consider that the very high density of gold (~19.30 g/cm$^3$) could potentially lead to falling out of entrainment before the source-representing zircon grains that it was eroded with. This source of error may become especially important to correct for if the placer deposits of interest were transported great distances, which we conclude to not be the case for the Pioneer District placers.

Second, a common assumption made in almost all detrital zircon studies is that zircon fertility in igneous sources and the relative abundance of zircon in sedimentary sources do not bias the source region interpretation (e.g. Dickinson, 2008). Varying bedrock mineral fertility near a placer lode source could lead to misinterpretation of age spectra or a complete absence of crucially important age domains. Increasing the number of grains analyzed per sample (*n)* is one way to reduce the likelihood of missing a potentially important source unit (Pullen et al., 2014). The large-n datasets collected for this study, combined with the well-understood configuration and well-constrained ages of possible plutonic source units, makes it unlikely that a significant bedrock source is being missed.

A source of error in the unmixing model may arise due to along-strike variability in the detrital zircon spectra of given unit. None of the potential sources input into the unmixing model (DZ samples) were collected directly from the hypothesized source area. As a preliminary investigation designed to test the utility of the method, we here assume that previously obtained samples from other localities provide sufficiently similar DZ spectra. To improve confidence in the unmixing modeling results, the input potential sources should be sampled from the hypothesized source area itself. However, even if this were done, the top-down modeling approach must still make a-priori assumptions about the potential sources and assume that the sink sample is a pure mixture of them. Therefore, it may be beneficial to complement future studies of this kind with recently developed "bottom-up" unmixing models, which create synthetic sources from mixed samples and do not require a-priori assumptions of source units ("DZNMF"; Saylor et al., 2019).

The wide-range of potential source rock ages in the northern Flint Creek range (Mesoproterozoic-Paleocene) adds an additional element of difficulty for DZ provenance interpretations. Other regions may have far more simple source regions, making use of the DZ spectra and modeling easier.

**Utility of technique and future possibilities**

Overall, our detrital zircon U-Pb results and modeling display that, even with abundant zircon recycling, the technique has great potential to determine the source of mineral deposits of high density. The complimentary collection of trace-element geochemical data allows a more detailed characterization of source, as it can be paired

with detrital U-Pb ages and serve as an independent provenance indicator (Gehrels, 2014). Similarly, Lu-Hf isotopic ratios, when paired with U-Pb ages, can provide information into the magmatic evolution of potential source areas. An increasing ability for unmixing models to account for zircon recycling and fertility will greatly improve the accuracy of results.

There are many mining districts around the world where the application of this technique may be of great value. U-Pb analyses of detrital zircons in the Witwatersrand basin of South Africa have given important insight into the controversial origin of the largest gold placer deposits on Earth (Gehrels, 2014), but further U-Pb dating and geochemical analysis of detrital zircons has the potential to provide more robust constraints on source units and transport history. The application of new modeling techniques would add another quantitative constraint on provenance.

Determining potential source areas for modern placer sediments holds potential as well and is a technique that has not yet been documented in the literature. We propose that a systematic investigation of detrital zircon grains from modern river placers in regions such as Alaska could ultimately assist in determining lode sources that are actively shedding gold. Identification of the weathering lode source would allow for more localized and potentially less environmentally impactful mining operations.

## CONCLUSION

Detrital zircon U-Pb geochronology and unmixing modeling suggest that gold from the Pioneer District placer deposits of southwest Montana was derived from vein and skarn lode sources in northern footwall of the Anaconda metamorphic core complex.

Our data offers the first quantitative support for previous interpretations (Loen, 1994; McCulloch et al., 2003) that the Late Cretaceous Royal Stock pluton precipitated gold along its contact with overlying Proterozoic through Mesozoic supracrustal rock, and was subsequently weathered, transported, and deposited in the AMCC supradetachment basin during the Late Oligocene-Early Miocene. Additionally, we identify the primary sedimentary rocks that were present in the catchment that sourced the gold. These results serve as confirmation of the utility of using DZ geochronology and emerging DZ unmixing modeling techniques to determine the source area of dense, economically-valuable minerals. The worldwide occurrence of gold placer deposits with unknown source areas provides abundant opportunity to apply these techniques.

## ACKNOWLEDGMENTS

We thank Devon Orme, Saré Campbell, and Colin Kennedy for field assistance and the entire staff of the University of Arizona Laserchron Center (Tucson, Arizona, USA) (support from National Science Foundation grant EAR-1649254) for analytical assistance. This research was funded by Montana State University and a Geological Society of America Graduate Student Research Grant.

## REFERENCES CITED

Baken, J.F., 1984, The structural geology and tectonic history of the northern Flint Creek Range, western Montana [M.Sc. thesis]: Montana State University, 140 p.

Balgord, E., Mahoney, J.B., and Gingras, M.K., 2009, Detrital zircon evidence requires revision of Belt stratigraphy in southwestern Montana: Geological Society of America Abstracts with Programs, v. 41, p. 590.

Bartschi, N., Saylor, J.E., Lapen, T.J., Blum, M.D., Pettit, B.S., and Andrea, R.A., 2018, Tectonic Controls On Late Cretaceous Sediment Provenance And Stratigraphic Architecture In The Book Cliffs, Utah. Geological Society of American Bulletin, v. 130, p. 1763-1781 doi:10 .1130 /B31927.1.

Baty, J.B., 1973, Fission track age dates from three granitic plutons in the Flint Creek Range, western Montana: Missoula, [M.Sc. Thesis]: The University of Montana, 37 p.

Boyle, R.W., 1979, The geochemistry of gold and its deposits, Geological Survey of Canada Bulletin 280, 584 p.

Brooks, J.A., 2002, Bedrock geologic maps of the Griffin Creek and Bailey Mountain 7.5 minute quadrangles, Powell County, Montana: Missoula, [M.Sc. Thesis]: University of Montana, 84 p.

Brooks, J.A., and Sears, J.W., 2009, Geologic map of the Bailey Mountain and Griffin Creek 7.5' quadrangles, Montana: Montana Bureau of Mines and Geology EDMAP portion of the National Geologic Mapping Program 1, 2 sheets, scale 1:24,000.

Chadwick, R.A., 1981, Chronology and structural setting of volcanism in southwestern and central Montana, in Tucker, T.E., ed., Field Conference and Symposium Guidebook to Southwest Montana: Montana Geological Society, p. 301–310.

Chapman, J.B., Ducea, M.N., Kapp, P., Gehrels, G.E., DeCelles, P.G., 2017, Spatial and temporal radiogenic isotopic trends of magmatism in Cordilleran orogens. Gondwana Res., v. 48, p. 189-204, doi:10.1016/j.gr.2017.04.019.

Chapman, A.D. and Laskowski, A.K., 2019, Detrital zircon U-Pb data reveal a Mississippian sediment dispersal network originating in the Appalachian orogen, traversing North America along its southern shelf, and reaching as far as the southwest United States. Lithosphere, v.11, p. 581-587, doi:10.1130/L1068.1.

Davis, D.W., Hirdes, W., Schaltegger, U., and Nunoo, E.A., 1994, U-Pb age constraints on deposition and provenance of Birimian and gold-bearing Tarkwaian sediments in Ghana, West Africa: Precambrian Research, v. 67, p. 89–107, doi:10.1016/0301-9268(94)90006-x.

DeCelles, P.G., 2004, Late Jurassic to Eocene evolution of the Cordilleran thrust belt and foreland basin system, western U.S.A. American Journal of Science, v. 304, p. 105–168, doi:10.2475/ajs.304.2.105.

Dickinson,W.R., 2008, Impact of differential zircon fertility of granitoid basement rocks in North America on age populations of detrital zircons and implications for granite petrogenesis. Earth and Planetary Science Letters, v. 275, p. 80–92, doi:10.1016/j.epsl.2008.08.003.

Dickinson, W. R., and G. E. Gehrels, 2008, Sediment delivery to the Cordilleran foreland basin: Insights from U-Pb ages of detrital zircons in Upper Jurassic and Cretaceous strata of the Colorado Plateau, Am. J. Sci., v. 308, p. 1041–1082, doi:10.2475/01.2008.01.

Dickinson, W.R., Lawton, T.F., and Gehrels, G.E., 2009, Recycling detrital zircons: A case study from the Cretaceous Bisbee Group of southern Arizona: Geology, v. 37, p. 503–506, doi:10.1130/g25646a.1.

Ducea, M.N., Barton, M.D., 2007, Igniting flare-up events in Cordilleran arcs, Geology, v. 35, p. 1047–1050, doi:10.1130/G23898A.1.

Dudás, F.O., Ispolatov, V.O., Harlan, S.S., and Snee, L.W., 2010, 40Ar/39Ar geochronology and geochemical reconnaissance of the Eocene Lowland Creek volcanic field, west-central Montana: The Journal of Geology, v. 118, p. 295–304, doi:10.1086/651523.

Edwards, R.P., and Atkinson, K., 1986, Ore Deposit Geology and its Influence on Mineral Exploration: London and New York, Chapman and Hall, p. 175-214.

Elliott, C.G., and Lonn, J.D., in review, Geologic map of the Long Peak 7.5' quadrangle, southwestern Montana: Montana Bureau of Mines and Geology Open-File Report, 1 sheet, scale 1:24,000.

Emmons W.H., and Calkins F.C., 1913, Geology and ore deposits of the Philipsburg Quadrangle Montana, U.S. Geological Survey Professional Paper 78, 271 p.

Feeley, T.C., and Cosca, M.A., 2003, Time vs. compositional trends of magmatism at Sunlight volcano, Absaroka volcanic province, Wyoming: Geological Society of America Bulletin, v. 115, p. 714–728, doi:10.1130/0016-7606(2003)115<0714:TVCTOM>2.0.CO;2.

Feeley, T.C., Cosca, M.A., and Lindsay, C.R., 2002, Petrogenesis and implications of calc-alkaline cryptic hybrid magmas from Washburn Volcano, Absaroka Volcanic Province, USA: Journal of Petrology, v. 43, p. 663–703, doi:10.1093/petrology/43.4.663.

Foster, D.A., and Raza, A., 2002, Low-temperature thermochronological record of exhumation of the Bitterroot metamorphic core complex, northern Cordilleran Orogen: Tectonophysics, v. 349, p. 23–36, doi:10.1016/s0040-1951(02)00044-6.

Foster, D.A., Doughty, P.T., Kalakay, T.J., Fanning, C.M., Coyner, S.C., Grice, W.C., and Vogl, J., 2007, Kinematics and timing of exhumation of metamorphic core complexes along the Lewis and Clark fault zone, northern Rocky Mountains, USA, in Till, A.B., Roeske, S.M., Sample, J.C., and Foster, D.A., eds., Exhumation Associated with Continental Strike-Slip Fault Systems: Geological Society of America Special Paper 434, p. 207–232, doi:10.1130/2007.2434(10).

Foster, D. A., Grice, W. C., & Kalakay, T. J., 2010, Extension of the Anaconda metamorphic core complex: 40Ar/39Ar thermochronology and implications for Eocene tectonics of the northern Rocky Mountains and the Boulder batholith. Lithosphere, v. 2, no. 4, p. 232-246. doi:10.1130/L94.1.

Foster, D.A., Mueller, P.A., Heatherington, A., Gifford, J.N., and Kalakay, T.J., 2012, Lu-Hf systematics of magmatic zircons reveal a Proterozoic crustal boundary under the Cretaceous Pioneer batholith, Montana: Lithos, v. 142–143, p. 216–225, doi:10.1016/j.lithos.2012.03.005 .

Fritz, W.J., Sears, J.W., McDowell, R.J., and Wampler, J.M., 2007, Cenozoic volcanic rocks of southwestern Montana: Northwest Geology, v. 36, p. 91–110.

Fuentes, F., DeCelles, P.G., and Gehrels, G.E., 2009, Jurassic onset of foreland basin deposition in northwestern Montana, USA: Implications for along-strike synchroneity of Cordilleran orogenic activity: Geology, v. 37, p. 379–382, doi:10.1130/G25557A.1.

Fuentes, F., DeCelles, P.G., and Constenius, K.N., 2012, Regional structure and kinematic history of the Cordilleran fold-thrust belt in northwestern Montana, USA: Geosphere, v. 8, p. 1104–1128, doi:10.1130/GES00773.1.

Gaschnig, R.M., Vervoort, J.D., Lewis, R.S., and McClelland, W.C., 2010, Migrating magmatism in the northern US Cordillera: In-situ U-Pb geochronology of the Idaho batholith: Contributions to Mineralogy and Petrology, v. 159, p. 863–883, doi:10.1007/s00410-009-0459-5.

Gaschnig, R.M., Vervoort, J.D., Lewis, R.S., and Tikoff, B., 2011, Isotopic Evolution of the Idaho Batholith and Challis Intrusive Province, Northern US Cordillera: Journal of Petrology, v. 52, p. 2397–2429, doi:10.1093/petrology/egr050.

Gaschnig, R.M., Vervoort, J.D., Lewis, R.S., and Tikoff, B., 2013, Probing for Proterozoic and Archean crust in the northern U.S. Cordillera with inherited zircon from the Idaho batholith: Geological Society of America Bulletin, v. 125, p. 73–88, doi:10.1130/B30583.1.

Gehrels, G. E., Valencia, V.A., Ruiz, J., 2008, Enhanced precision, accuracy, efficiency, and spatial resolution of U-Pb ages by laser ablation multicollector-inductively coupled plasma-mass spectrometry, Geochem. Geophys. Geosyst., v. 9, Q03017, doi:10.1029/2007GC001805.

Gehrels, G., 2014, Detrital Zircon U-Pb Geochronology Applied to Tectonics: The Annual Review of Earth and Planetary Sciences, p. 127–149, doi:10.1146/annurev-earth-050212-124012.

Goodge, J.W. and Vervoort, J.D., 2006, Origin of Mesoproterozoic A-type granites in Laurentia: Hf isotope evidence: Earth and Planetary Science Letters, v. 243, p. 711-731, doi:10.1016/j.epsl.2006.01.040.

Grice, W.C., Jr., 2006, Exhumation and cooling history of the middle Eocene Anaconda metamorphic core complex, western Montana [M.Sc. thesis]: Gainesville, University of Florida, 261 p.

Harlan, S.S., Snee, L.W., and Geissman, J.W., 1996, 40Ar/39Ar geochronology and paleomagnetism of Independence Volcano, Absaroka Volcanic Supergroup, Beartooth Mountains, Montana: Canadian Journal of Earth Sciences, v. 33, p. 1648–1654, doi:10.1139/e96-125.

Hiza, M.M., 1999, The Geochemistry and Geochronology of the Eocene Absaroka Volcanic Province, Northern Wyoming and Southwest Montana, USA [Ph.D. thesis]: Oregon State University, 243 p.

Howlett, C.J., Reynolds, A.N., Laskowski, A.K., Geologic Map of the Northern Half of the Pintler Lake 7.5' Quadrangle and the Southern Half of the Warren Peak 7.5’ Quadrangle, Southwestern Montana, Geological Society of America, Phoenix, AZ, September 2019. doi:10.1130/abs/2019AM-331565.

Janecke, S.U., VanDenburg, C.J., Blankenau, J.J., and M’Gonigle, J.W., 2000, Long-distance longitudinal transport of gravel across the Cordilleran thrust belt of Montana and Idaho: Geology, v. 28, n. 5, p. 439-442, doi:10.1130/00917613(2000)28<439:LL TOGA>2.0.CO;2.

Janecke, S.U., Dorsey, R. J., Kickham, J. C. Matoush, J. P., and McIntosh, W., 2005, Geologic Map of the Bachelor Mountain Quadrangle, Southwest Montana: Montana Bureau of Mines Open-File Report 525, scale 1:24,000, 28 p.

Kanouo NS, Zaw K, Yongue RF, Sutherland FL, Meffre S, et al., 2012, U-Pb zircon age constraining the source and provenance of gem-bearing Late Cenozoic detrital deposits, Mamfe Basin, SW Cameroon. Resource Geology, v. 62, p. 316–24, doi:10.1111/j.1751-3928.2012.00197.x.

Kanouo, N., Ngueutchoua, G., Kouske, A., Yongue, R., and Venkatesh, A., 2018, Trace Element and U–Pb Core Age for Zircons from Western Meiganga Gold Placer, Cameroon: Their Genesis and Archean-Proterozoic Sources: Minerals, v. 8, p. 194, doi:10.3390/min8050194.

Knight, J.B., Morison, S.R., and Mortensen, J.K., 1999, The relationship between placer gold particle shape, rimming, and distance of fluvial transport as exemplified by gold from the Klondike District, Yukon Territory, Canada: Economic Geology, v. 94, p. 635–648, doi:10.2113/gsecongeo.94.5.635.

Koglin N, Zeh A, Frimmel HE, Gerdes A. 2010. New constraints on the auriferous Witwatersrand sediment provenance from combined detrital zircon U-Pb and Lu-Hf isotope data for the Eldorado Reef (Central Rand Group, South Africa). Precambr. Res. v. 183, p. 817–824, doi:10.1016/jprecamres.2010.09.009.

Laskowski, A. K., DeCelles, P. G., Gehrels, G. E., 2013, Detrital zircon geochronology of Cordilleran retroarc foreland basin strata, western North America, Tectonics, v. 32, p. 1027–1048, doi:10.1002/tect.20065.

Lewis, R.S., 1998, Geologic Map of the Butte 1° x 2° Quadrangle: Open File Montana Bureau of Mines and Geology 363, 1 sheet, scale 1:250,000.

Link, P.K., Mahon, R.C., Beranek, L.P., Campbell-Stone, E.A., and Lynds, R., 2014, Detrital zircon provenance of Pennsylvanian to Permian sandstones from the Wyoming craton and Wood River Basin, Idaho, U.S.A.: Rocky Mountain Geology, v. 49, p. 115–136, doi:10.2113/gsrocky.49.2.115.

Loen, J.S., 1986, Origin of gold placers in the Pioneer District, Powell County, Montana, [M.Sc. thesis]: Colorado State University, 181 p.

Loen, J.S., 1994, Origin of placer gold nuggets and history of formation of glacial gold placers, Gold Creek, Granite County, Montana: Economic Geology, v. 89, p. 91–104, doi:10.2113/gsecongeo.89.1.91.

Loen, J.S., 1995, Use of placer gold characteristics to locate bedrock gold mineralization, Exploration & Mining Geology, v. 4, no. 4, p. 335-339.

Lund, K., Aleinikoff, J.N., Kunk, M.J., Unruh, D.M., Zeihen, G.D., Hodges, W.C., du Bray, E.A., and O'Neill, J.M., 2002, SHRIMP U-Pb and 40Ar/39Ar age constraints for relating plutonism and mineralization in the Boulder batholith region, Montana: Economic Geology and the Bulletin of the Society of Economic Geologists, v. 97, p. 241–267, doi:10.2113/gsecongeo.97.2.241.

Malusà, M.G., Resentini, A., and Garzanti, E., 2016, Hydraulic sorting and mineral fertility bias in detrital geochronology: Gondwana Research, v. 31, p. 1–19, doi:10.1016/j.gr.2015.09.002.

Marvin, R.F., Mehnert, H.H., Naeser, C.W., and Zartman, R.E., 1989, U.S. Geological Survey radiometric ages—compilation “C,” part five: Colorado, Montana, Utah, and Wyoming: Isochron-West, v. 53, p. 14–19.

McCulloch, R., 2003, Applied gold placer exploration and evaluation techniques: Butte, MT, Montana Bureau of Mines and Geology, 267 p.

Mueller, P., Mogk, D., Wooden, J., and Spake, D., 2016, U-Pb ages of zircons from the Lower Belt Supergroup and proximal crystalline basement: Implications for the early evolution of the Belt Basin, in MacLean, J.S., and Sears, J.W., eds., Belt Basin: Window to Mesoproterozoic Earth: Geological Society of America Special Paper 522, p. 283–303, doi:10.1130/2016.2522(11) .

Murphy, J.G., Foster, D.A., Kalakay, T.J., John, B.E., and Hamilton, M., 2002, U-Pb zircon geochronology of the eastern Pioneer igneous complex, SW Montana: Magmatism in the foreland of the Cordilleran fold and thrust belt: Northwest Geology, v. 31, p. 1–11.

Mutch, T.A., and McGill, G.E., 1962, Deformation In Host Rocks Adjacent To An Epizonal Pluton (The Royal Stock, Montana): Geological Society of America Bulletin, v. 73, p. 1541, doi:10.1130/0016-7606(1962)73[1541:dihrat]2.0.co;2.

Naibert, T.J., Geissman, J.W., and Heizler, M.T., 2010, Magnetic fabric, paleomagnetic, and 40Ar/39Ar geochronologic data bearing on the emplacement of the Late Cretaceous Philipsburg Batholith, SW Montana fold-and-thrust belt: Lithosphere, v. 2, p. 303–327, doi:10.1130/l83.1.

O’Neill, J.M., Lonn, J.D., Lageson, D.R., and Kunk, M.J., 2004, Early Tertiary Anaconda Metamorphic Core Complex: Canadian Journal of Earth Sciences, v. 41, p. 63–72. doi:10.1139/E03-086

Pardee, J.T., 1951, Gold placer deposits of the Pioneer district, Montana, U.S. Geological Survey Bulletin 978-C, p. 69-99.

Paterson, S.R., Okaya, D., Memeti, V., Economos, R., and Miller, R.B., 2011, Magma addition and flux calculations of incrementally constructed magma chambers in continental margin arcs: Combined field, geochronologic, and thermal modeling studies: Geosphere, v. 7, p. 1439–1468, doi:10.1130/ges00696.1.

Portner, R.A., Hendrix, M.S., Stalker, J.C., Miggins, D.P., and Sheriff, S.D., 2011, Sedimentary response to orogenic exhumation in the northern Rocky Mountain Basin and Range province, Flint Creek basin, west-central Montana: Canadian Journal of Earth Sciences, v. 48, p. 1131–1154, doi:10.1139/e10-107.

Pullen, A., Ibáñez-Mejía, M., Gehrels, G.E., Ibáñez-Mejía, J.C., and Pecha, M., 2014, What happens when n= 1000? Creating large-n geochronological datasets with LA-

ICP-MS for geologic investigations: J. Anal. At. Spectrom., v. 29, p. 971–980, doi:10.1039/c4ja00024b.

Reid, L., and Frostick, L.E., 1985, Beach orientation, bar morphology and the concentration of metalliferous placer deposits: a case study, Lake Turkana, N Kenya: Journal of the Geological Society, v. 142, p. 837–848, doi:10.1144/gsjgs.142.5.0837.

Ross, G.M., and Villeneuve, M., 2003, Provenance of the Mesoproterozoic (1.45 Ga) Belt basin (western North America): Another piece in the pre-Rodinia paleogeographic puzzle: Geological Society of America Bulletin, v. 115, p. 1191–1217, doi:10.1130/B25209.1.

Ruiz J, Valencia VA, Chesley JT, Kirk J, Gehrels G, Frimmel H, 2006, The source of gold for the Witswatersrand from Re-Os and U-Pb detrital zircon geochronology. *Geochim. Cosmochim Acta v.* 70, A543, doi:10.1016/jgca.2006.06.1002.

Saylor, J.E., Sundell, K.E., and Sharman, G.R., 2019, Characterizing sediment sources by non-negative matrix factorization of detrital geochronological data: Earth and Planetary Science Letters, v. 512, p. 46–58, doi:10.1016/j.epsl.2019.01.044.

Schwartz, T.M., and Graham, S.A., 2017, Depositional history and provenance of Paleogene strata in the Sage Creek basin, southwestern Montana: Geosphere, v. 13, no. 4, p. 1285–1309, doi:10.1130/GES01450.1.

Sharman, G.R., Sharman, J.P., Sylvester, Z., 2018, detritalPy: A Python-based toolset for visualizing and analysing detrital geo-thermochronologic data. *Depositional Rec*. v. 4, p. 202– 215, doi:10.1002/dep2.45.

Sircombe, K.N., 1999, Tracing provenance through the isotope ages of littoral and sedimentary detrital zircon, eastern Australia: Sedimentary Geology, v. 124, p. 47–67, doi:10.1016/s0037-0738(98)00120-1.

Stroup, C.N., Link, P.K., Janecke, S.U., Fanning, C.M., Yaxley, G., and Beranek, L.P., 2008, Eocene to Oligocene provenance and drainage in extensional basins of southwest Montana and east central Idaho: Evidence from detrital zircon populations in the Renova Formation and equivalent strata. In Ores and orogenesis: Circum-Pacific tectonics, geologic evolution, and ore deposits. Edited by J.E. Spencer and S.R. Titley. Arizona Geological Society Digest, 22, pp. 529–546.

Sundell, K. E., and Saylor J. E., 2017, Unmixing detrital geochronology age distributions, Geochem. Geophys. Geosyst., v. 18, p. 1-15, doi:10.1002/2016GC006774.

Tilling, R.I., 1974, Composition and time relations of plutonic and associated volcanic rocks, Boulder batholith region, Montana: Geological Society of America Bulletin, v. 85, p. 1925-1930, doi:10.1130/0016-7606(1974)85<1925:CATROP>2.0.CO;2.

Vervoort J., 2015, Lu-Hf Dating: The Lu-Hf Isotope System. In: Jack Rink W., Thompson J.W. (eds) Encyclopedia of Scientific Dating Methods. Encyclopedia of Earth Sciences Series. Springer, Dordrecht.

Wooden, J.L., Mazdab, F.K., Mueller, P.A., Aleinikoff, J.N., Lund, K., Wiegand, B., Kita, N., and Walley, J.W., 2008, Geochemical and isotopic evidence for the origin of the Boulder batholith, Montana: Geochimica et Cosmochimica Acta, v. 72, p. A1034.

Yeend, W. E., and Shawe, D. R., 1989, Gold in placer deposits: U.S. Geol. Survey Bull. 1857-C, p. G1-G13.

Zartman, R.E., Dyman, T.S., Tysdal, R.G., and Pearson, R.C., 1995, U-Pb ages of volcanogenic zircon from porcellanite beds in the Vaughn Member of the Mid-Cretaceous Blackleaf Formation, southwest Montana: Shorter Contributions to the Stratigraphy and Geochronology of Upper Cretaceous Rocks in the Western Interior of the United States, U.S. Geological Survey Bulletin 2113-B, p. B1–B16.

Zeh, A., and Gerdes, A., 2012, U–Pb and Hf isotope record of detrital zircons from gold-bearing sediments of the Pietersburg Greenstone Belt (South Africa)—Is there a common provenance with the Witwatersrand Basin?, Precambrian Research, v. 204-205, p. 46–56, doi:10.1016/j.precamres.2012.02.013.

Zen, E., 1996, Plutons in the eastern part of the Pioneer batholith: Field relations and petrographic descriptions: U.S. Geological Survey Open-File Report 96-97, 98 p.

# CHAPTER THREE

# FARALLON SLAB-REMOVAL AS A DRIVING FORCE OF METAMORPHIC CORE COMPLEX FORMATION IN THE WESTERN USA: DETAILS FROM THE ANACONDA METAMORPHIC CORE COMPLEX OF WESTERN MONTANA

## Contribution of Authors and Co-Authors

Manuscript in Chapter 3

Author: Caden J. Howlett

Contributions: Conceived the study, performed fieldwork and analyses, interpreted results, created figures, and wrote the manuscript.

Co-Author: Aislin N. Reynolds

Contributions: Performed fieldwork and analyses, interpreted results, contributed to writing manuscript.

Co-Author: Andrew K. Laskowski

Contributions: Conceived the study, performed fieldwork and analyses, discussed implications, and edited earlier manuscripts.

Manuscript Information Page

Caden J. Howlett, Aislin N. Reynolds, Andrew K. Laskowski

*Tectonics*

Status of Manuscript:
_**X**_ Prepared for submission to a peer-reviewed journal
____ Officially submitted to a peer-review journal
____ Accepted by a peer-reviewed journal
____ Published in a peer-reviewed journal

**Abstract**

Metamorphic core complexes (MCCs) are a product of extensional tectonics, but the driving force behind their exhumation is still debated. Early researchers suggested that the formation of MCCs in the western USA was due to gravitational collapse of Cordilleran crust that had been thickened through thrust faulting and addition of arc magmas to the orogenic wedge. However, the instability of overthickened crust alone cannot explain the diachronous formation of core complexes along strike, as there was relatively uniform thickening during development of the Cordillera. For this reason, there is growing interest in what role sublithospheric processes (such as subducted slab rollback or slab detachment) play in the initiation and evolution of MCC exhumation. We investigate the role of such processes by determining the relationship between igneous activity and extension in the Anaconda metamorphic core complex of western Montana. Geologic mapping, zircon U-Pb geochronology, zircon (U-Th)/He thermochronology, and Lu-Hf isotopic analysis reveal that the AMCC is an example of a core complex that was primed for large-magnitude extension through crustal thickening and voluminous magmatism. We suggest that buckling of the Farallon flat slab and the onset of the ignimbrite flareup in western Montana was responsible for the initiation of AMCC extension. Furthermore, we compile MCC cooling ages and ages of ignimbrite flareup related rocks across the western USA to suggest that removal of the Farallon Plate was a primary driver of Cordilleran core complex formation. Our results are consistent with the interpretation that slab removal resulted in asthenospheric mantle heating of the

hydrated continental lithosphere, migration of magmatic activity, elevated geotherms, and development of MCCs in the upper plate.

**Plain Language Summary**

Horizontal extension of the Earth's crust can lead to topographic uplift and uncover rocks from depths of 10-30 km (the middle crust). The resulting geologic structure, consisting of ductilely deformed rocks underlying a low-angle normal fault, is known as a metamorphic core complex. These structures are important because the rocks they expose record thermomechanical properties of crust that would be otherwise unreachable. Despite their importance, the mechanisms that cause core complexes to form are not well understood. In this study, we use field and radiometric dating techniques to determine the role that magmatism (intrusion of molten rock into the crust) served in the evolution of the Anaconda metamorphic core complex in western Montana. We also compile data from the western USA that suggests the removal of a previously subducted tectonic plate from beneath North America caused core complexes to form.

**1 Introduction**

As domal geologic structures that result from rapid exhumation of the mid-to-low crust, metamorphic core complexes (MCCs) provide illuminating windows into the thermomechanical properties of Earth's lithosphere (e.g. Crittenden et al., 1980; Whitney et al., 2013; Platt et al., 2015). First described in the western USA, MCCs consist of a ductilely deformed metamorphic-plutonic footwall separated from brittlely deformed hanging wall by a low-angle normal fault (detachment fault) (Coney, 1980; Wernicke, 1981; Coney and Harms, 1984). Despite their widespread occurrence and tectonic

significance, the origin of core complexes, specifically the mechanisms by which the footwall is exhumed from mid-crustal depths, remains controversial (e.g. Konstantinou et al., 2013). The spatial and temporal overlap of magmatic activity with MCC exhumation has led many researchers to consider the role of magmatism in the genesis of MCCs (e.g. Armstrong and Ward, 1991; Wernicke et al. 1992; Lister and Baldwin, 1993; Foster et al., 2001).

A comparison of metamorphic core complexes in the North American Cordillera indicates variability in the influence that magmatism plays on the initiation of exhumation (e.g. Armstrong, 1982; Whitney et al., 2013; Stevens et al. 2016). It has been established that the presence of melt and resulting decrease in crustal strength and viscosity can serve to facilitate large-magnitude extension and core complex exhumation during the collapse of an orogenic system (Armstrong & Ward, 1991; Stevens et al., 2016; and many others). However, studies of various core complexes in the North American Cordillera expose differences in the volume and timing of magmatism relative to the onset and duration of extension (Whitney et al., 2013). For example, main-phase plutonism and dike crystallization in the footwall of the Priest River and Clearwater Core Complexes occurred during exhumation (Stevens et al., 2016; Gaschnig et al., 2011), while plutonism and dike emplacement in the Bitterroot Core Complex of western Montana appear to largely predate the onset of extension (Foster et al., 2001). These examples outline two hypothetical end-member hypotheses that can be tested: either crustal extension facilitates magmatism or magmatism serves as a driving force of exhumation.

In this contribution, we determine the relationship between magmatism and extension in the Anaconda metamorphic core complex (AMCC) of western Montana through geologic mapping, zircon U-Pb geochronology, zircon (U-Th)/He thermochronology, and Lu-Hf isotopic analysis. U-Pb zircon ages from major plutons in the AMCC footwall, representing crystallization age, are compared to exhumation-related (U-Th)/He cooling ages, placing constraints on the relative timing of each. Hf-isotope signatures enable determination of whether melts were derived from crustal or mantle sources, which in turn gives insight into the sublithospheric processes that may be partially responsible for the exhumation of the AMCC footwall. Located within the Idaho-Montana segment of the Cordilleran Magmatic Arc, the AMCC may be a representative example of a core complex whose development was driven by magmatism that created a hot, weak, and over-thickened crust. Our results suggest that Cretaceous-Paleocene magmatism added sufficient material to the Cordilleran hinterland for the orogen to become gravitationally unstable (e.g. Constenius, 1996, 2003), and that the onset and southward sweep of the ignimbrite flare-up initiated core complex formation. Along with integrating our findings into a generalized tectonic model that explains the relationship between pluton emplacement and exhumation of the AMCC footwall, we compare our results with those from other Cordilleran core complexes, giving broader insight into the role that magmatic activity and sublithospheric processes play in the development of MCCs in the North American Cordillera (NAC).

Several orogen-scale dynamic models have been proposed for MCC formation in the NAC, including: (1) a change in plate motions, (2) dynamic processes of the

downgoing slab (e.g. slab rollback), and (3) late or post-orogenic collapse due to overthickened continental crust (e.g. Whitney et al., 2013). In the NAC, MCCs form a N-S trending belt that traces a pre-extensional lithospheric welt, where crustal thicknesses and gravitational potential energy would have been at their greatest prior to exhumation (Figure 3.1; Coney and Harms, 1984). This has led some researchers to conclude that

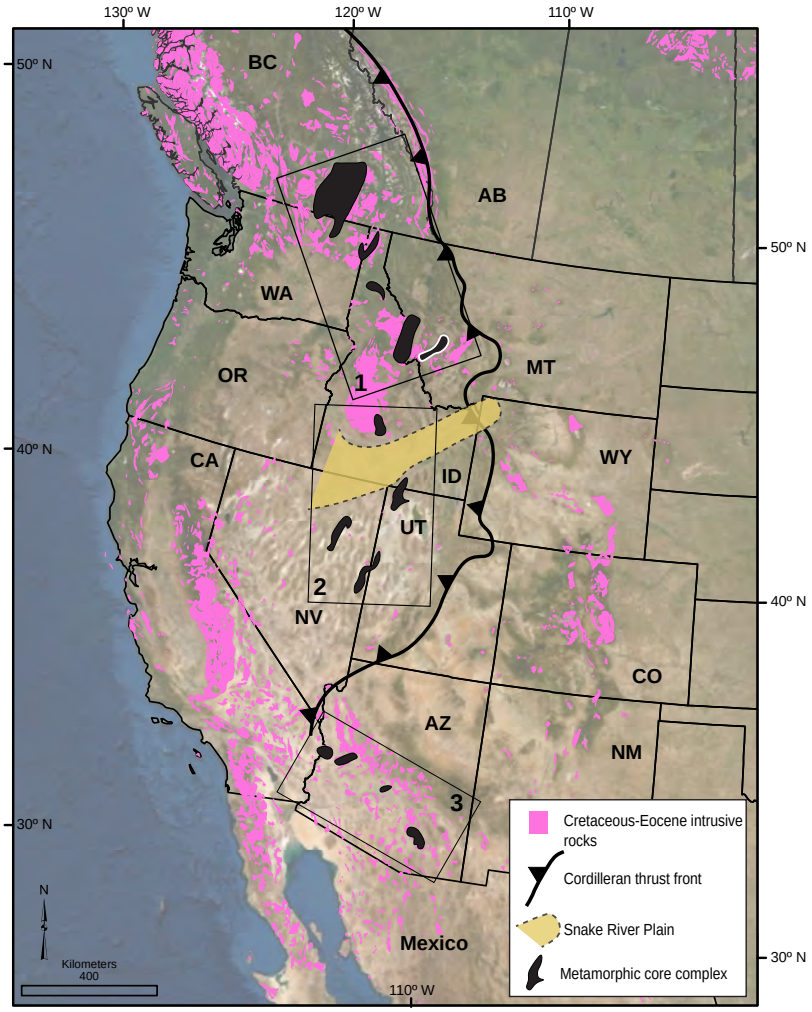


Figure 3.1. Tectonic overview map showing the distribution of major metamorphic core complexes and the aerial extent of Cretaceous-Cenozoic intrusive igneous rocks in the western USA (geology sourced from USGS National Map). MCC outlined in white represents Anaconda metamorphic core complex (AMCC). Black rectangles 1, 2, and 3 represent the northern, central, and southern MCC "belts" of the NA Cordillera, respectively. Basemap is satellite imagery from Esri/NOAA.

core complex formation was primarily driven by post-orogenic gravitational collapse (e.g. Coney and Harms, 1984; Wernicke et al. 1987). However, the instability of overthickened crust alone cannot explain the diachronous formation of core complexes (older in north, younger in south), as there was relatively uniform thickening during development of the Cordillera (Elison, 1991; Liu, 2001). For this reason, there is growing interest surrounding what role sub-lithospheric processes played in the formation of core complexes (e.g. Wernicke et al., 1992; Konstantinou et al., 2013; Stevens et al., 2016; Cassel et al., 2018).

A comparison across the three different core complex belts of the NAC (Figure 3.1) reveals that despite the localized variability in footwall plutonism across individual core complexes, there appears to be a strong spatial and temporal overlap between their formation and the transgressive migration of calc-alkaline magmatism known as the ignimbrite flare up (Armstrong and Ward, 1991; Konstantinou et al., 2013). The second part of this study, consisting of a synthesis of existing geo- and thermochronological data, combined with the new field and isotopic data from the AMCC, enables us to test the hypothesis that the MCCs of the NAC were triggered primarily by removal of the subducted Farallon plate by slab rollback and/or slab buckling. Our results are consistent with the interpretation that the progressive removal of the Farallon plate from beneath the NA Cordillera allowed for asthenospheric mantle heating of the hydrated continental lithosphere, ultimately resulting in the migration of magmatism, elevation of geotherms, and development of MCCs (e.g. Humphreys, 2009; Konstantinou et al., 2013; Cassel et al., 2018).

## 2 Regional Geologic Setting

Cordilleran-style orogenic belts and accompanying magmatic arcs form as a response to subduction of oceanic lithosphere beneath a continent (e.g. Dewey and Bird, 1970; Coney and Reynolds, 1977). The western USA developed into a Cordilleran-style margin in the Late Jurassic (~155 Ma; Hamilton, 1969; DeCelles et al., 2004) and over a span of ~100 My, contractile deformation and magmatism migrated inboard over 1,000 km from the modern trench (Coney and Reynolds, 1977). Low-angle and far-traveled subduction of the Farallon plate led to the development of a retroarc fold-thrust belt far from the trench, with active arc magmatism and consequent crustal thickening well into the craton (Dewey and Bird, 1970; Bird, 1988; DeCelles and Graham, 2015; Carrapa et al., 2019).

North of the Snake River Plain (SRP) in northeastern Idaho and western Montana, Late Cretaceous thrust faulting was accompanied by the voluminous magmatism of the Idaho and Boulder Batholiths (e.g. Foster et al., 2001) (Figure 3.2). Large-scale core complex related extension began immediately following the end of thrusting in this region at ~55 Ma (Constenius, 1996; Sears and Hendrix, 2004) and was contemporaneous with widespread explosive volcanism of the Challis–Absaroka–Colville–Kamloops–Bitterroot–Lowland Creek loop (Feeley, 2003; Foster et al., 2010). Stretching from the northwestern USA into central British Columbia, this belt of calc-alkaline and alkaline volcanic rocks broadly overlaps in space and time with exhumation of core complexes in the upper plate (Armstrong and Ward, 1991). Voluminous plutons that are present in the

lower plates of all northern belt MCCs overlap temporally with these volcanics as well (Grice, 2006; Foster et al. 2010).

In the Basin and Range Province south of the SNP, the period following regional folding and thrust faulting (Cretaceous-earliest Cenozoic; DeCelles, 2004) was dominated by the north to south sweep of ignimbrite flareup related magmatism (Lipman et al., 1971; Best and Christiansen, 1991; Best et al., 2016). Further to the south, in northern Mexico and across Arizona, similar magmatic activity occurred but migrated from SE to NW rather than N to S. Both fronts of magmatism met in southernmost Nevada at ~20 Ma (Humphreys, 1995; Christensen et al., 1992). Like the region north of the SRP, widespread volcanism in both of these regions was accompanied by large magnitude extension and core complex formation (Coney and Reynolds, 1977; Armstrong and Ward, 1991).

**3 The Anaconda Metamorphic Core Complex**

The Anaconda metamorphic core complex (AMCC) was one of the latest discovered core complexes in the western United States (O'Neill et al., 2004; Foster et al., 2010), and it represents one of nine MCCs north of the Snake River Plain that exhumed mid- to lower-crustal rock beginning in the Eocene (e.g. Coney and Harms, 1984; Whitney et al., 2013). The AMCC is located within the Idaho-Montana segment of the Cordilleran magmatic arc, along the eastern edge of the Cordilleran hinterland (O'Neill et al., 2004; Foster et al., 2010) (Figure 3.2). The voluminous Late Cretaceous Boulder and Idaho batholiths exist to the east and west of the AMCC, respectively (Lageson et al., 2001). These three major features of southwest Montana exist within the

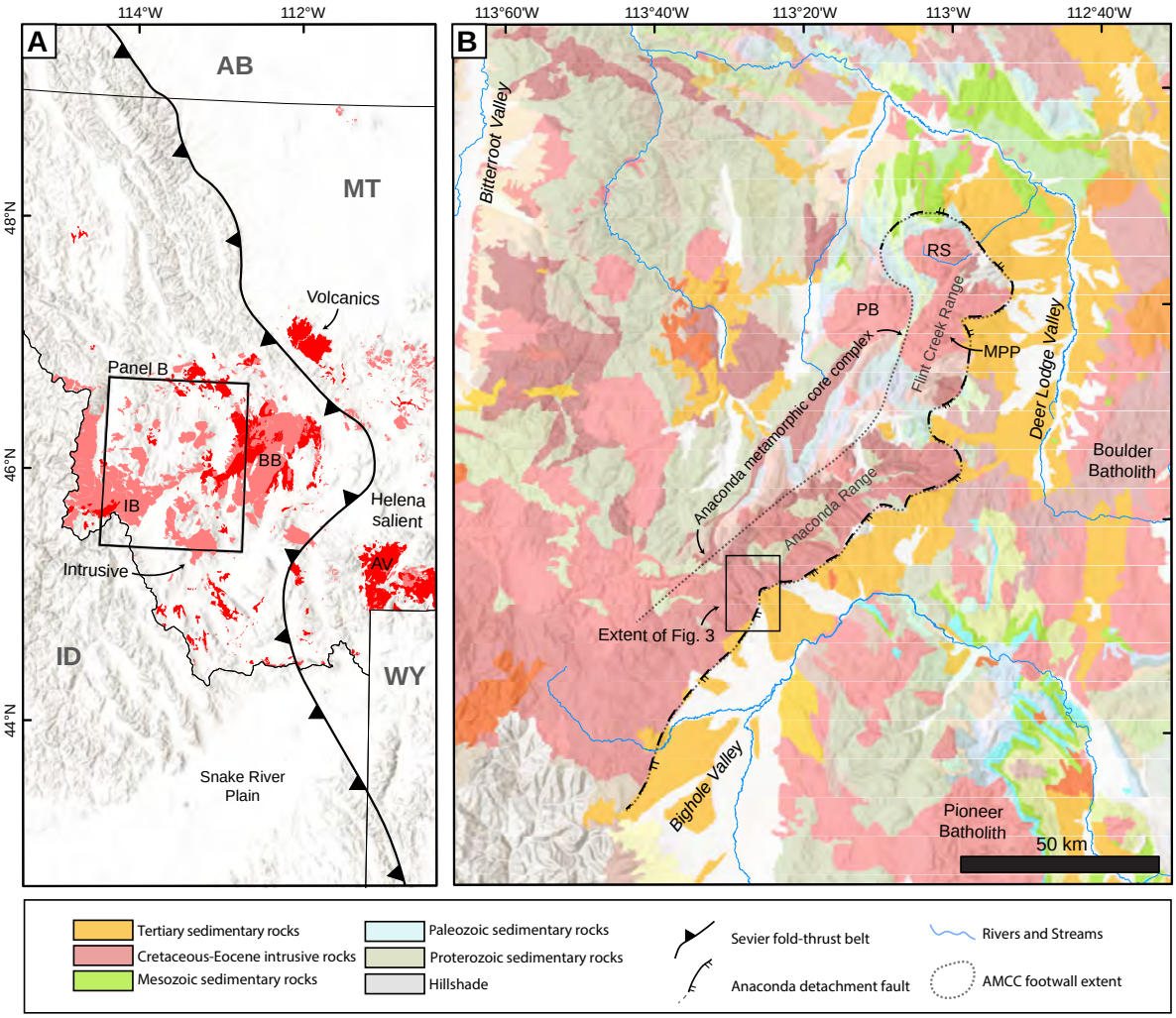


Figure 3.2. Tectonic overview maps showing (a) the AMCC in the context of the western Montana segment of the North American Cordillera, displaying the distribution of Cretaceous-Cenozoic plutonic and volcanic rocks in relation to the Bitterroot and Anaconda metamorphic core complexes. IB =Idaho Batholith; BB = Boulder Batholith; AV = Absaroka Volcanics. Map (b) displays a simplified geologic map of the Anaconda MCC, showing undivided Proterozoic-Tertiary sedimentary and metasedimentary rocks and major plutons. RS = Royal Stock; MPP = Mount Powell Pluton; PB = Philipsburg Batholith. Bedrock geology data and hill shade basemap sourced from the Montana Bureau of Mining and Geology and Esri Online/NOAA, respectively.

western and central parts of the Helena Salient, a major eastward-convex salient that marks the easternmost position of the Sevier fold-thrust belt (Lageson et al., 2001; DeCelles, 2004).

The AMCC can be subdivided into three domains that are characteristic of a Cordilleran-style metamorphic core complex: (1) a hanging wall consisting of largely unconsolidated synextensional sedimentary units, (2) a metamorphic-plutonic and metasedimentary footwall, and (3) a low-angle detachment fault along the eastern edge of the Anaconda Range that separates the hanging wall and footwall (Wallace et al., 1992; O'Neill et al., 2004; Foster et al., 2010).

The AMCC hanging wall consists of a series of fault-bound basins which contain Cenozoic-Quaternary clastic, volcaniclastic, and volcanic strata (Grice et al., 2006; Foster et al., 2010). Progressively less tilting of hanging wall strata moving up section suggest that it was deposited during active extension along the Anaconda detachment fault (Elliott and Lonn, in review; Grice et al., 2006).

The footwall of the AMCC, extending from the Flint Creek Range in the north to the Anaconda Range in the south (Figure 3.2), is made up of Late Cretaceous to Eocene granitic plutons and dikes that intruded into the metamorphosed Mesoproterozoic Belt Supergroup and Middle Cambrian to Cretaceous shelf-platform strata (Emmons and Calkins, 1913; Desmarais, 1983; Wallace et al., 1992; Lonn et al., 2003; Grice, 2006; Foster et al., 2010). The Flint Creek Range is cored primarily by Late Cretaceous plutons, including the Mount Powell batholith and Royal Stock (O'Neill et al., 2004). The Anaconda Range footwall contains volumetrically smaller Late Cretaceous plutons and a large variety of early to middle Eocene dikes and plutons (Wallace et al., 1992). The central Anaconda Range is dominated by the Eocene two-mica Pintler Granite, which has a consistent SE-dipping foliation and lineation direction (Figure 3.3a, 3.3b).

Two-mica granites, as well as a variety of deformed and undeformed dikes, intrude predominately mixed metasedimentary rocks of a Belt Supergroup protolith (Wallace et al., 1992).

Separating the metamorphic-crystalline footwall from the unconsolidated sedimentary rocks of the hanging wall is the Anaconda detachment fault (ADF). Along the Deer Lodge Valley, the ADF trends roughly N-S and dips gently (10-30°) to the east (Grice, 2006). In the south-central Anaconda Range, the detachment dips shallowly southeast (~12-15°) and has been recognized as a complex zone of anastomosing strain and possibly expressed as multiple detachments in certain stretches along strike (Elliott and Lonn, in review).

## 4 Methods

### 4.1 Field methods

We report data collected during field work in 2018 from the south-central AMCC, ~30 km north of the town of Wisdom, Montana, USA. Field work was conducted in all three structural domains of the AMCC (hanging wall, footwall, and along the Anaconda detachment fault (e.g. Elliott and Lonn, in review). Mapping was conducted at ~1:24,000 scale across the study area (Figure 3.3) atop paper 7.5' topographic basemaps generated by the United States Geological Survey. Basemaps were used for drafting geologic maps while in the field and all structural measurements and geologic mapping were digitized in Esri's ArcMap.

**4.2 Igneous zircon U-Pb geochronology**

Two samples of a two-mica granite were collected in the central field area from the AMCC footwall (45.860°N, 113.445°W). A strongly foliated granodiorite dike and dacite dike cross-cutting the Pintler Granite were obtained from (45.935°N, 113.477°W) and (45.824°N, 113.495°W), respectively. A fifth sample (071918CH7) was obtained from ~130 meters north of the northern extent of the mapped area (Figure 3.3; 43.939°N, 113.438°W).

Following collection, samples were prepared and analyzed using consistent protocols at the Arizona Laserchron Center (http://www.laserchron.org) (Gehrels et al., 2008). Zircons were separated from ~1.5 L bulk samples by pulverization in a jaw crusher, sieving, Frantz magnetic separation, heavy-liquid density separation, and hand-picking at GeoSepServices in Moscow, ID. Separated zircons were mounted (~45 zircons/sample) alongside the SLmix, R33, and FC zircon standards on a 1-inch epoxy ring mount in the sample preparation and mounting laboratory at Montana State University. Zircons were then polished to a depth of ~30 µm and imaged using a backscattered-electron detector (BSE) with a cathodoluminescence attachment at Montana Tech CAMP Laboratory for targeting specific age domains during analysis. Additionally, backscattered electron (BSE) images of mounts, which serve as generalized maps for isotopic analysis, were obtained at the Imaging and Chemical Analysis Laboratory (ICAL) at Montana State University.

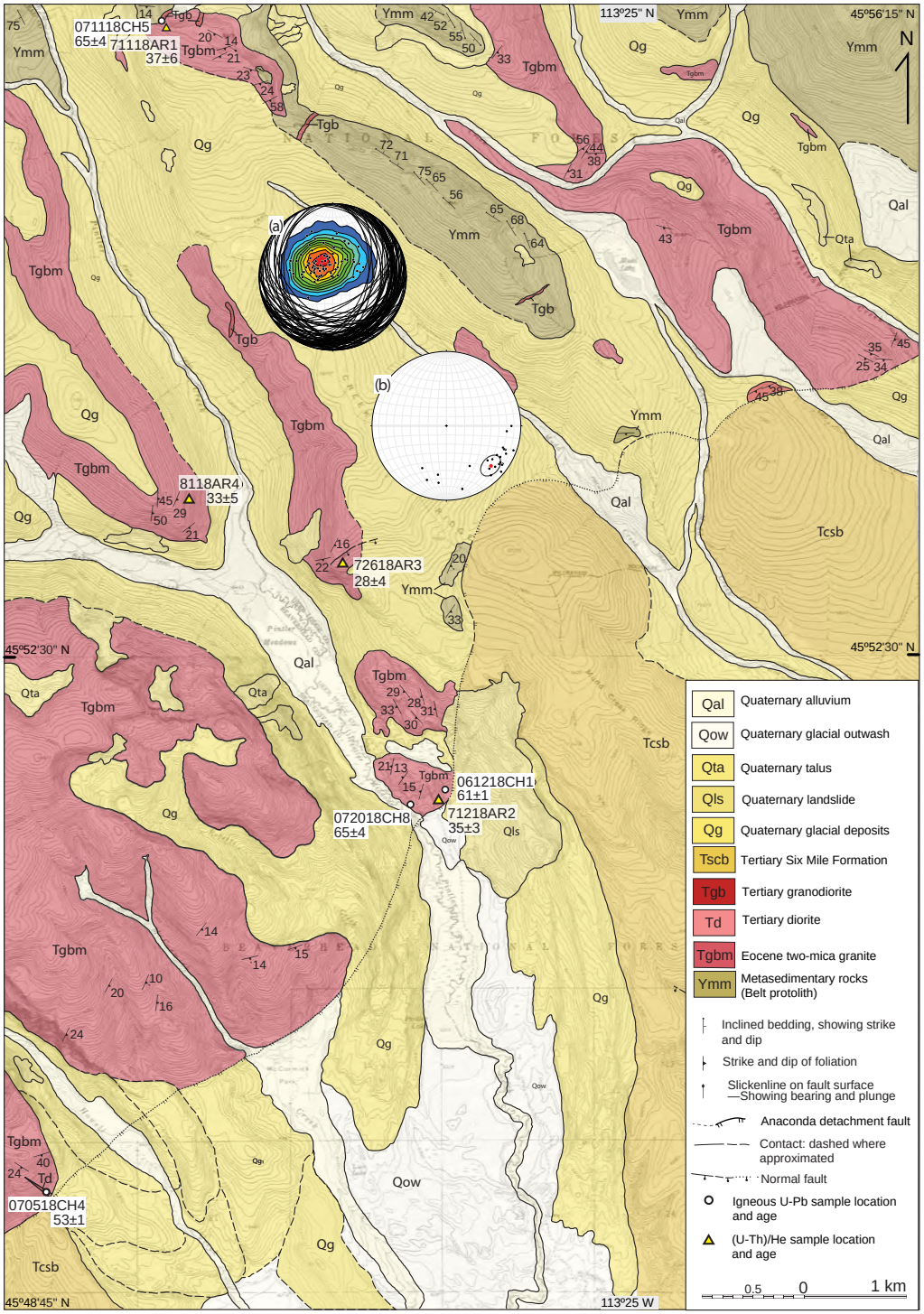


Figure 3.3. 1:24,000 scale geologic map of field area in south-central AMCC. Overlapping structural measurements of similar orientation were averaged for clarity. Lambert equal area stereonets present. (a) foliation planes and poles to foliation and (b) slip lineations from the AMCC footwall. Average zircon (U-Th)/He and U-Pb ages and their as¬sociated uncertainties were rounded to the nearest whole number.

Zircon U-Pb ages were obtained for ~25 zircon grains per sample using a Photon Machines Analyte G2 Excimer laser attached to a Thermo Element2 HR single-collector ICP-MS at the University of Arizona Laserchron Center. Analysis and data reduction followed the detailed methods in Gehrels and Pecha (2014).

**4.3 Igneous zircon Lu-Hf isotopic analysis**

Following U-Pb isotopic analysis, Hf isotope measurements were made for select zircon grains from samples 061218CH1 (n=15) and 071118CH5 (n=19) using an identical laser ablation system attached to a Nu Plasma multicollector ICP-MS at the Arizona Laserchron Center. Measurements were made from the same sample spots as LA-ICPMS U-Pb analysis to ensure that Hf isotopic data were determined from the same domain as the corresponding U-Pb age. Zircon fragments of MT, FC, SL, 91500, TEM, PLES, and R33 were used for standard sample bracketing during Lu-Hf analyses.

**4.4 Low-temperature thermochronology**

Four samples of two-mica granite were collected from the footwall of the Anaconda detachment along a pseudo-vertical sample transect (Figure 3.3). Bulk samples were sent to GeoSepServices for crushing and mineral separation, and all four samples yielded sufficient quantities of zircon grains suitable for (U-Th)/He analyses. Conversely, samples yielded impure apatite separates dominated by small grains (<60 μm). Zircon grains were selected based on size, morphology, and clarity at the Montana State University Tectonic Sedimentology and Thermochronology (TeST) laboratory; euhedral grains of similar size with half widths >60μm were selected and measured. Twenty zircon grains and sixteen apatite grains were chosen for analysis. The selected grains were then

individually packed into 1mm Nb foil tubes to ensure even heating of the grain and prevent volitization of parent nuclides during Helium extraction. He extraction and measurement, as well as isotopic dissolution for U-Th-Sm content, were conducted following methods outlined in Reiners et al. (2004) at the University of Arizona Radiogenic Helium Dating Laboratory (ARHDL). Fish Canyon Tuff zircon standards of a known age were analyzed alongside unknowns.

Inverse thermal modeling of low-temperature thermochronology data was completed using the HeFTy modeling software (Ketcham, 2005). HeFTy is based on a Monte-Carlo algorithm that accounts for both diffusive loss and radiogenic ingrowth of He for individual grains as a function of their thermal history, allowing the user to test a range of time-temperature (t-T) histories that could potentially provide good fits to the data.

### 4.6 Western USA data compilation

#### 4.6.1 Thermochronologic constraints on core complex exhumation

Thermochronologic cooling-ages were extracted from the literature to constrain the relative timing of exhumation across different Cordilleran metamorphic core complexes. MCCs were separated into three broad belts (Northern, Central, and Southern) according to their latitude/geographical location (e.g. Whitney et al., 2013). Due to the large number of useful decay systems and geo- and thermochronometers that exist, the timing of exhumation (i.e. cooling) was not determined using the same technique for all MCCs in the western US.

Despite a recent increase in the number of researchers applying new thermochronology techniques to MCCs, gaps in the data still exist. In cases where cooling ages did not exist, estimates on the timing of exhumation were determined from earlier published work that combined fieldwork and U-Pb geochronology (e.g. Ruby-Humboldt, MacCready et al., 1997).

### 4.6.2 Cenozoic volcanics data compilation

Age and geochemical data were compiled from the North American Volcanic and Intrusive Rock Database (NAVDAT) database for Cenozoic volcanics associated with the North American ignimbrite flareup. In order to track the migration of magmatism and volcanism during the Cenozoic, the western U.S. was compartmentalized into six volcanic "regions" based on latitude (50-46N, 46-43N, 43-41N, 41-39N, 39-37N, 37-33N). In order to constrain search results to ignimbrite flareup related Cenozoic volcanism, an age range of 15-65.5 Ma and a rock type of felsic-intermediate volcanic were specified, similar to that compiled in Konstantinou et al. (2013). Felsic-intermediate rocks were identified based on rock type name specified in respective papers. Database search results containing sample location, age and geochemical data for each region were exported from NAVDAT and probability density plots were created using the Isoplot4.15 Excel Add-In (Ludwig et al., 2012). Identical steps were taken for compiling Cenozoic volcanics data for southern Arizona, but the geographical bounds were more tightly constrained (latitudinally and longitudinally) to more accurately access the magmatic sweep in this region. The geographic constraints for southern Arizona

were: (33-32N, 111-110W; 34-33N, 112-111W; 34.5-33.5N, 114-113W; 35-34N, 115-114W).

Sample locations (latitude/longitude) for each latitudinal (and in the case of Arizona, longitudinal) region and imported to Esri's ArcMap as X-Y coordinates. Locations were symbolized according to their region and maps were created using open source data from Esri's ArcGIS Online.

## 5 Results

### 5.1 Geologic mapping

The two-mica granite known as the Pintler Creek Batholith dominates the footwall in the map area (Figure 3.3; Figure 3.4). The batholith intrudes into predominately deformed metasedimentary rocks of the Belt Supergroup and has a

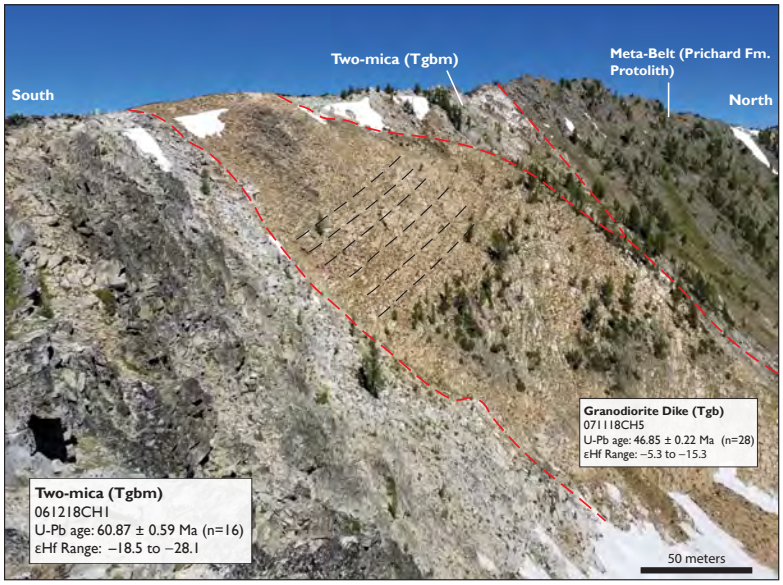


Figure 3.4. AMCC footwall exposing ~47 Ma granodiorite dike intruding between ~61 Ma two-mica granite and metasedimentary Belt rock. Dashed red lines are rock unit contacts and dashed black lines trace south-dipping foliation. The representative U-Pb ages and ranges of εHf values are included for each sample.

pervasive south-southeast dipping foliation (Figure 3.3a) with slip lineations that have a mean trend to the southeast (Figure 3.3b). The trend and plunge of slip lineations obtained from the granite suggest unroofing was directed to the southeast, with an average trend and plunge of 138°, 19 (Figure 3.3b). The Pintler Creek Batholith is crosscut by variably deformed dikes ranging in composition from dacite to granodiorite (Figure. 3.4).

Unlike many core complexes in the North American Cordillera, the AMCC footwall does not contain abundant mylonitic rocks or rocks that have undergone extensive migmatization. That said, the best exposure of proto-mylonitic rocks in the footwall of the Anaconda detachment is located in the central field area (adjacent to geochronology samples 061218CH1 and 072018CH8; Figure 3.3). This approximately one square kilometer region is host to anastomosing zones of high shear, two-mica granite, and gneiss.

The dominant structure is the Anaconda detachment fault (ADF), which trends approximately NE-SW across the central map area (Figure 3.3) and separates the crystalline footwall from the hanging wall. In many places, the ADF is concealed beneath Quaternary glacial and alluvial deposits. In places where the Anaconda detachment is covered by Quaternary sediments, there is usually an abrupt change from unconsolidated, well-rounded quartzite and granitic cobbles to the low-grade metamorphic (greenschist facies) and foliated rocks of the AMCC footwall.

Normal faults in the AMCC hanging wall are poorly exposed and are here inferred from topographic lineaments exposed by digital elevation models. Faults were

also identified by abrupt changes in float composition that can only be explained by rock unit juxtaposition.

## 5.2 Zircon U-Pb geochronology and Lu-Hf isotopic results

### *(061218CH1)*

Sample 061218CH1 is a fine- to medium-grained two-mica granite that is generally porphyritic. Many zircons display oscillatory zoning, with some zoning around distinct cores, suggesting igneous growth around inherited cores. Zircon U-Pb ages for 26 igneous rims range from 59.3 ± 0.8 to 67.0 ± 0.6 Ma, and ages for 6 cores range from 1662.5 ± 11.1 to 1799.2 ± 17.5 Ma. The weighted-mean age is 60.87 ± 0.59 Ma (n=14, MSWD=6.8) (Figure 3.5). Epsilon Hf values vary from −28.1 calculated at 61 Ma to –18.5 at 62 Ma (n =15) (Figure 3.6).

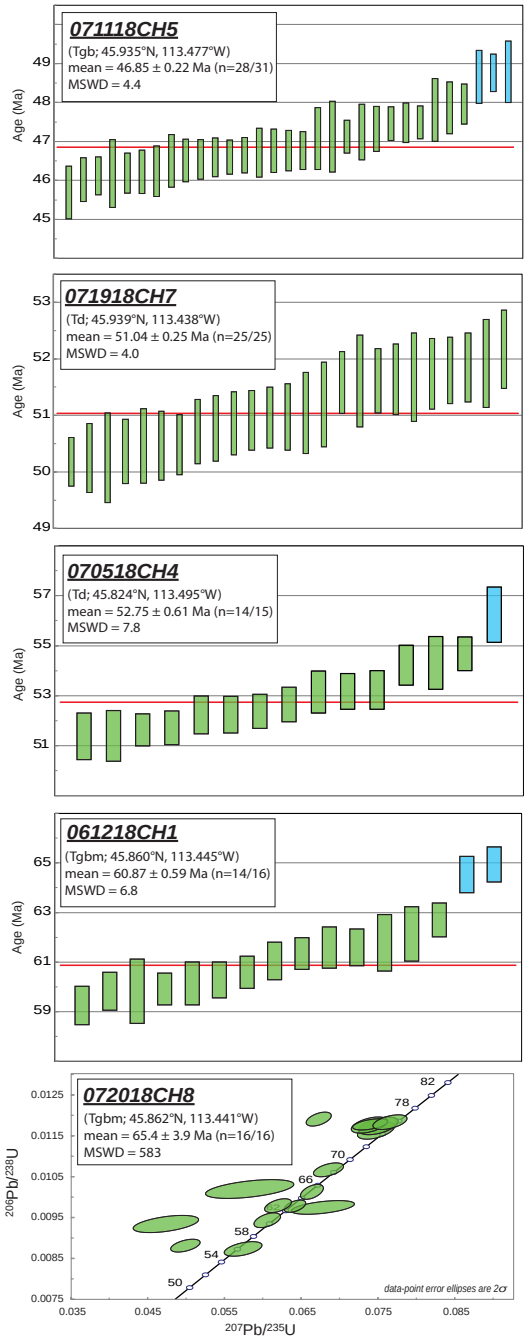


Figure 3.5. Igneous zircon U-Pb geochronology weighted mean plots from representative igneous rocks exposed in the AMCC footwall. Due to greater spread in U-Pb ages, sample 072018CH8 is displayed as a Wetherill concordia plot. Plots created using Isoplot4.15 Excel Add-in. Sample location shown and labeled on geologic map in Figure 3.3.

***(072018CH8)***

Sample 072018CH8 is the same rock type as 061218CH1, a porphyritic two-mica granite. Zircons extracted from the sample display oscillatory zoning, with some zoning around inherited cores. Ages for 17 zircon rims range from 56.1 ± 0.9 to 76.3 ± 0.9 Ma, and ages for 9 cores range from 1475.4 ± 17.7 to 2755.0 ± 10.9 Ma. The weighted-mean age of the 16 youngest rims is 65.4 ± 3.9 Ma, which are displayed on a Wetherill concordia plot due to large spread (Figure 3.5).

***(070518CH4)***

Sample 070518CH4 is from a dacite dike with large (>1 cm) plagioclase phenocrysts. The zircon yield from this sample was relatively low and small zircon size (50-60 μm) made any zircon zoning undiscernible. Zircon analyses provide U-Pb ages

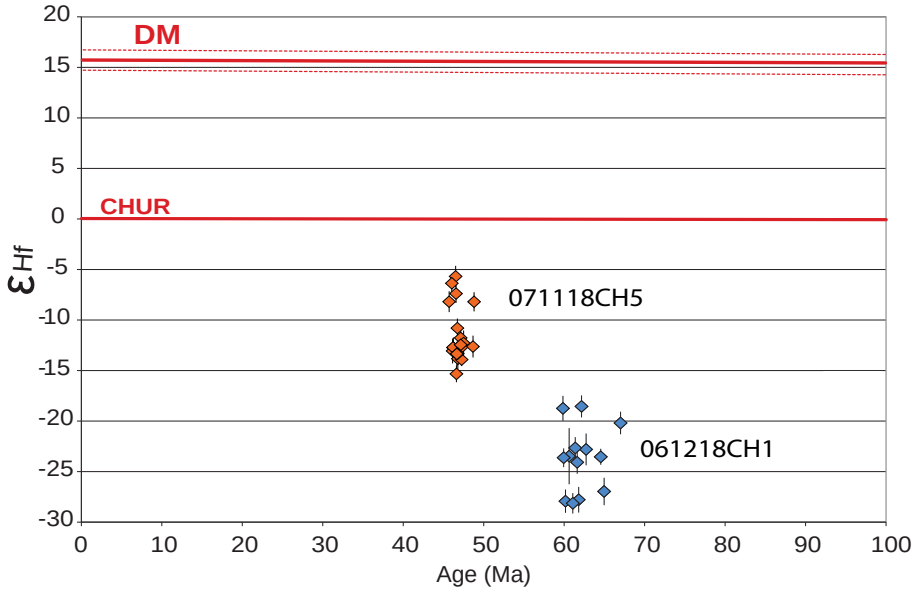


Figure 3.6. Epsilon plot displaying Lu-Hf results for 061218CH1 and 071118CH5. Both samples record negative epsilon values, suggesting moderately (CH5) to significantly (CH1) evolved melt derived from crustal sources. Red lines represent depleted mantle (DM) and chondritic uniform reservoir (CHUR) evolution lines.

that vary from 51.4 ± 0.9 to 56.3 ± 1.1 Ma (n=15). The weighted-mean age from 15 grains is 52.75 ± 0.61 Ma (MSWD=7.8) (Figure 3.5).

***(071118CH5)***

Sample 07110518 is a fine- to medium-grain granodiorite dike consisting of plagioclase, quartz, biotite, potassium feldspar. Quartz phenocrysts commonly are rounded. Zircons display simple igneous growth zoning and U-Pb ages range from 45.7 ± 0.7 to 48.8 ± 0.8 Ma (n=31). The weighted-mean age of 28 grains is 46.85 ± 0.22 Ma (MSWD=4.4) (Figure 3.5). Epsilon Hf values vary from –5.7 to -15.3 at 47 Ma (n=19) (Figure 3.6).

***(071918CH7)***

Sample 071918CH7 is a dacite dike with a composition identical to 070518CH4. Zircon grains display simple igneous growth zoning, with ages ranging from 50.2 ± 0.4 to 54.5 ± 0.8 Ma (n=29). The weighted-mean age of 25 grains is 51.04 ± 0.25 Ma (MSWD=4.0) (Figure 3.5).

**5.3 Zircon (U-Th)/He results**

Nineteen zircon grains were analyzed for (U-Th)/He from four two-mica granite samples collected from the footwall of the AMCC (detailed data can be found in Appendix C). A wide range of cooling ages is recorded for each sample, with individual zircon He ages range from 41.38 ± 0.56 Ma to 8.66 ± 0.12 Ma (Figure 3.7; Appendix C). Most grains yielded ages between 38 Ma and 28 Ma (Figure 3.7). Ages from sample 71118AR1 range from 41.38 ± 0.56 Ma to 31.55 ± 0.4 and ages from sample 71218AR2 range from 8.66 ± 0.12 Ma to 35.50 ± 0.51. Samples 72618AR3 and 8118AR4 show

cooling ages from 24.73 ± 0.33 to 29.74 ± 0.41 and 28.17 ± 0.39 to 38.36 ± 0.53, respectively (Figure 3.7).

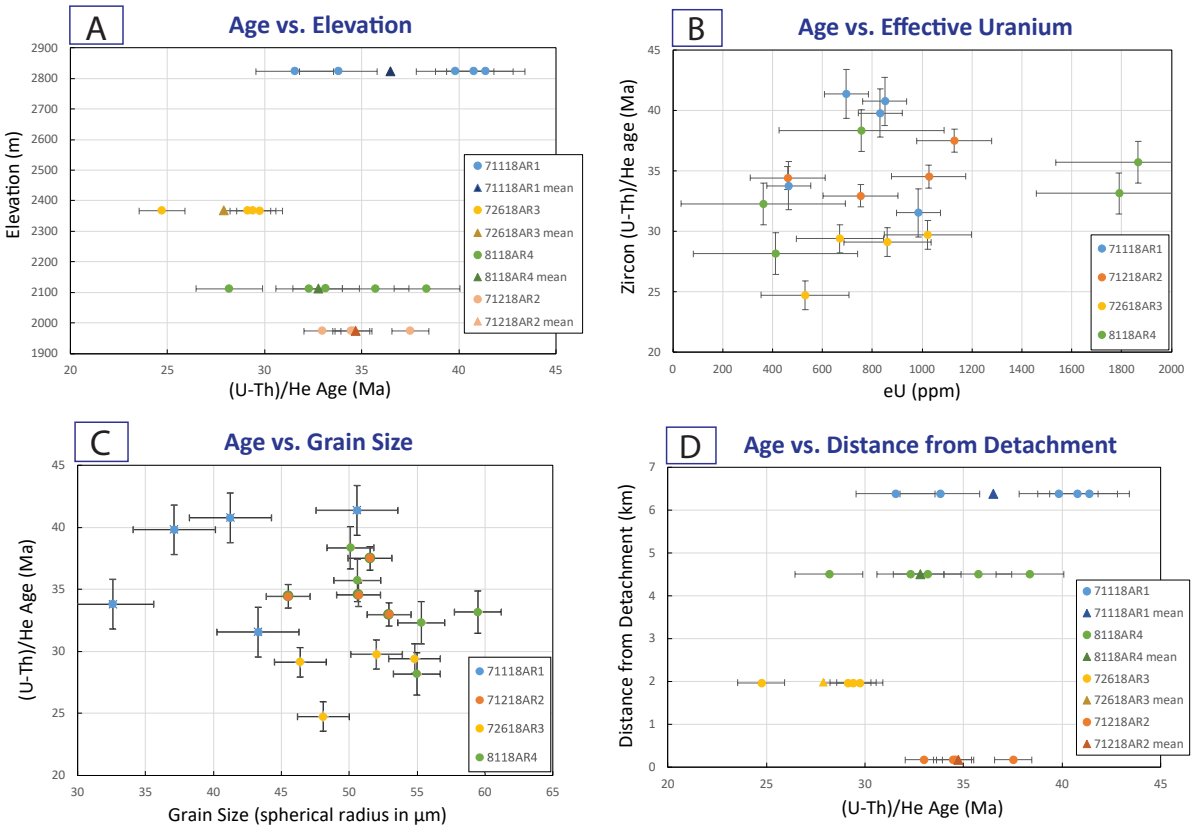


Figure 3.7. (a) Elevation versus zircon (U-Th)/He age, triangles are weighted means for each sample, plot shows anomalously young sample 72618AR3. (b) Zircon (U-Th)/He ages as a function of effective uranium (eU = 0.235Th × U). Slightly positive age-eU correlations are not interpreted to be strong enough evidence to cause the observed irregularity in ages. (c) Age versus grain size, showing no strong correlation. (d) Age as a function of sample distance from the Anaconda detachment. Sample ages show a clear trend of increasing cooling age with distance from the detachment, apart from the irregular sample nearest to the detachment which may indicate movement and exhumation along an older structure within the detachment zone.

### 5.3.1 HeFTy thermal modeling inputs and results

Inverse modeling of 8,000 paths for each sample was completed against t-T constraints defined by the zircon (U-Th)/He ages and zircon U-Pb crystallization ages from this study, and previously published apatite fission track and muscovite and biotite $^{40}Ar/^{39}Ar$ ages (Foster et al., 2010). Age inputs for each model were weighted means of the ages from each sample, including errors. The searchable t-T space for thermal history paths was defined by the following five input parameters, represented graphically in model runs as boxes through which the modeled t-T paths were forced:

a) Zircon U-Pb crystallization ages from two-mica granitic plutons from this study indicate that the sample was at temperatures >900 °C until 65 Ma and 60 Ma.
b) Muscovite (closure temperature 450-350 °C) and Biotite (closure temperature 380-330 °C) from two-mica granites recorded $^{40}Ar/^{39}Ar$ cooling ages between 53 Ma and 39 Ma, indicating that samples must have experienced rapid cooling through these temperatures by early to middle Eocene time (Foster et al. 2010).
c) Zircon (U-Th)/He ages from this study indicate that samples cooled between 190-170 °C from 42 Ma to 25 Ma. These constrains were enforced within the He model for each sample rather than as a t-T box.
d) Apatite fission track ages were less well constrained, yielding ages between 40 Ma and 20 Ma and indicating cooling through 110-60 °C (Foster et al. 2010).

The t-T paths resolved by the HeFTy thermal model for each sample are shown in Figure 3.8 as a series of good and acceptable fit paths, along with the single best fit (black) and weighted mean of good fit paths (blue). The first model that was run for each sample was

minimally restricted, with the only constraints being zircon U-Pb crystallization age, zircon (U-Th)/He data from the sample, and sample collection at the surface, allowing HeFTy to more freely produce thermal histories. The second model for each sample was restricted by all of the five constraints listed in the methods section, allowing for comparison of this study to results from Foster et al. (2010).

Under the less constrained model parameters, HeFTy produced a wide range of potential t-T paths, but all four samples generally show rapid cooling from ~60 Ma to ~30 Ma (Figure 3.8). The best fit line for sample 72618AR3 is an outlier, showing extremely rapid cooling at 60 Ma, followed by a long plateau between ~58 and ~10 Ma. The more heavily constrained models show rapid cooling between 60 Ma and ~50 Ma for samples 71118AR1 and 71218AR2, followed by an ~ 8 m.y. shallowing of slope. Both samples then exhibit rapid cooling starting at ~43 Ma. Sample 72618AR3 once again shows rapid cooling at 60 Ma, followed by a gradual slope until 25 Ma, at which point cooling slows dramatically. A similar trend is seen in the generated t-T paths for sample 81818AR4. Paths for all four samples show a flattening of slope between 30 and 25 Ma.

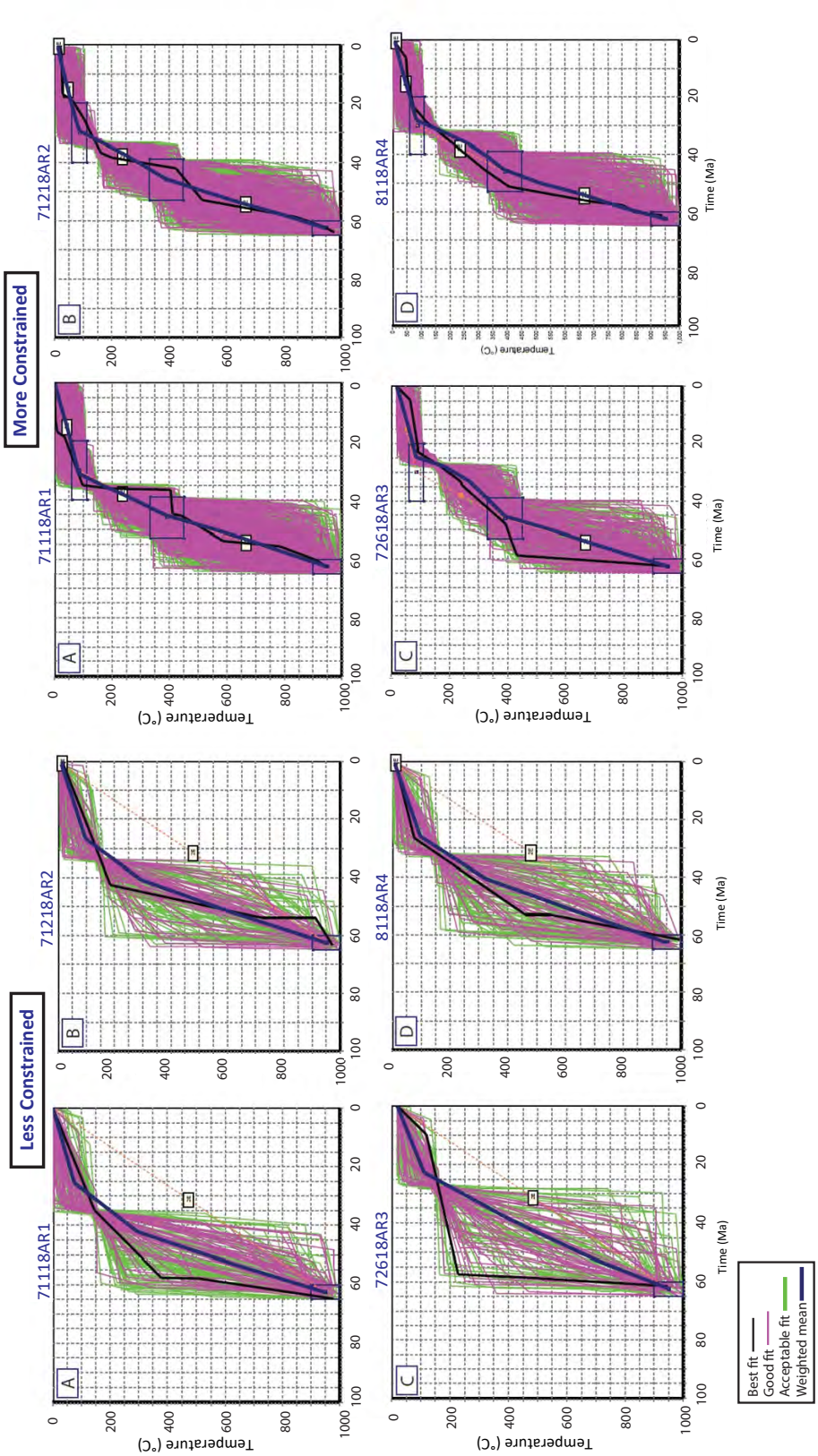


Figure 3.8. HeFTy model results for individual samples; left: minimal constraints (U-Pb crystallization ages, zircon He cooling ages, and surface temperature only) to allow as much freedom as possible for modeled t-T paths, and right: using five specific input constraints a) Zircon U-Pb crystallization ages indicate temperatures >900°C until 65-60 Ma. b) 40Ar/39Ar Muscovite (450-350°C) and Biotite (380-330°C) recorded cooling ages between 53-39 Ma. c) Zircon (U-Th)/He ages indicate cooling to 190-170°C from 42-25 Ma. d) Apatite fission track (110-60°C) yielded ages between 40-20 Ma. e) Samples were collected at the surface (20-0°C) at 0 Ma.

## 5.4 Western USA data compilation results

### 5.4.1 Metamorphic core complex cooling age compilation

The filtered and compiled cooling ages are displayed in Table 3.1 and the relative timing of MCC plutonism and exhumation for the three belts is shown in Figure 3.9.

Core complexes of the northern belt record an onset of extension in the Paleocene-Eocene, ranging from an ~60 Ma onset in the Shuswap complex of southern British Columbia (Vanderhaeghe et al., 2003) to ~53 Ma in the Anaconda metamorphic core complex of western Montana (Foster et al. 2010; Reynolds et al., 2019). Broadly speaking, exhumation of this belt of MCCs had slowed by Late Eocene-Early Oligocene (between 48 and 38 Ma). Apatite fission track data and zircon (U-Th)/He data from the Anaconda MCC suggest that extension may have lasted into the Mid-Late Oligocene (<27 Ma; Foster et al., 2010; Reynolds et al., 2019).

The central belt of MCCs experienced exhumation in the Mid-Late Eocene (Table 3.1; Figure 3.8). The Pioneer MCC of central Idaho represents the oldest of the central belt MCCs and was cooled between 50 and 46 Ma (Vogl et al., 2012). The Albion-Raft-River MCC and Ruby-Humboldt MCC both record several episodes of rapid extension but were mostly cooled from 41-20 Ma and 45-20 Ma, respectively (Lee et al., 2017; Snoke et al., 1988). Exhumation of the Snake Range MCC is constrained from ~37-22.5 Ma based on hornblende $^{40}Ar/^{39}Ar$ and U-Pb crystallization ages of cross-cutting footwall dikes (Lee et al., 2017).

Exhumation-related cooling of core complexes in the southern belt occurred in the Mid-Oligocene to Mid-Miocene (Table 3.1; Figure 3.9). The Catalina-Rincon, South

| MCCBelt | Core Complex | Cooling age(s) | References |
|---|---|---|---|
| Northern | Thor-Odin, Shuswap | 60-33 Ma ($^{40}Ar/^{39}Ar$ hbl, bio, sani) | Vanderhaeghe et al., 2003 |
| | Priest River | 58-48 Ma (U-Pb, $^{40}Ar/^{39}Ar$ bio, K-Ar bio) | Stevens et al., 2016; Doughty and Price, 1999 |
| | Clearwater | 58-38 Ma (U-Pb, $^{40}Ar/^{39}Ar$ mica) | Doughty et al. 2007 |
| | Bitterroot | 53-38 Ma (U-Pb, $^{40}Ar/^{39}Ar$ bio, ZFT) | Foster and Raza, 2002 |
| | Anaconda | 53-38 Ma, 27 Ma ($^{40}Ar/^{39}Ar$ bio, apatite FT), | Foster et al., 2010; unpublished data |
| Central | Pioneer | 50-46 Ma ($^{40}Ar/^{39}Ar$ bio) | Vogl et al., 2012 |
| | Albion/Raft-River | 41-20 Ma; 13.5-7 Ma (apatite fission track) | Lee et al., 2017; Konstantinou et al., 2013 |
| | Ruby-Humboldt | 45-20 ($^{40}Ar/^{39}Ar$ hbl); 29-20 (mylonitization) | Snoke and Miller, 1988; MacCready et al. 1997 |
| | Snake | 36-25 Ma ($^{40}Ar/^{39}Ar$ hbl); 37.8-22.5 Ma (U-Pb zircon) | Miller et al., 1988; Lee et al., 2017 |
| Southern | Catalina-Rincon | 28-22 Ma ($^{40}Ar/^{39}Ar$, AFT, ZFT); 25-20 Ma | Terrien, 2012; Reynolds et al, 1986 |
| | South Mountains | 21-17 Ma (AFT, K/Ar Hbl, $^{40}Ar/^{39}Ar$ bio) | Fitzgerald et al., 1993; Reynolds, 1986 |
| | Buckskin-Rawhide | 20-11 Ma (U-Th/He zircon + apatite, $^{40}Ar/^{39}Ar$ bio+sani) | Singleton et al., 2014 |
| | Whipple | 20.5-18.5 ($^{40}Ar/^{39}Ar$ sani, bio, hbl) | Gans and Gentry, 2016 |

Table 3.1. Timing of exhumation for MCCs in the North American cordillera.

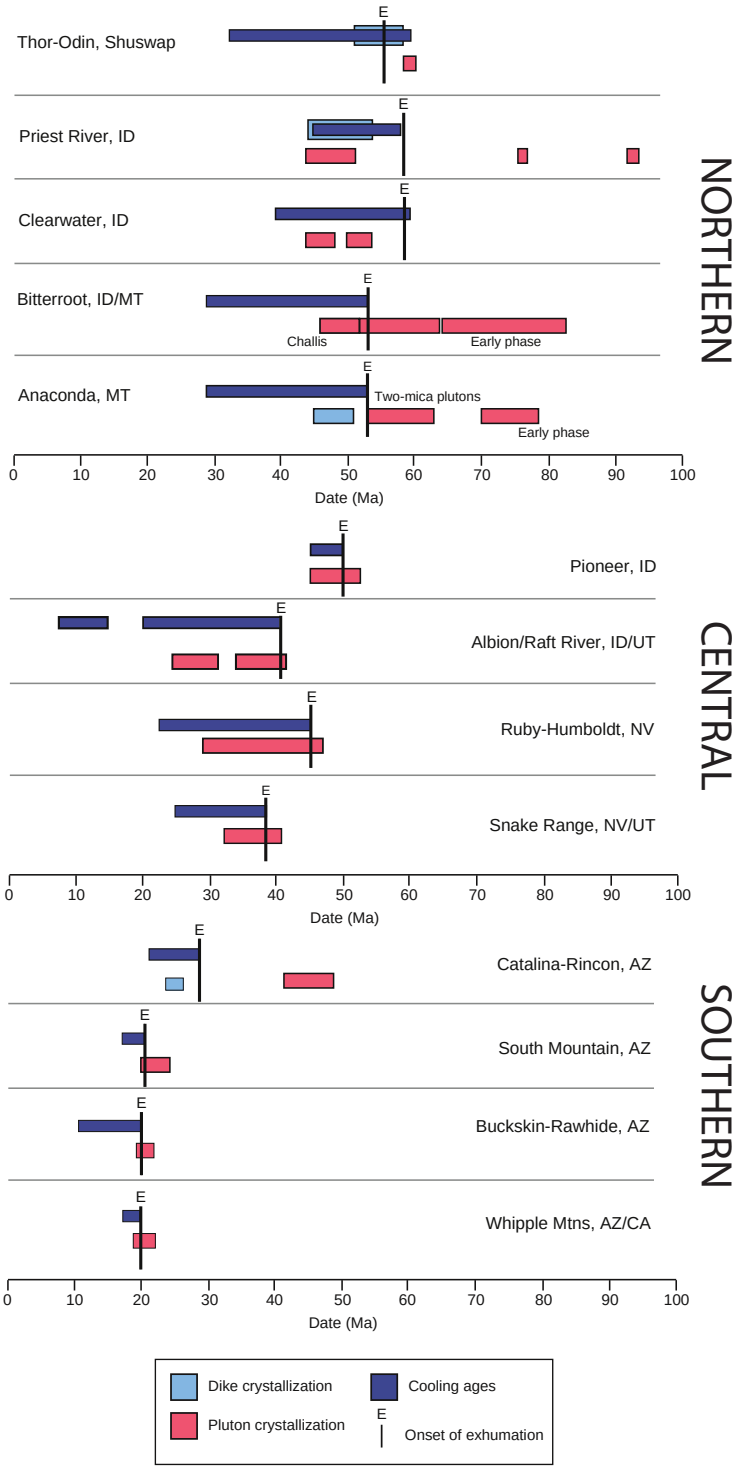


Figure 3.9. Comparison of the timing of main phase plutonism, dike crystallization, and exhumation of MCCs in North America. Data compiled from sources outlined in Table 3.1. Format adapted from Stevens et al. (2016).

Mountains, Buckskin-Rawhide, and Whipple MCCs record cooling ages of 28-22 Ma, 21-17 Ma, 20-11 Ma, and 20.5-18.5 Ma, respectively (Terrien, 2012; Fitzgerald et al., 1993; Singleton et al., 2014; Gans and Gentry, 2016).

### 5.4.2 Cenozoic volcanics compilation

Age-ranges from NAVDAT volcanics compilation are displayed as probability density plots (Figure 3.10). PDP "A" (50-46N) displays 141 radiometric ages for intermediate-felsic volcanic rocks, with ages ranging from 55-45 Ma. PDP B (46-43N) shows 505 ages that range primarily from 57 Ma to 39 Ma. PDPs C and D (43-41N, 41-39N) record ages primarily from 45-15 Ma, with peaks at 45 Ma and 25 Ma, respectively. PDP E (39-37N) displays ages from 35-15 Ma, with a prominent peak at ~17 Ma (n=628). Lastly, PDP F (37-33N) shows ages primarily from 20-12 Ma (n=1217).

#### 5.4.2.1 Cenozoic volcanics in southern Arizona

PDP A (Figure 3.11) displays intermediate-felsic volcanic ages for the region surrounding the Catalina-Rincon MCC and records ages between 40 Ma and 12 Ma, with a prominent peak around 27 Ma. PDP B (surrounding South Mountains MCC) displays ages from 26-16 Ma, and PDP C (surrounding Buckskin-Rawhide MCC) has ages from 33-18 Ma. PDP D (region surrounding Whipple Mountains MCC) records a prominent peak ~20 Ma and ~18 Ma, with a few younger ages at ~16 Ma.

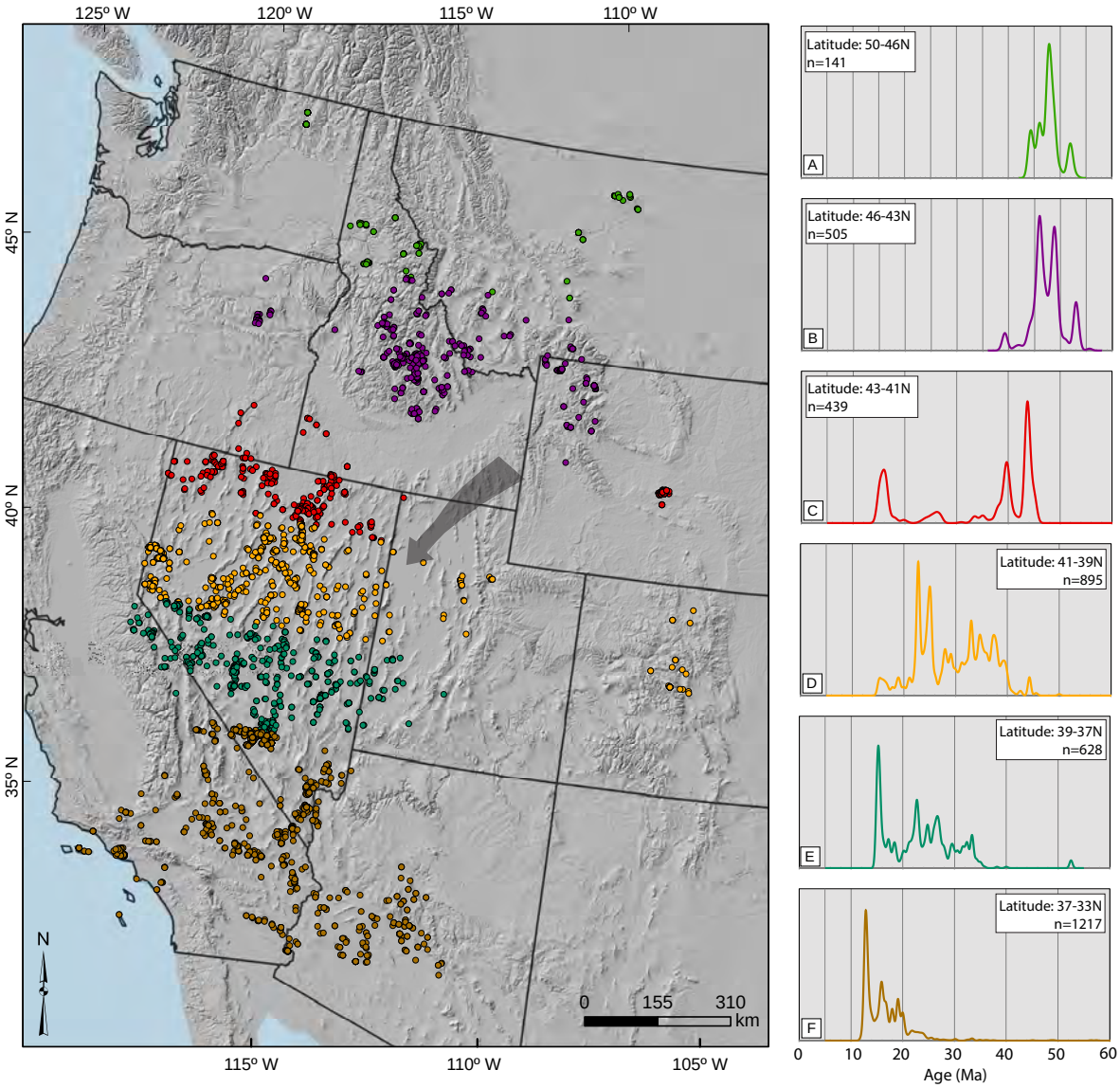


Figure 3.10. Shaded relief map of the western United States showing migration of intermediate-felsic volcanic rocks during the Cenozoic. Graphs A-F show relative probability plots of Cenozoic (60-0 Ma) volcanic rocks from six latitudinally-constrained regions in the western U.S. Latitudes specified in data compilation are listed on each graph and PDPs color-correspond to sample localities on map. Data compiled from the Western North American Volcanic and Intrusive Rock Database (NAVDAT). Gray arrow represents generalized direction of magmatic sweep.

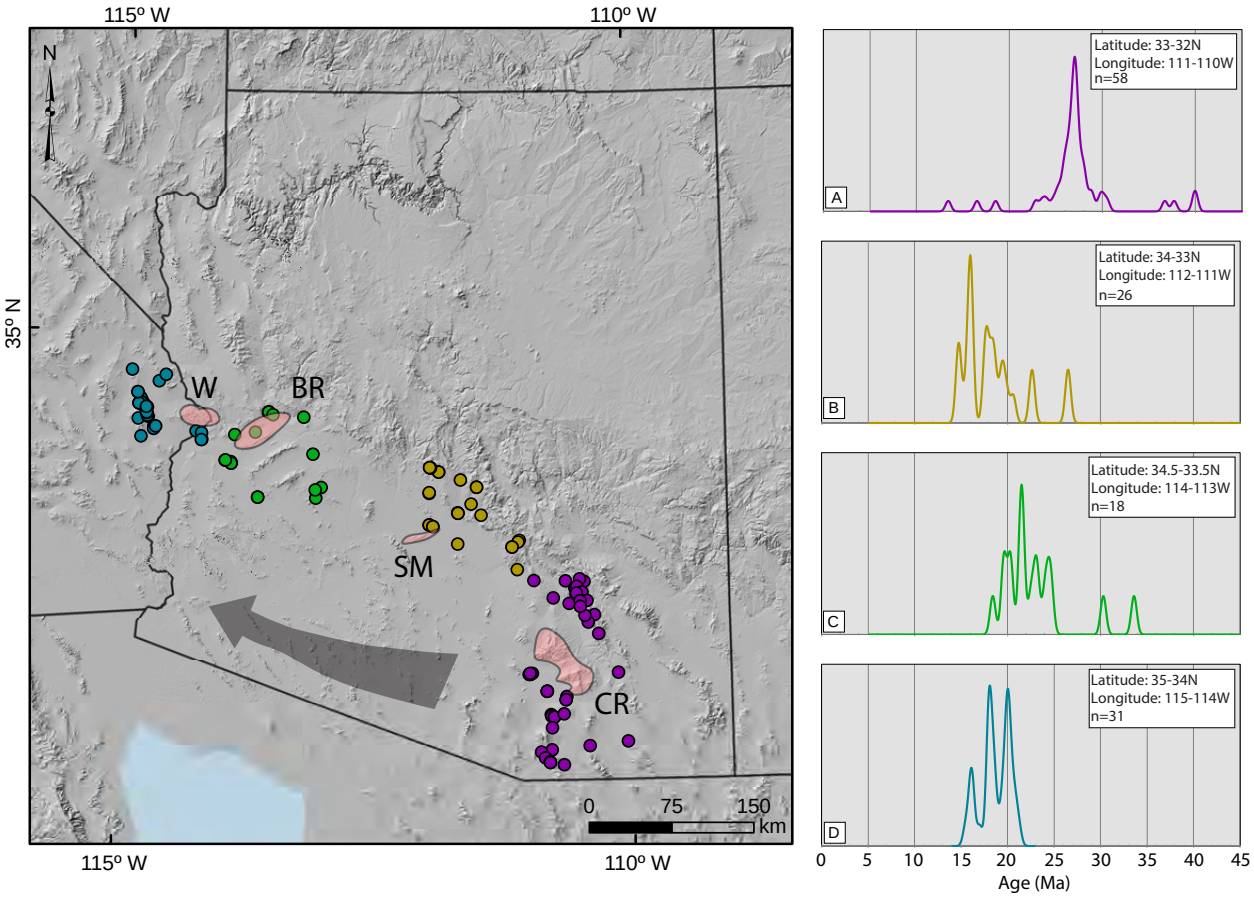


Figure 3.11. Shaded relief map of southern Arizona, USA showing migration of intermediate-felsic volcanic rocks during the Cenozoic. Graphs A-D show relative probability plots of Cenozoic (45-0 Ma) volcanic rocks from four latitudinally and longitudinally constrained regions in southern Arizona. Latitudes specified in data compilation are listed on each graph and PDPs color-correspond to sample localities on map. Data compiled from the Western North American Volcanic and Intrusive Rock Database (NAVDAT). Gray arrow shows generalized direction of magmatic sweep. Light red polygons represent Catalina-Rincon, South Mountain, Buckskin-Rawhide, and Whipple MCCs, respectively.

# 6 Discussion

## 6.1 AMCC footwall magmatism and cooling history

Conducting U-Pb zircon geochronology on variably deformed igneous rocks (ranging in composition from granodiorite to dacite) in the AMCC footwall provides constraints on the timing of pluton emplacement and dike crystallization. Pluton emplacement ages can be compared with previously existing and new thermochronologic cooling ages to gain insight into the relative timing of magmatism and extension.

### 6.1.1 Footwall magmatism and cooling ages

Previous workers have reported two-mica granites in the AMCC footwall to be Eocene in age, ranging from U-Pb ages of 53 ± 0.6 (Foster et al., 2007) to K-Ar ages between 54 and 49 Ma (Wallace et al., 1992), both of which overlap with early-stage exhumation as determined in this study and by Foster et al. (2010). The Paleocene (~61 Ma; Figure 3.5) U-Pb ages obtained in this study for the pervasive two-mica granite in the footwall of the AMCC indicates emplacement occurred at least 7 Ma before the onset of extension (Foster et al., 2010). Foster et al. (2010) reported Ar/Ar cooling ages on mica that indicate the initiation of AMCC exhumation at 53 ± 1 Ma, with slip along the detachment lasting until at least 39 Ma.

The older ages for the two-mica granite presented here reveal that these plutons were being emplaced before the initiation of AMCC exhumation and were contributing additional mass and thickness to the Cordilleran hinterland prior core complex related extnesion. It is possible that the younger ages produced by Foster et al. (2007) and Wallace et al. (1992) are from granites similar in composition and texture to the two-mica

granites dated in this study but were simply younger. The persistence and abundance of igneous activity in the footwalls of core complexes in general makes it very possible that there are separate generations of two-mica granite in the footwall of the AMCC. Regardless, our new data suggests that a significant amount of two-mica granite was emplaced around 61 Ma.

The U-Pb crystallization ages (~46.8 Ma, ~51.0 Ma, ~52.8 Ma) for three dikes within the AMCC footwall are all younger than the onset of extension at ~53 Ma (this study; Foster et al., 2010), suggesting synextensional emplacement. Synextensional igneous activity is common in metamorphic core complexes, and both plutons and dikes can be emplaced as a response to decompression during exhumation (Lister & Baldwin, 1993; Whitney et al., 2013). The dikes dated in this study—all of which display discordant contacts with foliated two-mica granite and surrounding host rock (Figure 3.4)—are interpreted as synextensional magmatism that occurred during early- to mid-stage slip on the Anaconda detachment fault.

### 6.1.2 New thermochronologic cooling ages

Individual cooling ages are plotted versus the elevation of sample collection in Figure 3.7. The highest elevation sample yielded the oldest cooling age, which is consistent that it passed through the partial retention zone earliest during exhumation-related cooling. However, the sample collected from the lowest elevation did not yield the youngest cooling age as expected. Large variations of zircon He ages in a given sample may potentially indicate that these samples were located in the zircon He partial retention zone (140-200 °C) between 38 Ma and 28 Ma. If the samples had cooled

through the PRZ very rapidly, the zircon grains would likely record a closer range of cooling ages. Four plots were constructed to analyze potential causes for the sample collected from the second-highest elevation (72618AR3) to unexpectedly yield the youngest cooling ages rather than the lowest elevation sample (Figure 3.7). Correlation between sample age and effective uranium (eU= 0.235Th × U) was explored as a possible explanation, with eU acting as a proxy for radiation damage that may have caused changes in the closure temperature of individual grains (Flowers et al., 2009; Guenthner et al., 2013). Figure 3.7b show slightly positive correlations between cooling age and eU, however, the youngest grains do not correlate with the highest eU (two grains >1700 ppm), and therefore eU does not appear to represent a significant control and cannot fully explain intrasample age variability or the anomalously young sample. Additionally, U-Pb crystallization ages of nearby samples are <80 Ma, limiting the amount of time in which radiation damage could have possibly accumulated. Ages also do not show any correlation to grain size (Figure 3.7c); the oldest sample (71118AR1) contains a cluster of three ages at ~40 Ma, regardless of variations in the grains' spherical radii (Rs) between ~37-50 μm. Therefore, potential grain size effects also cannot explain intrasample age variability or the anomalously young sample. Figure 3.7d plots cooling age as a function of the distance of the sample from the Anaconda detachment in order to analyze potential structural controls. Distances were measured from each sample's collection site to the mapped location of the Anaconda detachment in CalTopo, using a digital elevation model to aid in identification of the topographic expression of the detachment. Samples show a clear trend of increasing cooling age with distance from the

detachment, apart from the sample collected from the lowest elevation and very near to the detachment. It appears that although this sample was collected at the lowest elevation, it yields ages that are older than two of the higher elevation samples. This could potentially be explained by the presence of an older fault structure in the detachment zone that exhumed the sample at an earlier date and was then abandoned as movement and exhumation along younger portions of the detachment zone began.

The time-temperature paths generated by HeFTy favor two-mica pluton crystallization at ~60 Ma followed by initial rapid cooling through 450-300 °C by ~45 Ma (Figure 3.8). Further igneous activity, represented by synextensional dikes in the AMCC footwall and extrusive equivalents surrounding, drive a second episode of cooling due to exhumation along the Anaconda detachment from ~45 Ma to 25 Ma. These values are consistent with the data obtained in this study, as well as $^{40}Ar/^{39}Ar$ and apatite fission track ages from Foster et al. (2010). Therefore, we interpret that all voluminous pluton emplacement predates Eocene extension along the Anaconda detachment, acting as a driving factor for the formation of the Anaconda metamorphic core complex rather than a response.

**6.2 Lu-Hf systematics**

Analysis of Lu-Hf isotopic ratios in igneous rocks provides information into the how “isotopically evolved” a melt was at the time of crystallization (e.g. Vervoort, 2015). In the Lu-Hf system, the daughter product prefers to partition into melt, which results in crustal rocks having relatively depleted Hf values. We refer to such crustal rocks as being “evolved”, while referring to melts that have recently been derived from the mantle

as “juvenile” (e.g. Vervoort et al., 1999; Chapman et al., 2017). When paired with U-Pb geochronology ages, Lu-Hf isotopic ratios can be used to gain insight into the magmatic evolution of a region that has experienced multiple episodes of igneous activity (e.g. Gaschnig et al., 2011). This pairing technique of U-Pb and Lu-Hf (as well as with Sr-Rb, Sm-Nd, etc.) has been applied to now-exposed arc-magmatic rocks in Cordilleran-style margins around the world (e.g. Chapman et al., 2017).

The systematic trends that can be observed in Lu-Hf signatures are not well-studied for the plutons and dikes exposed in western Montana. However, various radio-isotopic systems have been used to investigate the evolution of the Idaho Batholith and Challis intrusions of eastern Idaho, which lies approximately 100 kilometers west of the Anaconda metamorphic core complex (Gaschnig et al., 2011). One of the isotopic trends observed in the Idaho Batholith is a steady decrease in epsilon Hf values from –8 εHf at ~90 Ma to approximately –25 εHf at ~50 Ma (Figure 3.12a), which was interpreted as progressive crustal thickening and incorporation of more crust into arc magmatism (Gaschnig et al., 2011). Epsilon Hf values in the almost immediately subsequent Challis Intrusives (~48 Ma; Gaschnig et al., 2011) display much more juvenile εHf values, ranging from –28 to –3 with an average around –11 (Figure 3.12a; Gaschnig et al., 2011). This “pull-up” in epsilon Hf space is interpreted to represent extensional collapse of the over-thickened Cordilleran arc crust and increased mantle input (hence more juvenile Hf values). Gaschnig et al. (2011) note that this influx of magmatism with relatively juvenile epsilon Hf values reflects a major regional shift to extensional tectonics in the western US.

Our new Lu-Hf data for two igneous samples obtained from the AMCC footwall and one detrital sample collected from within the AMCC supradetachment basin (Howlett and Laskowski, in review) reflect a nearly identical trend in epsilon Hf space (Figure 3.12b). The detrital grains—collected from the reworked Miocene conglomerate known as the Cabbage Patch Fm.—are hypothesized to have been largely sourced from the Late Cretaceous "Royal Stock" in the northern Flint Creek Range, approximately 10 km along-strike to the northeast of this map area (Loen, 1994; O'Neill et al., 2004; Howlett & Laskowski, in review). Having been eroded from the metamorphic-plutonic core of the AMCC, the epsilon Hf values of these detrital grains can be plotted alongside the two other igneous samples obtained from the field area of this study (Figure 3.12b). The detrital grains sourced from the northern Flint Creek AMCC footwall range from ~83 to ~68 Ma and display a clear decrease in εHf value as they get younger (Figure

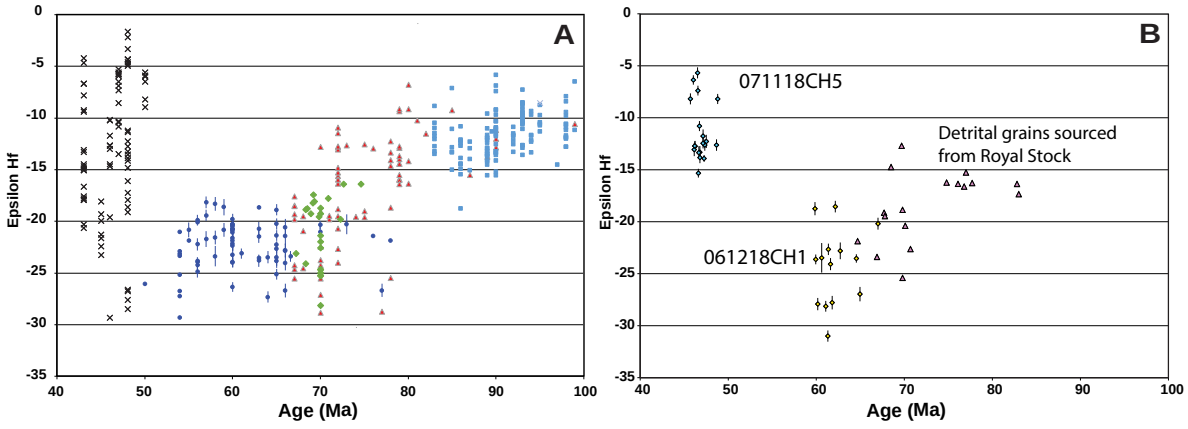


Figure 3.12. (a) Epsilon Hf values from igneous zircon rims plotted against correspfonding U-Pb geochronology ages, Idaho Batholith and related intrusions. Note decreasing εHf values from ~100-50 Ma, followed by pull-up at ~48 Ma. From Gaschnig et al. (2011). (b) Epsilon Hf values vs. U-Pb age for Cretaceous detrital zircons extracted from AMCC supradetachment basin, two-mica granite (061218CH1), and synextensional granodiorite dike (071118CH5). Axes of A and B have been set equal to expose the similarity in isotopic trend through time, interpreted to represent crustal thickening followed by extensional collapse and increased mantle input.

3.12b. The younger, ~61 Ma two-mica granite continues this isotopic trend of increasingly enriched Hf values with time (Figure 3.12b). Finally, the youngest dike dated using U-Pb (071118CH5) is plotted in εHf space and shows a remarkably similar "pull-up" to that seen in the Challis Intrusives of Gaschnig et al. (2011) (Figure 3.4; 3.12a and 3.12b).

It is noteworthy that Sm-Nd isotopic data from the nearby Lowland Creek volcanic field (LCVF) overlap in time and isotopic space with sample 071118CH5 (Dudas et al., 2010). This supports the interpretation that the LCVF is the surficial expression of magmatic activity that was occurring in the footwall of the AMCC during exhumation. The LCVF was active from 52.9 to 48.6 Ma (Dudas et al., 2010), initiating within error of when slip along the Anaconda detachment began (Foster et al., 2010; this study). As part of the widespread volcanism of the northern Cordilleran segment of the ignimbrite flare up, the temporally overlap suggests a linkage between the two (Feeley, 2003).

It has been recognized that the more juvenile Hf values in the mid-Eocene were likely a result of increased mantle input, but the specific cause of upwelling remains controversial (e.g. Gaschnig et al., 2011). We suggest that the increase in εHf values for the synextensional dike is a result of dynamic removal of the Farallon slab, which resulted in infilling of the mantle wedge with hot asthenosphere, heating of low-mid crust, elevation of the geotherm, and metamorphic core complex formation (Figure 3.13).

Lu-Hf signatures from the two-mica granite also have implications regarding the relationship between igneous activity and extension in the AMCC. If the two-mica

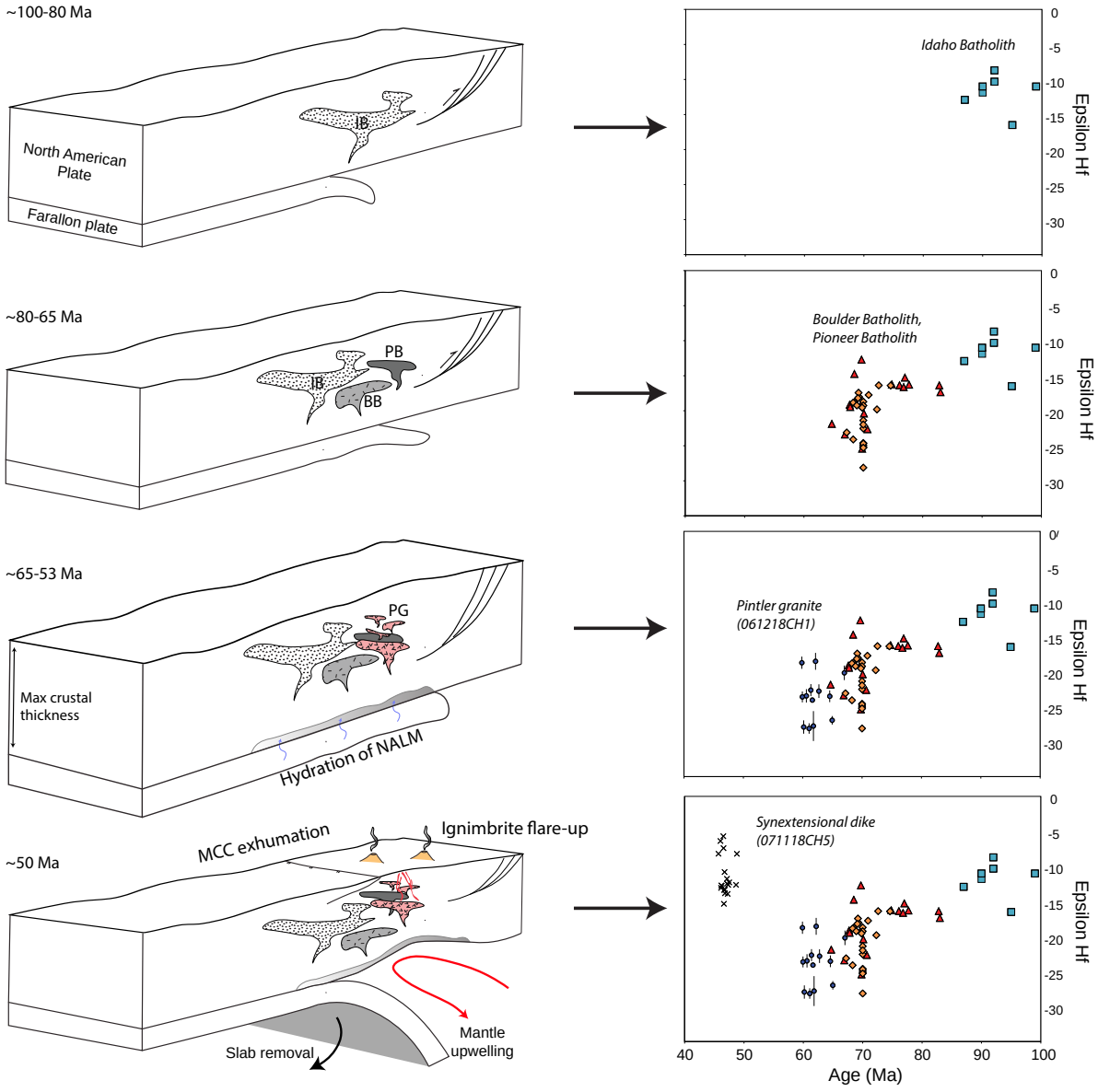


Figure 3.13. Schematic tectonic model to explain the systematic changes oberved in epsilon Hf space over time in the AMCC footwall. Increasingly evolved epsilon Hf values from 100 Ma to 60 Ma represent crustal thickening and incorporation of a larger crustal component into melt. The subsequent pull up in Hf space seen in synextensional footwall dike likely represents increased mantle input due to slab rollback, which elevated geotherms, caused ignimbrite flare up volcanism, and facilitated large-magnitude extension in the upper plate. NALM--North American lithospheric mantle.

granites that dominate the AMCC footwall were a response to extension, we would expect to see a pull-up in epsilon Hf space due to associated mantle upwelling. Our data shows a highly evolved melt for the two-mica that suggests crustal thickening and incorporation of crust into melt prior to collapse primed the crust for initiation of core complex extension.

**6.3 Tectonic evolution of the AMCC**

The Anaconda metamorphic core complex, as part of the northern belt of MCCs in the western USA (Figure 3.1), is situated in the hinterland of the Cordilleran fold-thrust belt (e.g. Coney and Harms, 1984). Core complexes in this region are the oldest in the NA Cordillera, with exhumation beginning in the Eocene between 50-55 Ma (Figure 3.9; Foster et al., 2001, 2007, 2010).

The Early Eocene onset of exhumation determined in the AMCC (~53 Ma; this study; Foster et al., 2010) fits into this time frame and corresponds with an episode of large-magnitude extension that began along the previously thickened Sevier hinterland at ~55 Ma (Constenius, 1996; Foster et al., 2001). In the approximately 45 Ma leading up to the onset of this extension episode (~100-55 Ma), both arc magmatism and eastward propagation of the fold and thrust belt led to extensive crustal thickening in eastern Idaho and western Montana (DeCelles, 2004; DeCelles & Graham, 2015). Spatially and temporally overlapping arc-magmatism included emplacement of the Idaho Batholith (~90 Ma) and the Boulder, Pioneer, and Tobacco Root Batholiths (~75-80 Ma), all of which contributed significant mass to the orogenic wedge (e.g. Gaschnig et al., 2011; Lageson et al., 2001). This study supports the interpretation that Cretaceous, Paleocene,

and earliest Eocene plutonism all contributed additional heat and mass to the already hot and overthickened Cordilleran lithosphere (e.g. Coney and Harms, 1984) prior to the onset of extension at ~53 Ma (Foster et al., 2010). It is proposed that these final pulses of magmatism in the hinterland primed the crust both thermally and gravitationally for collapse and extension in the northern NA Cordillera.

The initiation of large-magnitude extension in northern NA Cordillera subsequent to thrust faulting and extensive pluton emplacement was contemporaneous with widespread volcanism of the Challis–Absaroka–Colville–Kamloops–Bitterroot–Lowland Creek–Montana alkalic province, which lasted from 53–45 Ma (Foster and Fanning, 1997; Morris et al., 2000; Foster et al., 2001; House et al., 2002; Feeley et al., 2002; Feeley, 2003; Breitsprecher et al., 2003; du Bray et al., 2006; Dudas et al., 2010; Foster et al., 2010). The spatio-temporal overlap of this volcanism with extension in the upper plate necessitates a tectonic model that explains both (e.g. Foster et al., 2010). Several mechanisms have been proposed to explain this widespread volcanism, including subduction of the Farallon slab (Armstrong et al., 1977), a slab window (Breitsprecher et al., 2003), and regional extension (Morris et al., 2000). Isotopic and trace element analyses confirm that these volcanics were derived from partial melting of a mantle lithosphere that had been hydrated during the Mesozoic by an underlying oceanic slab (e.g. Feeley, 2003).

Dynamic removal of the subducted Farallon slab has been proposed as a cause of extension and volcanism in the northern MCC belt, as exposure of a refrigerated and metasomatized lower crust to upwelling asthenosphere would naturally cause both

(Humphreys, 2009). The exact mechanism by which the slab was removed remains a topic of discussion. Feeley (2003) points out that a simple steepening of the slab by rollback has difficulty explaining the contemporaneous nature of Eocene volcanism over a broad E-W swath in the northern Cordillera. Arguments have also been proposed that discount simple rollback as an explanation due to the limited velocity with which a slab can push through the asthenosphere (Tao and O'Connell, 1992; Kincaid and Olson, 1987). For these reasons, it was proposed that the slab was removed via downward buckling along an east-northeast trending axis (Humphreys, 1995). The buckling model consists of a tearing or necking separation of the Farallon plate near the northern and southern boundaries of the United States, followed by propagation of the separated edges towards the central axis. We believe that this model is the most fitting to explain the east-west extent of volcanism in the northern Cordillera, as well as the coeval formation of core complexes in the northern belt (Figure 3.9).

**6.4 MCC formation and ignimbrite flareup volcanism: tectonic implications**

A general age decrease in the onset of MCC exhumation is seen from north to south in metamorphic core complexes of the North American Cordillera (Figure 3.9). The average onset of extension in the northern belt of MCCs occurred in the Early Eocene, ca. 54 Ma. In the central belt, the onset of extension is on average 10 My later, occurring at ~45 Ma. In the MCCs of southern and central Arizona (the southern belt), the onset of extension occurs notably later, from ~28-20 Ma.

The PDPs displayed as heat maps in Figure 3.14 record a decrease in the age of Cenozoic volcanism from north to south. This decreasing age has been widely

recognized as a consequence of the transgressive north-to-south sweep of magmatism of the ignimbrite flareup (e.g. Coney and Reynolds, 1977; Humphreys, 1995; Best et al., 2016). In southern Arizona, the flareup of calc-alkaline magmatism did not occur until later (~25-20 Ma; Figure 3.11), and it migrated from east to west rather than north to south as seen across higher latitudes (Humphreys, 1995). Figure 3.11 subtly displays this east-west sweep as ages decrease from the area surrounding the Catalina-Rincon MCC to the region around the Whipple Mountains MCC.

By displaying the age of MCC exhumation atop the Cenozoic volcanics heatmaps, a pronounced spatio-temporal relationship between the migration of ignimbrite flareup magmatism and MCC formation is confirmed (Figure 3.14). It is most important to note that in many cases the onset of extension coincides with the most prominent peaks in volcanism. This result in the northern, central, and southern MCC belts supports the hypothesis that flareup magmatism and volcanism, which is intimately linked to rollback, foundering, or buckling of the subducted Farallon slab, served as a driving force of core complex formation from the Paleocene-Miocene in the western USA.

Some workers have suggested that the localization of northern belt MCCs along the craton margin rules out slab rollback, and that the confinement of MCCs to the crust makes them insensitive to slab dynamics at depth (Stevens et al., 2017). However, the pull up in epsilon-Hf space that coincides with AMCC footwall cooling (~46 Ma; Figure 3.6, 3.12) represents an influx of asthenospheric mantle into the wedge created by Farallon removal (e.g. Gaschnig et al., 2011; Figure 3.13). If the AMCC footwall were not sensitive to Farallon slab dynamics, we would not expect to see this abrupt input of

juvenile melt into the crust. Furthermore, geochemical and thermomechanical modeling on core complexes of the Bering Strait region and northern Basin and Range have concluded that mantle-derived magmatism plays an essential role in partial melting, pluton emplacement, and MCC formation (Gans et al., 1989; Amato and Miller, 2004; Konstantinou et al., 2013). Therefore, it is crucial to consider the role of sublithospheric processes that effect mantle input into theoretical and computational modeling of core complex formation.

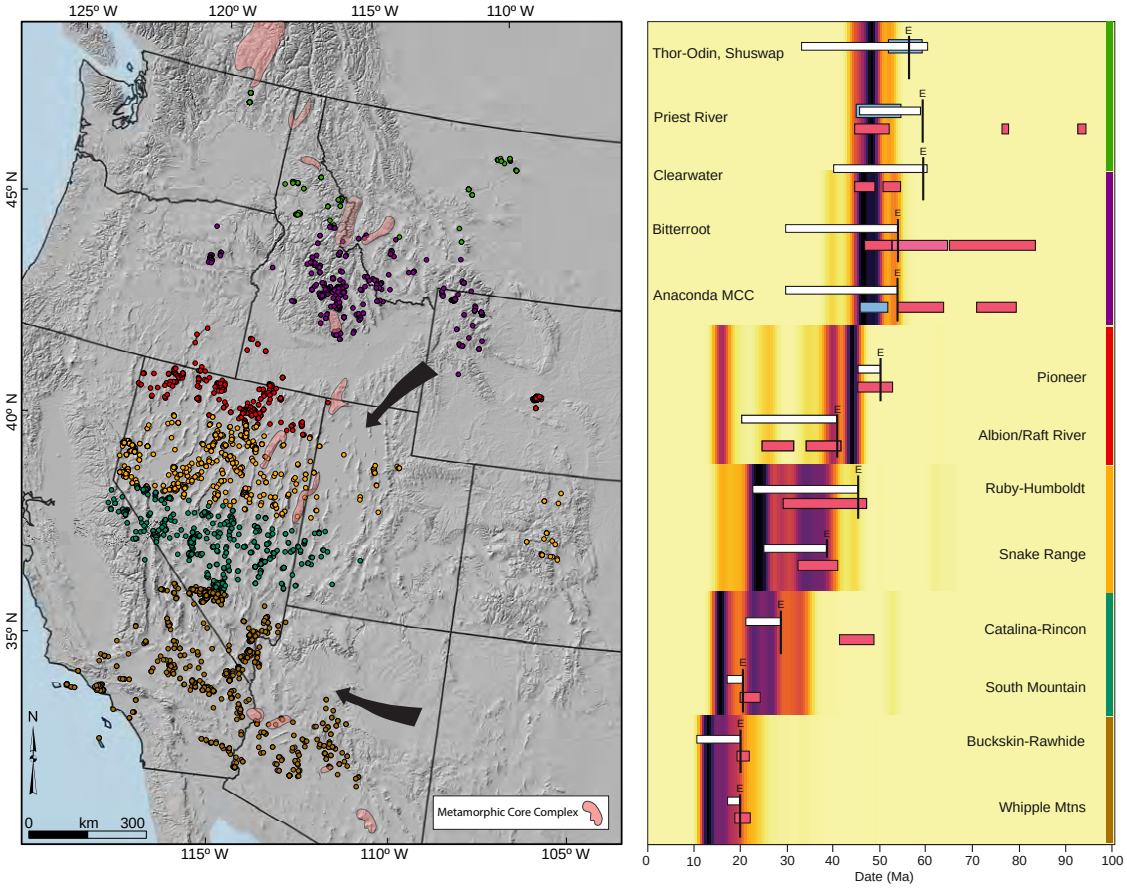


Figure 3.14. Comparing geographic location of major metamorphic core complexes, PDPs of ignimbrite flareup volcanism, and timing of MCC exhumation. Note the upper-right to bottom-left trend of both volcanic ages and onset of MCC extension. Black arrows show generalized direction of magmatic sweep. Light red polygons represent metamorphic core complexes included in this study. Horizontal white and magenta bars on chart represent timing of MCC cooling and plutonic activity, respectively. Colored bars along right side of heat maps correspond with sample location/latitudinal swath.

Regardless of the exact mechanism of Farallon slab removal, it is clear that sublithospheric processes play an important role in the generation of MCC footwall magmas, migration of Cenozoic volcanism, and general development of core complexes in the western USA.

## 7 Conclusions

The results of this integrated geologic, geochronologic, and thermochronologic study of the Anaconda metamorphic core complex of western Montana suggest that it is an example of a core complex whose development was primed by crustal thickening and magmatism. The overlap between the onset of extension (~53 Ma; Foster et al., 2010; this study) and widespread volcanism with a mantle origin (e.g. Feeley, 2003) supports dynamic lower plate processes as an initiating force of exhumation in the AMCC. The primary cause for the differences in timing of MCC exhumation in the NA Cordillera (i.e. younger exhumation of southern MCCs) has remained unclear. This synthesis of existing geo- and thermochronological data supports the hypothesis that the major MCCs of the NA Cordillera were triggered primarily by removal of the subducted Farallon plate by slab rollback/slab buckling. The progressive removal of the Farallon plate from beneath the NA Cordillera likely allowed asthenospheric mantle heating of the hydrated continental lithosphere, ultimately resulting in the migration of magmatism, elevation of geotherms, and development of MCCs.

## Acknowledgments, Samples, and Data

The data referenced in this paper can be accessed in the Supporting Information, or by request to the corresponding author. This research was supported by USGS

EDMAP grant G18AC00143, NSF Instrumentation and Facilities program grant NSF EAR-1649254 to the Arizona Laserchron Center, and Geological Society of America graduate student research grants to C. Howlett and A. Reynolds. We express our gratitude for all our collaborators at the Montana Bureau of Mining and Geology (MBMG)—especially Dr. Colleen Elliott, whose expertise on the AMCC was invaluable. This manuscript benefited greatly from constructive conversation with Dr. Devon Orme and Dr. David Lageson. We also thank the staff of GeoSepServices, the Arizona LaserChron Center, and the Arizona Radiogenic Helium Dating Laboratory for help with mineral separation and analyses.

Supplementary Tables S1, S2, and S3, containing igneous zircon U-Pb analytical data, igneous zircon Lu-Hf analytical data and zircon (U-Th/He) analytical data can be accessed at (insert web address here).

**References**

Amato, J. M., & Miller, E. L. (2004). Geologic map and summary of the evolution of the Kigluaik Mountains gneiss dome, Seward Peninsula, Alaska. In Donna L. Whitney, C. Teyssier, & C. S. Siddoway, Gneiss Domes in Orogeny. Geological Society of America. doi:10.1130/0-8137-2380-9.295

Armstrong, R., & Ward, P. (1991). Evolving geographic patterns of Cenozoic magmatism in the North American Cordillera: The temporal and spatial association of magmatism and metamorphic core complexes. Journal of Geophysical Research: Solid Earth, 96(B8), 13201–13224. doi:10.1029/91JB00412

Armstrong, R. L. (1982). Cordilleran Metamorphic Core Complexes -- From Arizona to Southern Canada. Annual Review of Earth and Planetary Sciences, 10(1), 129–154. doi:10.1146/annurev.ea.10.050182.001021

Armstrong, R. L., Taubeneck, W. H., & Hales, P. O. (1977). Rb-Sr and K-Ar geochronometry of Mesozoic granitic rocks and their Sr isotopic composition, Oregon, Washington, and Idaho. GSA Bulletin, 88(3), 397–411. doi:10.1130/0016-7606(1977)88<397:RAKGOM>2.0.CO;2

Best, M. G., Christiansen, E. H., de Silva, S., & Lipman, P. W. (2016). Slab-rollback ignimbrite flareups in the southern Great Basin and other Cenozoic American arcs: A distinct style of arc volcanism. Geosphere, 12(4), 1097–1135. doi:10.1130/GES01285.1

Bird, P. (1988). Formation of the Rocky Mountains, Western United States: A continuum computer model. Science, 239(4847), 1501–1507. doi:10.1126/science.239.4847.1501

Breitsprecher, K., Thorkelson, D. J., Groome, W. G., & Dostal, J. (2003). Geochemical confirmation of the Kula-Farallon slab window beneath the Pacific Northwest in Eocene time. Geology, 31(4), 351–354. doi:10.1130/0091-7613(2003)031<0351:GCOTKF>2.0.CO;2

Carrapa, B., DeCelles, P. G., & Romero, M. (2019). Early Inception of the Laramide Orogeny in Southwestern Montana and Northern Wyoming: Implications for Models of Flat-Slab Subduction. Journal of Geophysical Research: Solid Earth, 124(2), 2102–2123. doi:10.1029/2018JB016888

Cassel, E. J., Smith, M. E., & Jicha, B. R. (2018). The Impact of Slab Rollback on Earth's Surface: Uplift and Extension in the Hinterland of the North American Cordillera. Geophysical Research Letters, 45(20). doi:10.1029/2018GL079887

Chapman, J. B., Ducea, M. N., Kapp, P., Gehrels, G. E., & DeCelles, P. G. (2017). Spatial and temporal radiogenic isotopic trends of magmatism in Cordilleran orogens. Gondwana Research, 48, 189–204. doi:10.1016/j.gr.2017.04.019

Christiansen, R. L., Yeats, R. S., Graham, S. A., Niem, W. A., Niem, A. R., & Snavely, P. D. (1992). Post-Laramide geology of the U.S. Cordilleran region. In B. C. Burchfiel, P. W. Lipman, & M. L. Zoback (Eds.), The Cordilleran Orogen (pp. 261-R-111). Boulder, Colorado 80301: Geological Society of America. doi:10.1130/DNAG-GNA-G3.261

Coney, P. J., & Harms, T. A. (1984). Cordilleran metamorphic core complexes: Cenozoic extensional relics of Mesozoic compression. Geology, 12(9), 550–554. doi:10.1130/0091-7613(1984)12<550:CMCCCE>2.0.CO;2

Coney, P. J., & Reynolds, S. J. (1977). Cordilleran Benioff zones. Nature, 270(5636), 403–406. doi:10.1038/270403a0

Constenius, K. N. (1996). Late Paleogene extensional collapse of the Cordilleran foreland fold and thrust belt. GSA Bulletin, 108(1), 20–39. doi:10.1130/00167606(1996)108<0020:LPECOT>2.3.CO;2

Constenius, K. N., Esser, R. P., & Layer, P. W. (2003). Extensional Collapse of the Charleston-Nebo Salient and Its Relationship To Space-Time Variations In Cordilleran Orogenic Belt Tectonism and Continental Stratigraphy, 52 p.

Crittenden, M. D., Coney, P. J., & Davis, G. H. (Eds.). (1980). Cordilleran metamorphic core complexes. Boulder, Colo: Geological Society of America.

DeCelles, P. G. (2004). Late Jurassic to Eocene evolution of the Cordilleran thrust belt and foreland basin system, western U.S.A. American Journal of Science, 304(2), 105–168. doi:10.2475/ajs.304.2.105

DeCelles, P. G., & Graham, S. A. (2015). Cyclical processes in the North American Cordilleran orogenic system. Geology, 43(6), 499–502. doi:10.1130/G36482.1

Desmarais, N.R. (1983). Geology and geochronology of the Chief Joseph plutonic-metamorphic core complex, Idaho-Montana, dissertation, University of Washington, 125 pp.

Dewey, J. F., and Bird, J. M. (1970), Mountain belts and the new global tectonics, J. Geophys. Res., 75(14), 2625– 2647, doi:10.1029/JB075i014p02625.

du Bray, E.A., Harlan, S.S., and Wilson, A.B., 2006, Petrology of the Crazy Mountains Dike Swarm and Geochronology of Associated Sills, South-Central Montana: U.S. Geological Survey Professional Paper 1714, 21 p.

Dudás, F. Ö., Ispolatov, V. O., Harlan, S. S., & Snee, L. W. (2010). Ar Geochronology and Geochemical Reconnaissance of the Eocene Lowland Creek Volcanic Field, West-Central Montana. The Journal of Geology, 118(3), 295–304. doi:10.1086/651523

Elison, M. W. (1991). Intracontinental contraction in western North America: Continuity and episodicity. GSA Bulletin, 103(9), 1226–1238. doi:10.1130/00167606(1991)103<1226:ICIWNA>2.3.CO;2

Elliott, C.G., and Lonn, J.D., in review, Geologic map of the Long Peak 7.5' quadrangle, southwestern Montana: Montana Bureau of Mines and Geology Open-File Report, 1 sheet, scale 1:24,000.

Emmons, W., & Calkins, F. (1913). Geology and ore deposits of the Philipsburg quadrangle, Montana (Professional Paper No. 78) (p. 271).

Feeley, T. C. (2003). Origin and Tectonic Implications of Across-Strike Geochemical Variations in the Eocene Absaroka Volcanic Province, United States. The Journal of Geology, 111(3), 329–346. doi:10.1086/373972

Feeley, T. C., Cosca, M. A., & Lindsay, C. R. (2002). Petrogenesis and Implications of Calc-Alkaline Cryptic Hybrid Magmas from Washburn Volcano, Absaroka Volcanic Province, USA. Journal of Petrology, 43(4), 663–703. doi:10.1093/petrology/43.4.663

Fitzgerald, P. G., Reynolds, S. J., Stump, E., Foster, D. A., & Gleadow, A. J. W. (1993). Thermochronologic evidence for timing of denudation and rate of crustal extension of the south mountains metamorphic core complex and sierra estrella, Arizona. Nuclear Tracks and Radiation Measurements, 21(4), 555–563. doi:10.1016/1359-0189(93)90196-G

Flowers, R. M., Ketcham, R. A., Shuster, D. L., & Farley, K. A. (2009). Apatite (U-Th)/He thermochronometry using a radiation damage accumulation and annealing model. Geochimica et Cosmochimica Acta, 73(8), 2347–2365. doi:1016/j.gca.2009.01.015

Foster, D. A., Schafer, C., Fanning, C. M., & Hyndman, D. W. (2001). Relationships between crustal partial melting, plutonism, orogeny, and exhumation: Idaho–Bitterroot batholith. Tectonophysics, 342(3–4), 313–350. doi:10.1016/S0040-1951(01)00169-X

Foster, D. A., Doughty, P. T., Kalakay, T. J., Fanning, C. M., Coyner, S., Grice, W. C., & Vogl, J. (2007). Kinematics and timing of exhumation of metamorphic core complexes along the Lewis and Clark fault zone, northern Rocky Mountains, USA. In Special Paper 434: Exhumation Associated with Continental Strike-Slip

Fault Systems (Vol. 434, pp. 207–232). Geological Society of America. doi:10.1130/2007.2434(10)

Foster, D. A., Grice, W. C., & Kalakay, T. J. (2010). Extension of the Anaconda metamorphic core complex: 40Ar/39Ar thermochronology and implications for Eocene tectonics of the northern Rocky Mountains and the Boulder batholith. Lithosphere, 2(4), 232–246. doi:10.1130/L94.1

Foster, D. A., Mueller, P. A., Heatherington, A., Gifford, J. N., & Kalakay, T. J. (2012). Lu–Hf systematics of magmatic zircons reveal a Proterozoic crustal boundary under the Cretaceous Pioneer batholith, Montana. Lithos, 142–143, 216–225. doi:10.1016/j.lithos.2012.03.005

Gans, P. B., & Gentry, B. J. (2016). Dike emplacement, footwall rotation, and the transition from magmatic to tectonic extension in the Whipple Mountains metamorphic core complex, southeastern California: Dike Emplacement and Footwall Rotation. Tectonics, 35(11), 2564–2608. doi:10.1002/2016TC004215

Gaschnig, R. M., Vervoort, J. D., Lewis, R. S., & Tikoff, B. (2011). Isotopic Evolution of the Idaho Batholith and Challis Intrusive Province, Northern US Cordillera. Journal of Petrology, 52(12), 2397–2429. doi:10.1093/petrology/egr050

Gehrels, G., & Pecha, M. (2014). Detrital zircon U-Pb geochronology and Hf isotope geochemistry of Paleozoic and Triassic passive margin strata of western North America. Geosphere, 10(1), 49–65. doi:10.1130/GES00889.1

Gehrels, G. E., Valencia, V. A., & Ruiz, J. (2008). Enhanced precision, accuracy, efficiency, and spatial resolution of U-Pb ages by laser ablation-multicollector-inductively coupled plasma-mass spectrometry: TECHNICAL BRIEF. Geochemistry, Geophysics, Geosystems, 9(3), n/a-n/a. doi:10.1029/2007GC001805

Grice, W. C. (2006). Exhumation and cooling history of the Middle Eocene Anaconda metamorphic core complex, western Montana, 276.

Guenthner, W. R., Reiners, P. W., Ketcham, R. A., Nasdala, L., & Giester, G. (2013). Helium diffusion in natural zircon: Radiation damage, anisotropy, and the interpretation of zircon (U-Th)/He thermochronology. American Journal of Science, 313(3), 145–198. doi:10.2475/03.2013.01

Hamilton, W.B., 1969, Mesozoic California and the underflow of the Pacific mantle: Geological Society of America Bulletin, 80, 2409–2430, doi:10.1130 /0016-7606(1969)80[2409:MCATUO]2.0.CO;2.

House, M. A., Bowring, S. A., & Hodges, K. V. (2002). Implications of middle Eocene epizonal plutonism for the unroofing history of the Bitterroot metamorphic core

complex, Idaho-Montana. GSA Bulletin, 114(4), 448–461. doi:10.1130/0016-7606(2002)114<0448:IOMEEP>2.0.CO;2

Howlett, C. J., Reynolds, A. N., & Laskowski, A. K. (2019). Geologic map of the northern half of the Pintler Lake 7.5’ quadrangle and the southern half of the Warren Peak 7.5’ quadrangle, southwestern montana (p. 331565). GSA Annual Meeting, Phoenix, Arizona, USA. doi:10.1130/abs/2019AM-331565

Humphreys, E., Hessler, E., Dueker, K., Farmer, G. L., Erslev, E., & Atwater, T. (2003). How Laramide-Age Hydration of North American Lithosphere by the Farallon Slab Controlled Subsequent Activity in the Western United States. International Geology Review, 45(7), 575–595. doi:10.2747/0020-6814.45.7.575

Humphreys, E. D. (1995). Post-Laramide removal of the Farallon slab, western United States. Geology, 23(11), 987–990. doi:10.1130/00917613(1995)023<0987:PLROTF>2.3.CO;2

Ketcham, R. A. (2005). Forward and Inverse Modeling of Low-Temperature Thermochronometry Data. Reviews in Mineralogy and Geochemistry, 58(1), 275–314. doi:10.2138/rmg.2005.58.11

Kincaid, C., & Olson, P. (1987). An experimental study of subduction and slab migration. Journal of Geophysical Research: Solid Earth, 92(B13), 13832–13840. doi:10.1029/JB092iB13p13832

Konstantinou, A., Strickland, A., Miller, E., Vervoort, J., Fisher, C. M., Wooden, J., & Valley, J. (2013). Synextensional magmatism leading to crustal flow in the Albion-Raft River-Grouse Creek metamorphic core complex, northeastern Basin and Range: Synextensional magmatism in the ARG. Tectonics, 32(5), 1384–1403. doi:10.1002/tect.20085

Lageson, D. R., Schmitt, J. G., Horton, B. K., Kalakay, T. J., & Burton, B. R. (2001). Influence of Late Cretaceous magmatism on the Sevier orogenic wedge, western Montana, 4.

Lee, J., Blackburn, T., & Johnston, S. (2017). Timing of mid-crustal ductile extension in the northern Snake Range metamorphic core complex, Nevada: Evidence from U/Pb zircon ages. Geosphere, 13(2), 439–459. doi:10.1130/GES01429.1

Lipman, P. W., Prostka, H. J., & Christiansen, R. L. (1971). Evolving Subduction Zones in the Western United States, as Interpreted from Igneous Rocks. Science, 174(4011), 821–825. doi:10.1126/science.174.4011.821

Lister, G. S., & Baldwin, S. L. (1993). Plutonism and the origin of metamorphic core complexes. Geology, 21, 607–610.

Liu, M. (2001). Cenozoic extension and magmatism in the North American Cordillera: the role of gravitational collapse. Tectonophysics, 342(3–4), 407–433. doi:10.1016/S0040-1951(01)00173-1

Loen, J. S. (1994). Origin of placer gold nuggets and history of formation of glacial gold placers, Gold Creek, Granite County, Montana. Economic Geology, 89(1), 91–104. doi:10.2113/gsecongeo.89.1.91

Lonn, J.D., McDonald, C., Lewis, R.S., Kalakay, T.J., O'Neill, J.M., Berg, R.B., and Hargrave, P. (2003). Preliminary geologic map of the Philipsburg 30′ × 60′ quadrangle, western Montana: Montana Bureau of Mines and Geology Open-File Report MBMG 483, scale 1:100,000.

Ludwig, K. (2012). User's Manual for Isoplot Version 3.75–4.15: A Geochronological Toolkit for Microsoft Excel: Berkeley Geochronological Center Special Publication 5, 75 p.

MacCready, T., Snoke, A. W., Wright, J. E., & Howard, K. A. (1997). Mid-crustal flow during Tertiary extension in the Ruby Mountains core complex, Nevada. GSA Bulletin, 109(12), 1576–1594. doi:10.1130/0016-7606(1997)109<1576:MCFDTE>2.3.CO;2

Morris, G. A., Larson, P. B., & Hooper, P. R. (2000). 'Subduction Style' Magmatism in a Non-subduction Setting: the Colville Igneous Complex, NE Washington State, USA. Journal of Petrology, 41(1), 43–67. doi:10.1093/petrology/41.1.43

O'Neill, J. M., Lonn, J. D., Lageson, D. R., & Kunk, M. J. (2004). Early Tertiary Anaconda Metamorphic Core Complex, southwestern Montana. Canadian Journal of Earth Sciences, 41(1), 63–72. doi:10.1139/e03-086

Platt, J. P., Behr, W. M., & Cooper, F. J. (2015). Metamorphic core complexes: windows into the mechanics and rheology of the crust. Journal of the Geological Society, 172(1), 9–27. doi:10.1144/jgs2014-036

Reynolds, A. N., Howlett, C. J., & Laskowski, A. K. (2019). Extension Of The Anaconda Metamorphic Core Complex: Low-Temperature Thermochronology From The Footwall Of The Anaconda Detachment, Southwest Montana (p. 335709). GSA Annual Meeting, Phoenix, Arizona, USA - 2019. doi:10.1130/abs/2019AM-335709

Sears, J. W., & Hendrix, M. S. (2004). Lewis and Clark line and the rotational origin of the Alberta and Helena salients, North American Cordillera. In Special Paper 383: Orogenic curvature: Integrating paleomagnetic and structural analyses (Vol. 383, pp. 173–186). Geological Society of America. doi:10.1130/0-8137-2383-3(2004)383[173:LACLAT]2.0.CO;2

Singleton, J. S., Stockli, D. F., Gans, P. B., & Prior, M. G. (2014). Timing, rate, and magnitude of slip on the Buckskin-Rawhide detachment fault, west central Arizona. Tectonics, 33(8), 1596–1615. https://doi.org/10.1002/2013TC003517

Snoke, A. W., Howard, K. A., McGrew, A. J., Burton, B. R., Barnes, C. G., Peters, M. T., & Wright, J. E. (1997). The grand tour of the Ruby-East Humboldt metamorphic core complex, northeastern Nevada: Part 1 - Introduction & road log. Brigham Young University Geology Studies, 42(1), 225–296.

Stevens, Liane M., Bendick, R., & Baldwin, J. A. (2017). Synconvergent exhumation of metamorphic core complexes in the northern North American Cordillera. Geology, 45(6), 495–498. doi:10.1130/G38802.1

Stevens, L.M., Baldwin, J. A., Crowley, J. L., Fisher, C. M., & Vervoort, J. D. (2016). Magmatism as a response to exhumation of the Priest River complex, northern Idaho: Constraints from zircon U–Pb geochronology and Hf isotopes. Lithos, 262, 285–297. doi:10.1016/j.lithos.2016.07.006

Tao, W. C., & O'connell, R. J. (1992). Ablative subduction: A two-sided alternative to the conventional subduction model. Journal of Geophysical Research, 97(B6), 8877. doi:10.1029/91JB02422

Terrien, J. (2012), Thermochronological And Geochemical Insights On The Transition Between The Metamorphic Core Complex And The North American Cordillera, Southern Arizona, dissertation, 245 pp.

Vanderhaeghe, O., Teyssier, C., McDougall, I., & Dunlap, W. J. (2003). Cooling and exhumation of the Shuswap Metamorphic Core Complex constrained by 40Ar/39Ar thermochronology. GSA Bulletin, 115(2), 200–216. doi:10.1130/00167606(2003)115<0200:CAEOTS>2.0.CO;2

Vervoort, J. D., Patchett, P. J., Blichert-Toft, J., & Albarède, F. (1999). Relationships between Lu–Hf and Sm–Nd isotopic systems in the global sedimentary system. Earth and Planetary Science Letters, 168(1–2), 79–99. doi:10.1016/S0012-821X(99)00047-3

Vogl, J. J., Foster, D. A., Fanning, C. M., Kent, K. A., Rodgers, D. W., & Diedesch, T. (2012). Timing of extension in the Pioneer metamorphic core complex with implications for the spatial-temporal pattern of Cenozoic extension and exhumation in the northern U.S. Cordillera: Extension in the Pioneer core complex. Tectonics, 31(1), doi:10.1029/2011TC002981

Wallace, C.A., Lidke, D.J., Elliott, J.E., Desmarais, N.R., Obradovich, J.D., Lopez, D.A., Zarske, S.E., Heise, B.A., Blaskowski, M.J., and Loen, J.S. (1992). Geologic map of the Anaconda-Pintlar wilderness and contiguous roadless area, Granite, Deer

Lodge, Beaverhead, and Ravalli counties, western Montana: U.S. Geological Survey Miscellaneous Field Studies Map MF-1633-C, scale 1:50,000.

Wernicke, B. (1981). Low-angle normal faults in the Basin and Range Province: nappe tectonics in an extending orogen. Nature, 291(5817), 645–648. doi:10.1038/291645a0

Wernicke, B. P., England, P. C., Sonder, L. J., & Christiansen, R. L. (1987). Tectonomagmatic evolution of Cenozoic extension in the North American Cordillera. Geological Society, London, Special Publications, 28(1), 203–221. doi:10.1144/GSL.SP.1987.028.01.15

Wernicke, B. (1992). Cenozoic extensional tectonics of the U.S. Cordillera. In B. C. Burchfiel, P. W. Lipman, & M. L. Zoback (Eds.), The Cordilleran Orogen (pp. 553–17). Boulder, Colorado 80301: Geological Society of America. doi:10.1130/DNAG-GNA-G3.553

Whitney, D. L., Teyssier, C., Rey, P., & Buck, W. R. (2013). Continental and oceanic core complexes. Geological Society of America Bulletin, 125(3–4), 273–298. doi:10.1130/B30754.1

# CHAPTER FOUR

# CONCLUSIONS

This first manuscript provided in this thesis consists of a provenance analysis of gold placer deposits deposited in the supradetachment basin of the northern Anaconda metamorphic core complex in western Montana. New detrital zircon U-Pb geochronology data, DZ isotopic data, and DZ unmixing modeling results suggest that the placer gold was sourced from the northern footwall of the Anaconda MCC. Along with offering quantitative support for previous interpretations regarding the source of the gold, our study serves as a confirmation of the utility of using DZ geochronology and isotopic data, as well as emerging modeling techniques, to determine the source of economically valuable minerals.

The second manuscript contains an investigation of plutonism and extension in the central AMCC. A combination of geologic mapping, igneous zircon U-Pb geochronology, zircon Lu-Hf isotopic analysis, and zircon (U-Th)/He thermochronology provides new insights into the evolution of the AMCC: (1) The footwall of the Anaconda Range segment of the AMCC is dominated by Paleocene-Eocene two-mica granites. U-Pb ages that precede the onset of extension (~53 Ma; Foster et al., 2010), combined with evolved Lu-Hf signatures, suggests that this magmatism was not a response to extension, but rather served as a driving force of exhumation. Additionally, (2) New zircon (U-Th)/He thermochronology ages suggest cooling through 450-300 °C by ~45 Ma, with extension lasting until ~25 Ma. These new cooling ages further constrain the timing of slip along the Anaconda detachment fault (ADF), which was broadly bracketed between

53 Ma and 39 Ma by Foster et al. (2010). Apatite fission track ages (Foster et al., 2010), combined with these new zircon (U-Th)/He results, confirm that exhumation of the footwall continued into the Oligocene (~27-25 Ma). This extended duration of slip is supported further by anomalously old cooling ages close to the Anaconda detachment, which we interpret to be a consequence of an older strand of the ADF that was abandoned as movement and exhumation along younger portions of the detachment fault began. (3) A comparison of Lu-Hf data from the AMCC footwall and the Idaho Batholith exposes a systematic change over time. From ~100 Ma to ~50 Ma, zircon epsilon Hf values become increasingly negative, suggesting incorporation of more existing crust into melt. After 50 Ma (and coinciding with large-magnitude extension of the AMCC), a dramatic pull in up epsilon Hf space is seen. We suggest these trends represent crustal thickening followed by increased mantle input as a result of removal of the subhorizontally-subducted Farallon slab.

Taken together, our results from the AMCC suggest that Mesozoic-Early Cenozoic contraction and magmatism created an overthickened and gravitationally unstable crust (e.g. Coney and Harms, 1984), and that removal of the Farallon slab from beneath the northern Cordillera triggered core complex formation. In addition, an orogen-scale compilation of MCC cooling ages and the timing of Cenozoic volcanism suggests that there is an intimate linkage between large-magnitude extension and migration of igneous activity believed to be the result of slab removal.

It should be emphasized that no single driving force can explain core complex formation in the NA cordillera, as their formation was likely a cumulative result of many

changing variables (gravitational instability, changes in far-field plate boundary conditions, etc.). That being said, the work presented here confirms a strong correlation between Cenozoic magmatism associated with slab removal and upper plate extension, suggesting that it played a crucial role in MCC formation. The mechanism by which the Farallon slab was removed remains speculative, but the coeval formation of northern MCCs and widely distributed volcanic activity agrees well with the slab buckling hypothesis of Humphreys (1995), in which the Farallon flat slab was removed via buckling/collapse perpendicular to an east-northeast trending axis. This model not only accounts best for timing of northern belt MCCs, but also for the evolution of Cenozoic igneous activity through the Great Basin and across southern Arizona. Regardless of how the slab was removed, it appears that post-Laramide upwelling of asthenosphere and increased input from the mantle contributed to the evolution of the western USA during the Cenozoic. Therefore, it is important that future theoretical and computational modeling of core complex formation consider the role of sublithospheric processes.

## Literature Cited

Coney, P. J., & Harms, T. A. (1984). Cordilleran metamorphic core complexes: Cenozoic extensional relics of Mesozoic compression. Geology, 12(9), 550–554. doi:10.1130/0091-7613(1984)12<550:CMCCCE>2.0.CO;2

Foster, D. A., Grice, W. C., & Kalakay, T. J. (2010). Extension of the Anaconda metamorphic core complex: 40Ar/39Ar thermochronology and implications for Eocene tectonics of the northern Rocky Mountains and the Boulder batholith. Lithosphere, 2(4), 232–246. doi:10.1130/L94.1

Humphreys, E. D. (1995). Post-Laramide removal of the Farallon slab, western United States. Geology, 23(11), 987–990. doi:10.1130/00917613(1995)023<0987:PLROTF>2.3.CO;2

# CUMULATIVE LITERATURE CITED

Amato, J. M., & Miller, E. L. (2004). Geologic map and summary of the evolution of the Kigluaik Mountains gneiss dome, Seward Peninsula, Alaska. In Donna L. Whitney, C. Teyssier, & C. S. Siddoway, *Gneiss Domes in Orogeny*. Geological Society of America.

Armstrong, R. L. (1972). Low-Angle (Denudation) Faults, Hinterland of the Sevier Orogenic Belt, Eastern Nevada and Western Utah. *Geological Society of America Bulletin, 83*(6), 1729.

Armstrong, R. L. (1982). Cordilleran Metamorphic Core Complexes -- From Arizona to Southern Canada. Annual Review of Earth and Planetary Sciences, 10(1), 129–154. doi:10.1146/annurev.ea.10.050182.001021

Armstrong, R. L., Taubeneck, W. H., & Hales, P. O. (1977). Rb-Sr and K-Ar geochronometry of Mesozoic granitic rocks and their Sr isotopic composition, Oregon, Washington, and Idaho. GSA Bulletin, 88(3), 397–411. doi:10.1130/0016-7606(1977)88<397:RAKGOM>2.0.CO;2

Armstrong, R., & Ward, P. (1991). Evolving geographic patterns of Cenozoic magmatism in the North American Cordillera: The temporal and spatial association of magmatism and metamorphic core complexes. Journal of Geophysical Research: Solid Earth, 96(B8), 13201–13224. doi:10.1029/91JB00412

Baken, J.F., 1984, The structural geology and tectonic history of the northern Flint Creek Range, western Montana [M.Sc. thesis]: Montana State University, 140 p.

Balgord, E., Mahoney, J.B., and Gingras, M.K., 2009, Detrital zircon evidence requires revision of Belt stratigraphy in southwestern Montana: Geological Society of America Abstracts with Programs, v. 41, p. 590.

Bartschi, N., Saylor, J.E., Lapen, T.J., Blum, M.D., Pettit, B.S., and Andrea, R.A., 2018, Tectonic Controls On Late Cretaceous Sediment Provenance And Stratigraphic Architecture In The Book Cliffs, Utah. Geological Society of American Bulletin, v. 130, p. 1763-1781 doi:10 .1130 /B31927.1.

Baty, J.B., 1973, Fission track age dates from three granitic plutons in the Flint Creek Range, western Montana: Missoula, [M.Sc. Thesis]: The University of Montana, 37 p.

Best, M. G., Christiansen, E. H., de Silva, S., & Lipman, P. W. (2016). Slab-rollback ignimbrite flareups in the southern Great Basin and other Cenozoic American arcs: A distinct style of arc volcanism. Geosphere, 12(4), 1097–1135. doi:10.1130/GES01285.1

Bird, P. (1988). Formation of the Rocky Mountains, Western United States: A continuum computer model. Science, 239(4847), 1501–1507. doi:10.1126/science.239.4847.1501

Boyle, R.W., 1979, The geochemistry of gold and its deposits, Geological Survey of Canada Bulletin 280, 584 p.

Breitsprecher, K., Thorkelson, D. J., Groome, W. G., & Dostal, J. (2003). Geochemical confirmation of the Kula-Farallon slab window beneath the Pacific Northwest in Eocene time. Geology, 31(4), 351–354. doi:10.1130/0091-7613(2003)031<0351:GCOTKF>2.0.CO;2

Brooks, J.A., 2002, Bedrock geologic maps of the Griffin Creek and Bailey Mountain 7.5 minute quadrangles, Powell County, Montana: Missoula, [M.Sc. Thesis]: University of Montana, 84 p.

Brooks, J.A., and Sears, J.W., 2009, Geologic map of the Bailey Mountain and Griffin Creek 7.5' quadrangles, Montana: Montana Bureau of Mines and Geology EDMAP portion of the National Geologic Mapping Program 1, 2 sheets, scale 1:24,000.

Carrapa, B., DeCelles, P. G., & Romero, M. (2019). Early Inception of the Laramide Orogeny in Southwestern Montana and Northern Wyoming: Implications for Models of Flat-Slab Subduction. Journal of Geophysical Research: Solid Earth, 124(2), 2102–2123. doi:10.1029/2018JB016888

Cassel, E. J., Smith, M. E., & Jicha, B. R. (2018). The Impact of Slab Rollback on Earth's Surface: Uplift and Extension in the Hinterland of the North American Cordillera. Geophysical Research Letters, 45(20). doi:10.1029/2018GL079887

Chadwick, R.A., 1981, Chronology and structural setting of volcanism in southwestern and central Montana, in Tucker, T.E., ed., Field Conference and Symposium Guidebook to Southwest Montana: Montana Geological Society, p. 301–310.

Chapman, A.D. and Laskowski, A.K., 2019, Detrital zircon U-Pb data reveal a Mississippian sediment dispersal network originating in the Appalachian orogen, traversing North America along its southern shelf, and reaching as far as the southwest United States. Lithosphere, v.11, p. 581-587, doi:10.1130/L1068.1.

Chapman, J. B., Ducea, M. N., Kapp, P., Gehrels, G. E., & DeCelles, P. G. (2017). Spatial and temporal radiogenic isotopic trends of magmatism in Cordilleran orogens. Gondwana Research, 48, 189–204. doi:10.1016/j.gr.2017.04.019

Christiansen, R. L., Yeats, R. S., Graham, S. A., Niem, W. A., Niem, A. R., & Snavely, P. D. (1992). Post-Laramide geology of the U.S. Cordilleran region. In B. C. Burchfiel, P. W. Lipman, & M. L. Zoback (Eds.), The Cordilleran Orogen (pp.

261-R-111). Boulder, Colorado 80301: Geological Society of America. doi:10.1130/DNAG-GNA-G3.261

Coney, P. J., & Harms, T. A. (1984). Cordilleran metamorphic core complexes: Cenozoic extensional relics of Mesozoic compression. *Geology*, *12*(9), 550–554.

Coney, P. J., & Reynolds, S. J. (1977). Cordilleran Benioff zones. Nature, 270(5636), 403–406. doi:10.1038/270403a0

Constenius, K. N. (1996). Late Paleogene extensional collapse of the Cordilleran foreland fold and thrust belt. GSA Bulletin, 108(1), 20–39. doi:10.1130/00167606(1996)108<0020:LPECOT>2.3.CO;2

Constenius, K. N., Esser, R. P., & Layer, P. W. (2003). Extensional Collapse of the Charleston-Nebo Salient and Its Relationship To Space-Time Variations In Cordilleran Orogenic Belt Tectonism and Continental Stratigraphy, 52 p.

Crittenden, M. D., Coney, P. J., & Davis, G. H. (Eds.). (1980). *Cordilleran metamorphic core complexes*. Boulder, Colo: Geological Society of America.

Davis, D.W., Hirdes, W., Schaltegger, U., and Nunoo, E.A., 1994, U-Pb age constraints on deposition and provenance of Birimian and gold-bearing Tarkwaian sediments in Ghana, West Africa: Precambrian Research, v. 67, p. 89–107, doi:10.1016/0301-9268(94)90006-x.

DeCelles, P. G. (2004). Late Jurassic to Eocene evolution of the Cordilleran thrust belt and foreland basin system, western U.S.A. American Journal of Science, 304(2), 105–168. doi:10.2475/ajs.304.2.105

DeCelles, P. G., & Graham, S. A. (2015). Cyclical processes in the North American Cordilleran orogenic system. Geology, 43(6), 499–502. doi:10.1130/G36482.1

Desmarais, N.R. (1983). Geology and geochronology of the Chief Joseph plutonic-metamorphic core complex, Idaho-Montana, dissertation, University of Washington, 125 pp.

Dewey, J. F., and Bird, J. M. (1970), Mountain belts and the new global tectonics, J. Geophys. Res., 75(14), 2625– 2647, doi:10.1029/JB075i014p02625.

Dickinson, W. R., and G. E. Gehrels, 2008, Sediment delivery to the Cordilleran foreland basin: Insights from U-Pb ages of detrital zircons in Upper Jurassic and Cretaceous strata of the Colorado Plateau, Am. J. Sci., v. 308, p. 1041–1082, doi:10.2475/01.2008.01.

Dickinson, W.R., Lawton, T.F., and Gehrels, G.E., 2009, Recycling detrital zircons: A case study from the Cretaceous Bisbee Group of southern Arizona: Geology, v. 37, p. 503–506, doi:10.1130/g25646a.1.

Dickinson,W.R., 2008, Impact of differential zircon fertility of granitoid basement rocks in North America on age populations of detrital zircons and implications for granite petrogenesis. Earth and Planetary Science Letters, v. 275, p. 80–92, doi:10.1016/j.epsl.2008.08.003.

du Bray, E.A., Harlan, S.S., and Wilson, A.B., 2006, Petrology of the Crazy Mountains Dike Swarm and Geochronology of Associated Sills, South-Central Montana: U.S. Geological Survey Professional Paper 1714, 21 p.

Ducea, M.N., Barton, M.D., 2007, Igniting flare-up events in Cordilleran arcs, Geology, v. 35, p. 1047–1050, doi:10.1130/G23898A.1.

Dudás, F. Ö., Ispolatov, V. O., Harlan, S. S., & Snee, L. W. (2010). Ar Geochronology and Geochemical Reconnaissance of the Eocene Lowland Creek Volcanic Field, West-Central Montana. The Journal of Geology, 118(3), 295–304. doi:10.1086/651523

Edwards, R.P., and Atkinson, K., 1986, Ore Deposit Geology and its Influence on Mineral Exploration: London and New York, Chapman and Hall, p. 175-214.

Elison, M. W. (1991). Intracontinental contraction in western North America: Continuity and episodicity. GSA Bulletin, 103(9), 1226–1238. doi:10.1130/00167606(1991)103<1226:ICIWNA>2.3.CO;2

Elliott, C.G., and Lonn, J.D., in review, Geologic map of the Long Peak 7.5' quadrangle, southwestern Montana: Montana Bureau of Mines and Geology Open-File Report, 1 sheet, scale 1:24,000.

Emmons W.H., and Calkins F.C., 1913, Geology and ore deposits of the Philipsburg Quadrangle Montana, U.S. Geological Survey Professional Paper 78, 271 p.

Feeley, T. C. (2003). Origin and Tectonic Implications of Across-Strike Geochemical Variations in the Eocene Absaroka Volcanic Province, United States. The Journal of Geology, 111(3), 329–346. doi:10.1086/373972

Feeley, T. C., Cosca, M. A., & Lindsay, C. R. (2002). Petrogenesis and Implications of Calc-Alkaline Cryptic Hybrid Magmas from Washburn Volcano, Absaroka Volcanic Province, USA. Journal of Petrology, 43(4), 663–703. doi:10.1093/petrology/43.4.663

Feeley, T.C., and Cosca, M.A., 2003, Time vs. compositional trends of magmatism at Sunlight volcano, Absaroka volcanic province, Wyoming: Geological Society of America Bulletin, v. 115, p. 714–728, doi:10.1130/0016-7606(2003)115<0714:TVCTOM>2.0.CO;2.

Fitzgerald, P. G., Reynolds, S. J., Stump, E., Foster, D. A., & Gleadow, A. J. W. (1993). Thermochronologic evidence for timing of denudation and rate of crustal extension of the south mountains metamorphic core complex and sierra estrella, Arizona. Nuclear Tracks and Radiation Measurements, 21(4), 555–563. doi:10.1016/1359-0189(93)90196-G

Flowers, R. M., Ketcham, R. A., Shuster, D. L., & Farley, K. A. (2009). Apatite (U-Th)/He thermochronometry using a radiation damage accumulation and annealing model. Geochimica et Cosmochimica Acta, 73(8), 2347–2365. doi:1016/j.gca.2009.01.015

Foster, D. A., & Fanning, C. M. (1997). Geochronology of the northern Idaho batholith and the Bitterroot metamorphic core complex: Magmatism preceding and contemporaneous with extension. *Geological Society of America Bulletin*, 16.

Foster, D. A., Doughty, P. T., Kalakay, T. J., Fanning, C. M., Coyner, S., Grice, W. C., & Vogl, J. (2007). Kinematics and timing of exhumation of metamorphic core complexes along the Lewis and Clark fault zone, northern Rocky Mountains, USA. In Special Paper 434: Exhumation Associated with Continental Strike-Slip Fault Systems (Vol. 434, pp. 207–232). Geological Society of America. doi:10.1130/2007.2434(10)

Foster, D. A., Grice, W. C., & Kalakay, T. J. (2010). Extension of the Anaconda metamorphic core complex: 40Ar/39Ar thermochronology and implications for Eocene tectonics of the northern Rocky Mountains and the Boulder batholith. Lithosphere, 2(4), 232–246. doi:10.1130/L94.1

Foster, D. A., Mueller, P. A., Heatherington, A., Gifford, J. N., & Kalakay, T. J. (2012). Lu–Hf systematics of magmatic zircons reveal a Proterozoic crustal boundary under the Cretaceous Pioneer batholith, Montana. Lithos, 142–143, 216–225. doi:10.1016/j.lithos.2012.03.005

Foster, D. A., Schafer, C., Fanning, C. M., & Hyndman, D. W. (2001). Relationships between crustal partial melting, plutonism, orogeny, and exhumation: Idaho–Bitterroot batholith. Tectonophysics, 342(3–4), 313–350. doi:10.1016/S0040-1951(01)00169-X

Foster, D.A., and Raza, A., 2002, Low-temperature thermochronological record of exhumation of the Bitterroot metamorphic core complex, northern Cordilleran Orogen: Tectonophysics, v. 349, p. 23–36, doi:10.1016/s0040-1951(02)00044-6.

Fritz, W.J., Sears, J.W., McDowell, R.J., and Wampler, J.M., 2007, Cenozoic volcanic rocks of southwestern Montana: Northwest Geology, v. 36, p. 91–110.

Fuentes, F., DeCelles, P.G., and Constenius, K.N., 2012, Regional structure and kinematic history of the Cordilleran fold-thrust belt in northwestern Montana, USA: Geosphere, v. 8, p. 1104–1128, doi:10.1130/GES00773.1.

Fuentes, F., DeCelles, P.G., and Gehrels, G.E., 2009, Jurassic onset of foreland basin deposition in northwestern Montana, USA: Implications for along-strike synchroneity of Cordilleran orogenic activity: Geology, v. 37, p. 379–382, doi:10.1130/G25557A.1.

Gans, P. B., & Gentry, B. J. (2016). Dike emplacement, footwall rotation, and the transition from magmatic to tectonic extension in the Whipple Mountains metamorphic core complex, southeastern California: Dike Emplacement and Footwall Rotation. Tectonics, 35(11), 2564–2608. doi:10.1002/2016TC004215

Gans, P. B., Mahood, G. A., & Schermer, E. (1989). Synextensional magmatism in the Basin and Range Province; A case study from the eastern Great Basin. In *Geological Society of America Special Papers* (Vol. 233, pp. 1–53). Geological Society of America.

Gaschnig, R.M., Vervoort, J.D., Lewis, R.S., and McClelland, W.C., 2010, Migrating magmatism in the northern US Cordillera: In-situ U-Pb geochronology of the Idaho batholith: Contributions to Mineralogy and Petrology, v. 159, p. 863–883, doi:10.1007/s00410-009-0459-5.

Gaschnig, R.M., Vervoort, J.D., Lewis, R.S., and Tikoff, B., 2011, Isotopic Evolution of the Idaho Batholith and Challis Intrusive Province, Northern US Cordillera: Journal of Petrology, v. 52, p. 2397–2429, doi:10.1093/petrology/egr050.

Gaschnig, R.M., Vervoort, J.D., Lewis, R.S., and Tikoff, B., 2013, Probing for Proterozoic and Archean crust in the northern U.S. Cordillera with inherited zircon from the Idaho batholith: Geological Society of America Bulletin, v. 125, p. 73–88, doi:10.1130/B30583.1.

Gehrels, G. E., Valencia, V. A., & Ruiz, J. (2008). Enhanced precision, accuracy, efficiency, and spatial resolution of U-Pb ages by laser ablation-multicollector-inductively coupled plasma-mass spectrometry: TECHNICAL BRIEF. Geochemistry, Geophysics, Geosystems, 9(3), n/a-n/a. doi:10.1029/2007GC001805

Gehrels, G., & Pecha, M. (2014). Detrital zircon U-Pb geochronology and Hf isotope geochemistry of Paleozoic and Triassic passive margin strata of western North America. Geosphere, 10(1), 49–65. doi:10.1130/GES00889.1

Goodge, J.W. and Vervoort, J.D., 2006, Origin of Mesoproterozoic A-type granites in Laurentia: Hf isotope evidence: Earth and Planetary Science Letters, v. 243, p. 711-731, doi:10.1016/j.epsl.2006.01.040.

Grice, W.C., Jr., 2006, Exhumation and cooling history of the middle Eocene Anaconda metamorphic core complex, western Montana [M.Sc. thesis]: Gainesville, University of Florida, 261 p.

Guenthner, W. R., Reiners, P. W., Ketcham, R. A., Nasdala, L., & Giester, G. (2013). Helium diffusion in natural zircon: Radiation damage, anisotropy, and the interpretation of zircon (U-Th)/He thermochronology. American Journal of Science, 313(3), 145–198. doi:10.2475/03.2013.01

Hamilton, W.B., 1969, Mesozoic California and the underflow of the Pacific mantle: Geological Society of America Bulletin, 80, 2409–2430, doi:10.1130 /0016-7606(1969)80[2409:MCATUO]2.0.CO;2.

Harlan, S.S., Snee, L.W., and Geissman, J.W., 1996, 40Ar/39Ar geochronology and paleomagnetism of Independence Volcano, Absaroka Volcanic Supergroup, Beartooth Mountains, Montana: Canadian Journal of Earth Sciences, v. 33, p. 1648–1654, doi:10.1139/e96-125.

Hill, E. J., Baldwin, S. L., & Lister, G. S. (1995). Magmatism as an essential driving force for formation of active metamorphic core complexes in eastern Papua New Guinea. *Journal of Geophysical Research: Solid Earth, 100*(B6), 10441–10451.

Hiza, M.M., 1999, The Geochemistry and Geochronology of the Eocene Absaroka Volcanic Province, Northern Wyoming and Southwest Montana, USA [Ph.D. thesis]: Oregon State University, 243 p.

House, M. A., Bowring, S. A., & Hodges, K. V. (2002). Implications of middle Eocene epizonal plutonism for the unroofing history of the Bitterroot metamorphic core complex, Idaho-Montana. GSA Bulletin, 114(4), 448–461. doi:10.1130/0016-7606(2002)114<0448:IOMEEP>2.0.CO;2

Howlett, C. J., Reynolds, A. N., & Laskowski, A. K. (2019). Geologic map of the northern half of the Pintler Lake 7.5’ quadrangle and the southern half of the Warren Peak 7.5’ quadrangle, southwestern montana (p. 331565). GSA Annual Meeting, Phoenix, Arizona, USA. doi:10.1130/abs/2019AM-331565

Humphreys, E. D. (1995). Post-Laramide removal of the Farallon slab, western United States. Geology, 23(11), 987–990. doi:10.1130/00917613(1995)023<0987:PLROTF>2.3.CO;2

Humphreys, E., Hessler, E., Dueker, K., Farmer, G. L., Erslev, E., & Atwater, T. (2003). How Laramide-Age Hydration of North American Lithosphere by the Farallon Slab Controlled Subsequent Activity in the Western United States. International Geology Review, 45(7), 575–595. doi:10.2747/0020-6814.45.7.575

Janecke, S.U., Dorsey, R. J., Kickham, J. C. Matoush, J. P., and McIntosh, W., 2005, Geologic Map of the Bachelor Mountain Quadrangle, Southwest Montana: Montana Bureau of Mines Open-File Report 525, scale 1:24,000, 28 p.

Janecke, S.U., VanDenburg, C.J., Blankenau, J.J., and M'Gonigle, J.W., 2000, Long-distance longitudinal transport of gravel across the Cordilleran thrust belt of Montana and Idaho: Geology, v. 28, n. 5, p. 439-442, doi:10.1130/00917613(2000)28<439:LL TOGA>2.0.CO;2.

Kanouo NS, Zaw K, Yongue RF, Sutherland FL, Meffre S, et al., 2012, U-Pb zircon age constraining the source and provenance of gem-bearing Late Cenozoic detrital deposits, Mamfe Basin, SW Cameroon. Resource Geology, v. 62, p. 316–24, doi:10.1111/j.1751-3928.2012.00197.x.

Kanouo, N., Ngueutchoua, G., Kouske, A., Yongue, R., and Venkatesh, A., 2018, Trace Element and U–Pb Core Age for Zircons from Western Meiganga Gold Placer, Cameroon: Their Genesis and Archean-Proterozoic Sources: Minerals, v. 8, p. 194, doi:10.3390/min8050194.

Ketcham, R. A. (2005). Forward and Inverse Modeling of Low-Temperature Thermochronometry Data. Reviews in Mineralogy and Geochemistry, 58(1), 275–314. doi:10.2138/rmg.2005.58.11

Kincaid, C., & Olson, P. (1987). An experimental study of subduction and slab migration. Journal of Geophysical Research: Solid Earth, 92(B13), 13832–13840. doi:10.1029/JB092iB13p13832

Knight, J.B., Morison, S.R., and Mortensen, J.K., 1999, The relationship between placer gold particle shape, rimming, and distance of fluvial transport as exemplified by gold from the Klondike District, Yukon Territory, Canada: Economic Geology, v. 94, p. 635–648, doi:10.2113/gsecongeo.94.5.635.

Koglin N, Zeh A, Frimmel HE, Gerdes A. 2010. New constraints on the auriferous Witwatersrand sediment provenance from combined detrital zircon U-Pb and Lu-Hf isotope data for the Eldorado Reef (Central Rand Group, South Africa). Precambr. Res. v. 183, p. 817–824, doi:10.1016/jprecamres.2010.09.009.

Konstantinou, A., Strickland, A., Miller, E., Vervoort, J., Fisher, C. M., Wooden, J., & Valley, J. (2013). Synextensional magmatism leading to crustal flow in the Albion-Raft River-Grouse Creek metamorphic core complex, northeastern Basin and Range: Synextensional magmatism in the ARG. Tectonics, 32(5), 1384–1403. doi:10.1002/tect.20085

Lageson, D. R., Schmitt, J. G., Horton, B. K., Kalakay, T. J., & Burton, B. R. (2001). Influence of Late Cretaceous magmatism on the Sevier orogenic wedge, western Montana, 4.

Laskowski, A. K., DeCelles, P. G., Gehrels, G. E., 2013, Detrital zircon geochronology of Cordilleran retroarc foreland basin strata, western North America, Tectonics, v. 32, p. 1027–1048, doi:10.1002/tect.20065.

Lee Armstrong, R., & Ward, P. (1991). Evolving geographic patterns of Cenozoic magmatism in the North American Cordillera: The temporal and spatial association of magmatism and metamorphic core complexes. *Journal of Geophysical Research: Solid Earth*, *96*(B8), 13201–13224.

Lee, J., Blackburn, T., & Johnston, S. (2017). Timing of mid-crustal ductile extension in the northern Snake Range metamorphic core complex, Nevada: Evidence from U/Pb zircon ages. Geosphere, 13(2), 439–459. doi:10.1130/GES01429.1

Lewis, R.S., 1998, Geologic Map of the Butte 1° x 2° Quadrangle: Open File Montana Bureau of Mines and Geology 363, 1 sheet, scale 1:250,000.

Link, P.K., Mahon, R.C., Beranek, L.P., Campbell-Stone, E.A., and Lynds, R., 2014, Detrital zircon provenance of Pennsylvanian to Permian sandstones from the Wyoming craton and Wood River Basin, Idaho, U.S.A.: Rocky Mountain Geology, v. 49, p. 115–136, doi:10.2113/gsrocky.49.2.115.

Lipman, P. W., Prostka, H. J., & Christiansen, R. L. (1971). Evolving Subduction Zones in the Western United States, as Interpreted from Igneous Rocks. Science, 174(4011), 821–825. doi:10.1126/science.174.4011.821

Lister, G. S., & Baldwin, S. L. (1993). Plutonism and the origin of metamorphic core complexes. Geology, 21, 607–610.

Liu, M. (2001). Cenozoic extension and magmatism in the North American Cordillera: the role of gravitational collapse. Tectonophysics, 342(3–4), 407–433. doi:10.1016/S0040-1951(01)00173-1

Loen, J. S. (1994). Origin of placer gold nuggets and history of formation of glacial gold placers, Gold Creek, Granite County, Montana. Economic Geology, 89(1), 91–104. doi:10.2113/gsecongeo.89.1.91

Loen, J.S., 1986, Origin of gold placers in the Pioneer District, Powell County, Montana, [M.Sc. thesis]: Colorado State University, 181 p.

Loen, J.S., 1995, Use of placer gold characteristics to locate bedrock gold mineralization, Exploration & Mining Geology, v. 4, no. 4, p. 335-339.

Lonn, J.D., McDonald, C., Lewis, R.S., Kalakay, T.J., O'Neill, J.M., Berg, R.B., and Hargrave, P. (2003). Preliminary geologic map of the Philipsburg 30′ × 60′ quadrangle, western Montana: Montana Bureau of Mines and Geology Open-File Report MBMG 483, scale 1:100,000.

Ludwig, K. (2012). User's Manual for Isoplot Version 3.75–4.15: A Geochronological Toolkit for Microsoft Excel: Berkeley Geochronological Center Special Publication 5, 75 p.

Lund, K., Aleinikoff, J.N., Kunk, M.J., Unruh, D.M., Zeihen, G.D., Hodges, W.C., du Bray, E.A., and O'Neill, J.M., 2002, SHRIMP U-Pb and 40Ar/39Ar age constraints for relating plutonism and mineralization in the Boulder batholith region, Montana: Economic Geology and the Bulletin of the Society of Economic Geologists, v. 97, p. 241–267, doi:10.2113/gsecongeo.97.2.241.

MacCready, T., Snoke, A. W., Wright, J. E., & Howard, K. A. (1997). Mid-crustal flow during Tertiary extension in the Ruby Mountains core complex, Nevada. GSA Bulletin, 109(12), 1576–1594. doi:10.1130/0016-7606(1997)109<1576:MCFDTE>2.3.CO;2

Malusà, M.G., Resentini, A., and Garzanti, E., 2016, Hydraulic sorting and mineral fertility bias in detrital geochronology: Gondwana Research, v. 31, p. 1–19, doi:10.1016/j.gr.2015.09.002.

Marchev, P., Kaiser-Rohrmeier, M., Heinrich, C., Ovtcharova, M., von Quadt, A., & Raicheva, R. (2005). Hydrothermal ore deposits related to post-orogenic extensional magmatism and core complex formation: The Rhodope Massif of Bulgaria and Greece. *Ore Geology Reviews*, *27*(1–4), 53–89.

Marvin, R.F., Mehnert, H.H., Naeser, C.W., and Zartman, R.E., 1989, U.S. Geological Survey radiometric ages—compilation "C," part five: Colorado, Montana, Utah, and Wyoming: Isochron-West, v. 53, p. 14–19.

McCulloch, R., 2003, Applied gold placer exploration and evaluation techniques: Butte, MT, Montana Bureau of Mines and Geology, 267 p.

Morris, G. A., Larson, P. B., & Hooper, P. R. (2000). 'Subduction Style' Magmatism in a Non-subduction Setting: the Colville Igneous Complex, NE Washington State, USA. Journal of Petrology, 41(1), 43–67. doi:10.1093/petrology/41.1.43

Mueller, P., Mogk, D., Wooden, J., and Spake, D., 2016, U-Pb ages of zircons from the Lower Belt Supergroup and proximal crystalline basement: Implications for the early evolution of the Belt Basin, in MacLean, J.S., and Sears, J.W., eds., Belt Basin: Window to Mesoproterozoic Earth: Geological Society of America Special Paper 522, p. 283–303, doi:10.1130/2016.2522(11) .

Murphy, J.G., Foster, D.A., Kalakay, T.J., John, B.E., and Hamilton, M., 2002, U-Pb zircon geochronology of the eastern Pioneer igneous complex, SW Montana: Magmatism in the foreland of the Cordilleran fold and thrust belt: Northwest Geology, v. 31, p. 1–11.

Mutch, T.A., and McGill, G.E., 1962, Deformation In Host Rocks Adjacent To An Epizonal Pluton (The Royal Stock, Montana): Geological Society of America Bulletin, v. 73, p. 1541, doi:10.1130/0016-7606(1962)73[1541:dihrat]2.0.co;2.

Naibert, T.J., Geissman, J.W., and Heizler, M.T., 2010, Magnetic fabric, paleomagnetic, and 40Ar/39Ar geochronologic data bearing on the emplacement of the Late Cretaceous Philipsburg Batholith, SW Montana fold-and-thrust belt: Lithosphere, v. 2, p. 303–327, doi:10.1130/l83.1.

O'Neill, J. M., Lonn, J. D., Lageson, D. R., & Kunk, M. J. (2004). Early Tertiary Anaconda Metamorphic Core Complex, southwestern Montana. Canadian Journal of Earth Sciences, 41(1), 63–72. doi:10.1139/e03-086

Pardee, J.T., 1951, Gold placer deposits of the Pioneer district, Montana, U.S. Geological Survey Bulletin 978-C, p. 69-99.

Paterson, S.R., Okaya, D., Memeti, V., Economos, R., and Miller, R.B., 2011, Magma addition and flux calculations of incrementally constructed magma chambers in continental margin arcs: Combined field, geochronologic, and thermal modeling studies: Geosphere, v. 7, p. 1439–1468, doi:10.1130/ges00696.1.

Platt, J. P., Behr, W. M., & Cooper, F. J. (2015). Metamorphic core complexes: windows into the mechanics and rheology of the crust. Journal of the Geological Society, 172(1), 9–27. doi:10.1144/jgs2014-036

Portner, R.A., Hendrix, M.S., Stalker, J.C., Miggins, D.P., and Sheriff, S.D., 2011, Sedimentary response to orogenic exhumation in the northern Rocky Mountain Basin and Range province, Flint Creek basin, west-central Montana: Canadian Journal of Earth Sciences, v. 48, p. 1131–1154, doi:10.1139/e10-107.

Pullen, A., Ibáñez-Mejía, M., Gehrels, G.E., Ibáñez-Mejía, J.C., and Pecha, M., 2014, What happens when n= 1000? Creating large-n geochronological datasets with LA-ICP-MS for geologic investigations: J. Anal. At. Spectrom., v. 29, p. 971–980, doi:10.1039/c4ja00024b.

Reid, L., and Frostick, L.E., 1985, Beach orientation, bar morphology and the concentration of metalliferous placer deposits: a case study, Lake Turkana, N Kenya: Journal of the Geological Society, v. 142, p. 837–848, doi:10.1144/gsjgs.142.5.0837.

Reynolds, A. N., Howlett, C. J., & Laskowski, A. K. (2019). Extension Of The Anaconda Metamorphic Core Complex: Low-Temperature Thermochronology From The

Footwall Of The Anaconda Detachment, Southwest Montana (p. 335709). GSA Annual Meeting, Phoenix, Arizona, USA - 2019. doi:10.1130/abs/2019AM-335709

Ross, G.M., and Villeneuve, M., 2003, Provenance of the Mesoproterozoic (1.45 Ga) Belt basin (western North America): Another piece in the pre-Rodinia paleogeographic puzzle: Geological Society of America Bulletin, v. 115, p. 1191–1217, doi:10.1130/B25209.1.

Ruiz, J., Valencia, V.A., Chesley, J.T., Kirk, J., Gehrels, G., Frimmel, H., 2006, The source of gold for the Witswatersrand from Re-Os and U-Pb detrital zircon geochronology. *Geochim. Cosmochim Acta v.* 70, A543, doi:10.1016/jgca.2006.06.1002.

Saylor, J.E., Sundell, K.E., and Sharman, G.R., 2019, Characterizing sediment sources by non-negative matrix factorization of detrital geochronological data: Earth and Planetary Science Letters, v. 512, p. 46–58, doi:10.1016/j.epsl.2019.01.044.

Schwartz, T.M., and Graham, S.A., 2017, Depositional history and provenance of Paleogene strata in the Sage Creek basin, southwestern Montana: Geosphere, v. 13, no. 4, p. 1285–1309, doi:10.1130/GES01450.1.

Sears, J. W., & Hendrix, M. S. (2004). Lewis and Clark line and the rotational origin of the Alberta and Helena salients, North American Cordillera. In Special Paper 383: Orogenic curvature: Integrating paleomagnetic and structural analyses (Vol. 383, pp. 173–186). Geological Society of America. doi:10.1130/0-8137-2383-3(2004)383[173:LACLAT]2.0.CO;2

Sharman, G.R., Sharman, J.P., Sylvester, Z., 2018, detritalPy: A Python-based toolset for visualizing and analysing detrital geo-thermochronologic data. *Depositional Rec*. v. 4, p. 202– 215, doi:10.1002/dep2.45.

Singleton, J. S., Stockli, D. F., Gans, P. B., & Prior, M. G. (2014). Timing, rate, and magnitude of slip on the Buckskin-Rawhide detachment fault, west central Arizona. Tectonics, 33(8), 1596–1615. https://doi.org/10.1002/2013TC003517

Sircombe, K.N., 1999, Tracing provenance through the isotope ages of littoral and sedimentary detrital zircon, eastern Australia: Sedimentary Geology, v. 124, p. 47–67, doi:10.1016/s0037-0738(98)00120-1.

Snoke, A. W., Howard, K. A., McGrew, A. J., Burton, B. R., Barnes, C. G., Peters, M. T., & Wright, J. E. (1997). The grand tour of the Ruby-East Humboldt metamorphic core complex, northeastern Nevada: Part 1 - Introduction & road log. Brigham Young University Geology Studies, 42(1), 225–296.

Stevens, L.M., Baldwin, J. A., Crowley, J. L., Fisher, C. M., & Vervoort, J. D. (2016). Magmatism as a response to exhumation of the Priest River complex, northern Idaho: Constraints from zircon U–Pb geochronology and Hf isotopes. Lithos, 262, 285–297. doi:10.1016/j.lithos.2016.07.006

Stevens, Liane M., Bendick, R., & Baldwin, J. A. (2017). Synconvergent exhumation of metamorphic core complexes in the northern North American Cordillera. Geology, 45(6), 495–498. doi:10.1130/G38802.1

Stroup, C.N., Link, P.K., Janecke, S.U., Fanning, C.M., Yaxley, G., and Beranek, L.P., 2008, Eocene to Oligocene provenance and drainage in extensional basins of southwest Montana and east central Idaho: Evidence from detrital zircon populations in the Renova Formation and equivalent strata. In Ores and orogenesis: Circum-Pacific tectonics, geologic evolution, and ore deposits. Edited by J.E. Spencer and S.R. Titley. Arizona Geological Society Digest, 22, pp. 529–546.

Sundell, K. E., and Saylor J. E., 2017, Unmixing detrital geochronology age distributions, Geochem. Geophys. Geosyst., v. 18, p. 1-15, doi:10.1002/2016GC006774.

Tao, W. C., & O'connell, R. J. (1992). Ablative subduction: A two-sided alternative to the conventional subduction model. Journal of Geophysical Research, 97(B6), 8877. doi:10.1029/91JB02422

Terrien, J. (2012), Thermochronological And Geochemical Insights On The Transition Between The Metamorphic Core Complex And The North American Cordillera, Southern Arizona, dissertation, 245 pp.

Tilling, R.I., 1974, Composition and time relations of plutonic and associated volcanic rocks, Boulder batholith region, Montana: Geological Society of America Bulletin, v. 85, p. 1925-1930, doi:10.1130/0016-7606(1974)85<1925:CATROP>2.0.CO;2.

Vanderhaeghe, O., Teyssier, C., McDougall, I., & Dunlap, W. J. (2003). Cooling and exhumation of the Shuswap Metamorphic Core Complex constrained by 40Ar/39Ar thermochronology. GSA Bulletin, 115(2), 200–216. doi:10.1130/00167606(2003)115<0200:CAEOTS>2.0.CO;2

Vervoort J., 2015, Lu-Hf Dating: The Lu-Hf Isotope System. In: Jack Rink W., Thompson J.W. (eds) Encyclopedia of Scientific Dating Methods. Encyclopedia of Earth Sciences Series. Springer, Dordrecht.

Vervoort, J. D., Patchett, P. J., Blichert-Toft, J., & Albarède, F. (1999). Relationships between Lu–Hf and Sm–Nd isotopic systems in the global sedimentary system. Earth and Planetary Science Letters, 168(1–2), 79–99. doi:10.1016/S0012-821X(99)00047-3

Vogl, J. J., Foster, D. A., Fanning, C. M., Kent, K. A., Rodgers, D. W., & Diedesch, T. (2012). Timing of extension in the Pioneer metamorphic core complex with implications for the spatial-temporal pattern of Cenozoic extension and exhumation in the northern U.S. Cordillera: Extension in the Pioneer core complex. Tectonics, 31(1), doi:10.1029/2011TC002981

Wallace, C.A., Lidke, D.J., Elliott, J.E., Desmarais, N.R., Obradovich, J.D., Lopez, D.A., Zarske, S.E., Heise, B.A., Blaskowski, M.J., and Loen, J.S. (1992). Geologic map of the Anaconda-Pintlar wilderness and contiguous roadless area, Granite, Deer Lodge, Beaverhead, and Ravalli counties, western Montana: U.S. Geological Survey Miscellaneous Field Studies Map MF-1633-C, scale 1:50,000.

Wernicke, B. (1981). Low-angle normal faults in the Basin and Range Province: nappe tectonics in an extending orogen. Nature, 291(5817), 645–648. doi:10.1038/291645a0

Wernicke, B. (1992). Cenozoic extensional tectonics of the U.S. Cordillera. In B. C. Burchfiel, P. W. Lipman, & M. L. Zoback (Eds.), The Cordilleran Orogen (pp. 553–17). Boulder, Colorado 80301: Geological Society of America. doi:10.1130/DNAG-GNA-G3.553

Wernicke, B. P., England, P. C., Sonder, L. J., & Christiansen, R. L. (1987). Tectonomagmatic evolution of Cenozoic extension in the North American Cordillera. Geological Society, London, Special Publications, 28(1), 203–221. doi:10.1144/GSL.SP.1987.028.01.15

Whitney, D. L., Teyssier, C., Rey, P., & Buck, W. R. (2013). Continental and oceanic core complexes. Geological Society of America Bulletin, 125(3–4), 273–298. doi:10.1130/B30754.1

Wooden, J.L., Mazdab, F.K., Mueller, P.A., Aleinikoff, J.N., Lund, K., Wiegand, B., Kita, N., and Walley, J.W., 2008, Geochemical and isotopic evidence for the origin of the Boulder batholith, Montana: Geochimica et Cosmochimica Acta, v. 72, p. A1034.

Yeend, W. E., and Shawe, D. R., 1989, Gold in placer deposits: U.S. Geol. Survey Bull. 1857-C, p. G1-G13.

Zartman, R.E., Dyman, T.S., Tysdal, R.G., and Pearson, R.C., 1995, U-Pb ages of volcanogenic zircon from porcellanite beds in the Vaughn Member of the Mid-Cretaceous Blackleaf Formation, southwest Montana: Shorter Contributions to the Stratigraphy and Geochronology of Upper Cretaceous Rocks in the Western Interior of the United States, U.S. Geological Survey Bulletin 2113-B, p. B1–B16.

Zeh, A., and Gerdes, A., 2012, U–Pb and Hf isotope record of detrital zircons from gold-bearing sediments of the Pietersburg Greenstone Belt (South Africa)—Is there a common provenance with the Witwatersrand Basin?, Precambrian Research, v. 204-205, p. 46–56, doi:10.1016/j.precamres.2012.02.013.

Zen, E., 1996, Plutons in the eastern part of the Pioneer batholith: Field relations and petrographic descriptions: U.S. Geological Survey Open-File Report 96-97, 98 p.

# APPENDICES

# APPENDIX A

## PIONEER DISTRICT SAMPLE LOCATIONS, DETRITAL ZIRCON U-PB GEOCHRONOLOGY RESULTS, AND DETRITAL ZIRCON LU-HF ANALYSES

**(THIS DATA CAN BE FOUND IN SUPPLEMENTARY DATA ITEM 1)**

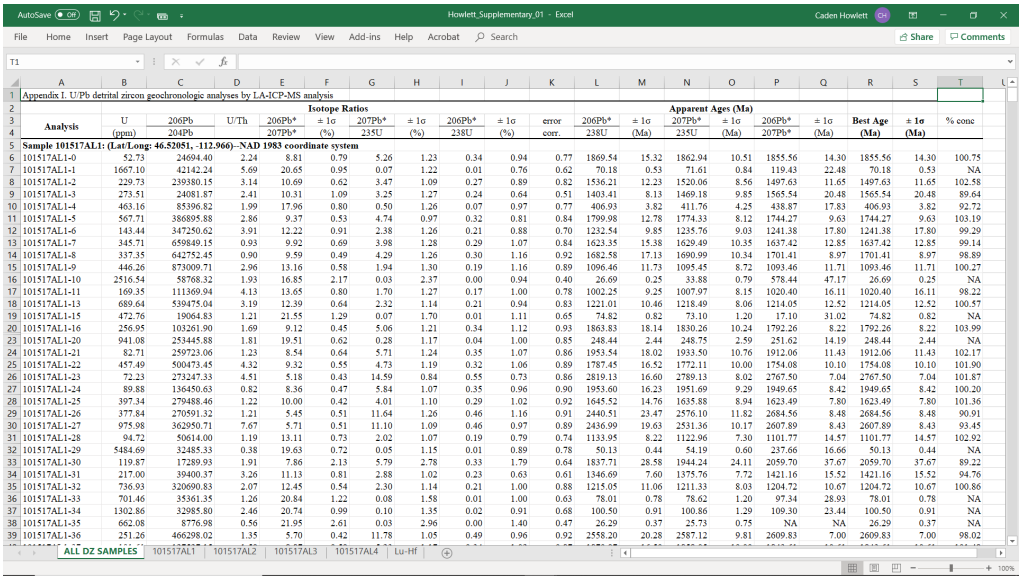

AutoSave Howlett_Supplementary_01 - Excel Caden Howlett

File Home Insert Page Layout Formulas Data Review View Add-ins Help Acrobat Search Share Comments

Appendix 1. U/Pb detrital zircon geochronologic analyses by LA-ICP-MS analysis

| Analysis | U (ppm) | 206Pb 204Pb | U/Th | 206Pb* 207Pb* | ± 1σ (%) | 207Pb* 235U | ± 1σ (%) | 206Pb* 238U | ± 1σ (%) | error corr. | 206Pb* 238U | ± 1σ (Ma) | 207Pb* 235U | ± 1σ (Ma) | 206Pb* 207Pb* | ± 1σ (Ma) | Best Age (Ma) | ± 1σ (Ma) | % conc |
|---|---|---|---|---|---|---|---|---|---|---|---|---|---|---|---|---|---|---|---|
| | | | | Isotope Ratios | | | | | | | Apparent Ages (Ma) | | | | | | | | |
| **Sample 101517AL1: (Lat/Long: 46.52051, -112.966)--NAD 1983 coordinate system** | | | | | | | | | | | | | | | | | | | |
| 101517AL1-0 | 52.73 | 24694.40 | 2.24 | 8.81 | 0.79 | 5.26 | 1.23 | 0.34 | 0.94 | 0.77 | 1869.54 | 15.32 | 1862.94 | 10.51 | 1855.56 | 14.30 | 1855.56 | 14.30 | 100.75 |
| 101517AL1-1 | 1667.10 | 42142.24 | 5.69 | 20.65 | 0.95 | 0.07 | 1.22 | 0.01 | 0.76 | 0.62 | 70.18 | 0.53 | 71.61 | 0.84 | 119.43 | 22.48 | 70.18 | 0.53 | NA |
| 101517AL1-2 | 229.73 | 239380.15 | 3.14 | 10.69 | 0.62 | 3.47 | 1.09 | 0.27 | 0.89 | 0.82 | 1536.21 | 12.23 | 1520.06 | 8.56 | 1497.63 | 11.65 | 1497.63 | 11.65 | 102.58 |
| 101517AL1-3 | 273.51 | 24081.87 | 2.41 | 10.31 | 1.09 | 3.25 | 1.27 | 0.24 | 0.64 | 0.51 | 1403.41 | 8.13 | 1469.18 | 9.85 | 1565.54 | 20.48 | 1565.54 | 20.48 | 89.64 |
| 101517AL1-4 | 463.16 | 85396.82 | 1.99 | 17.96 | 0.80 | 0.50 | 1.26 | 0.07 | 0.97 | 0.77 | 406.93 | 3.82 | 411.76 | 4.25 | 438.87 | 17.83 | 406.93 | 3.82 | 92.72 |
| 101517AL1-5 | 567.71 | 386895.88 | 2.86 | 9.37 | 0.53 | 4.74 | 0.97 | 0.32 | 0.81 | 0.84 | 1799.98 | 12.78 | 1774.33 | 8.12 | 1744.27 | 9.63 | 1744.27 | 9.63 | 103.19 |
| 101517AL1-6 | 143.44 | 347250.62 | 3.91 | 12.22 | 0.91 | 2.38 | 1.26 | 0.21 | 0.88 | 0.70 | 1232.54 | 9.85 | 1235.76 | 9.03 | 1241.38 | 17.80 | 1241.38 | 17.80 | 99.29 |
| 101517AL1-7 | 345.71 | 659849.15 | 0.93 | 9.92 | 0.69 | 3.98 | 1.28 | 0.29 | 1.07 | 0.84 | 1623.35 | 15.38 | 1629.49 | 10.35 | 1637.42 | 12.85 | 1637.42 | 12.85 | 99.14 |
| 101517AL1-8 | 337.35 | 642752.45 | 0.90 | 9.59 | 0.49 | 4.29 | 1.26 | 0.30 | 1.16 | 0.92 | 1682.58 | 17.13 | 1690.99 | 10.34 | 1701.41 | 8.97 | 1701.41 | 8.97 | 98.89 |
| 101517AL1-9 | 446.26 | 873009.71 | 2.96 | 13.16 | 0.58 | 1.94 | 1.30 | 0.19 | 1.16 | 0.89 | 1096.46 | 11.73 | 1095.45 | 8.72 | 1093.46 | 11.71 | 1093.46 | 11.71 | 100.27 |
| 101517AL1-10 | 2516.54 | 58768.32 | 1.93 | 16.85 | 2.17 | 0.03 | 2.37 | 0.00 | 0.94 | 0.40 | 26.69 | 0.25 | 33.88 | 0.79 | 578.44 | 47.17 | 26.69 | 0.25 | NA |
| 101517AL1-11 | 169.35 | 111369.94 | 4.13 | 13.65 | 0.80 | 1.70 | 1.27 | 0.17 | 1.00 | 0.78 | 1002.25 | 9.25 | 1007.97 | 8.15 | 1020.40 | 16.11 | 1020.40 | 16.11 | 98.22 |
| 101517AL1-13 | 689.64 | 539475.04 | 3.19 | 12.39 | 0.64 | 2.32 | 1.14 | 0.21 | 0.94 | 0.83 | 1221.01 | 10.46 | 1218.49 | 8.06 | 1214.05 | 12.52 | 1214.05 | 12.52 | 100.57 |
| 101517AL1-15 | 472.76 | 19064.83 | 1.21 | 21.55 | 1.29 | 0.07 | 1.70 | 0.01 | 1.11 | 0.65 | 74.82 | 0.82 | 73.10 | 1.20 | 17.10 | 31.02 | 74.82 | 0.82 | NA |
| 101517AL1-16 | 256.95 | 103261.90 | 1.69 | 9.12 | 0.45 | 5.06 | 1.21 | 0.34 | 1.12 | 0.93 | 1863.83 | 18.14 | 1830.26 | 10.24 | 1792.26 | 8.22 | 1792.26 | 8.22 | 103.99 |
| 101517AL1-20 | 941.08 | 253445.88 | 1.81 | 19.51 | 0.62 | 0.28 | 1.17 | 0.04 | 1.00 | 0.85 | 248.44 | 2.44 | 248.75 | 2.59 | 251.62 | 14.19 | 248.44 | 2.44 | NA |
| 101517AL1-21 | 82.71 | 259723.06 | 1.23 | 8.54 | 0.64 | 5.71 | 1.24 | 0.35 | 1.07 | 0.86 | 1953.54 | 18.02 | 1933.50 | 10.76 | 1912.06 | 11.43 | 1912.06 | 11.43 | 102.17 |
| 101517AL1-22 | 457.49 | 500473.45 | 4.32 | 9.32 | 0.55 | 4.73 | 1.19 | 0.32 | 1.06 | 0.89 | 1787.45 | 16.52 | 1772.11 | 10.00 | 1754.08 | 10.10 | 1754.08 | 10.10 | 101.90 |
| 101517AL1-23 | 72.23 | 273247.33 | 4.51 | 5.18 | 0.43 | 14.59 | 0.84 | 0.55 | 0.73 | 0.86 | 2819.13 | 16.60 | 2789.13 | 8.02 | 2767.50 | 7.04 | 2767.50 | 7.04 | 101.87 |
| 101517AL1-24 | 89.88 | 136450.63 | 0.82 | 8.36 | 0.47 | 5.84 | 1.07 | 0.35 | 0.96 | 0.90 | 1953.60 | 16.23 | 1951.69 | 9.29 | 1949.65 | 8.42 | 1949.65 | 8.42 | 100.20 |
| 101517AL1-25 | 397.34 | 279488.46 | 1.22 | 10.00 | 0.42 | 4.01 | 1.10 | 0.29 | 1.02 | 0.92 | 1645.52 | 14.76 | 1635.88 | 8.94 | 1623.49 | 7.80 | 1623.49 | 7.80 | 101.36 |
| 101517AL1-26 | 377.84 | 270591.32 | 1.21 | 5.45 | 0.51 | 11.64 | 1.26 | 0.46 | 1.16 | 0.91 | 2440.51 | 23.47 | 2576.10 | 11.82 | 2684.56 | 8.48 | 2684.56 | 8.48 | 90.91 |
| 101517AL1-27 | 975.98 | 362950.71 | 7.67 | 5.71 | 0.51 | 11.10 | 1.09 | 0.46 | 0.97 | 0.89 | 2436.99 | 19.63 | 2531.36 | 10.17 | 2607.89 | 8.43 | 2607.89 | 8.43 | 93.45 |
| 101517AL1-28 | 94.72 | 50614.00 | 1.19 | 13.11 | 0.73 | 2.02 | 1.07 | 0.19 | 0.79 | 0.74 | 1133.95 | 8.22 | 1122.96 | 7.30 | 1101.77 | 14.57 | 1101.77 | 14.57 | 102.92 |
| 101517AL1-29 | 5484.69 | 32485.33 | 0.38 | 19.63 | 0.72 | 0.05 | 1.15 | 0.01 | 0.89 | 0.78 | 50.13 | 0.44 | 54.19 | 0.60 | 237.66 | 16.66 | 50.13 | 0.44 | NA |
| 101517AL1-30 | 119.87 | 17289.93 | 1.91 | 7.86 | 2.13 | 5.79 | 2.78 | 0.33 | 1.79 | 0.64 | 1837.71 | 28.58 | 1944.24 | 24.11 | 2059.70 | 37.67 | 2059.70 | 37.67 | 89.22 |
| 101517AL1-31 | 217.00 | 39400.37 | 3.26 | 11.13 | 0.81 | 2.88 | 1.02 | 0.23 | 0.63 | 0.61 | 1346.69 | 7.60 | 1375.76 | 7.72 | 1421.16 | 15.52 | 1421.16 | 15.52 | 94.76 |
| 101517AL1-32 | 736.93 | 320690.83 | 2.07 | 12.45 | 0.54 | 2.30 | 1.14 | 0.21 | 1.00 | 0.88 | 1215.05 | 11.06 | 1211.33 | 8.03 | 1204.72 | 10.67 | 1204.72 | 10.67 | 100.86 |
| 101517AL1-33 | 701.46 | 35361.35 | 1.26 | 20.84 | 1.22 | 0.08 | 1.58 | 0.01 | 1.00 | 0.63 | 78.01 | 0.78 | 78.62 | 1.20 | 97.34 | 28.93 | 78.01 | 0.78 | NA |
| 101517AL1-34 | 1302.86 | 32985.80 | 2.46 | 20.74 | 0.99 | 0.10 | 1.35 | 0.02 | 0.91 | 0.68 | 100.50 | 0.91 | 100.86 | 1.29 | 109.30 | 23.44 | 100.50 | 0.91 | NA |
| 101517AL1-35 | 662.08 | 8776.98 | 0.56 | 21.95 | 2.61 | 0.03 | 2.96 | 0.00 | 1.40 | 0.47 | 26.29 | 0.37 | 25.73 | 0.75 | NA | NA | 26.29 | 0.37 | NA |
| 101517AL1-36 | 251.26 | 466298.02 | 1.35 | 5.70 | 0.42 | 11.78 | 1.05 | 0.49 | 0.96 | 0.92 | 2558.20 | 20.28 | 2587.12 | 9.81 | 2609.83 | 7.00 | 2609.83 | 7.00 | 98.02 |

ALL DZ SAMPLES | 101517AL1 | 101517AL2 | 101517AL3 | 101517AL4 | Lu-Hf

# APPENDIX B

## ANACONDA RANGE SAMPLE LOCATIONS, IGNEOUS ZIRCON U-PB GEOCHRONOLOGY, AND LU-HF ISOTOPIC RESULTS

**(THIS DATA CAN BE FOUND IN SUPPLEMENTARY DATA ITEM 2)**

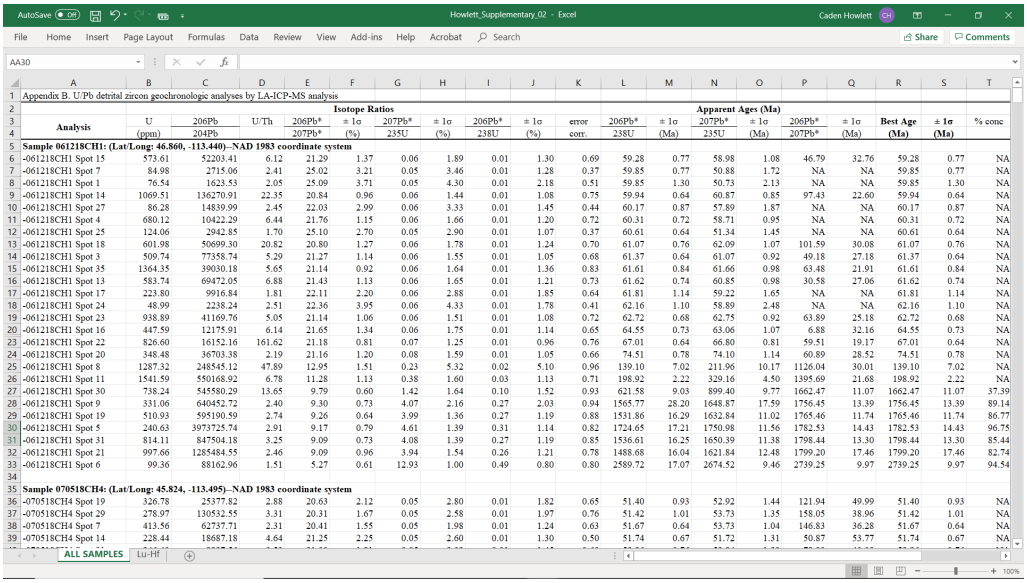

Howlett_Supplementary_02 - Excel

Appendix B. U/Pb detrital zircon geochronologic analyses by LA-ICP-MS analysis

| Analysis | U (ppm) | 206Pb 204Pb | U/Th | 206Pb* 207Pb* | ± 1σ (%) | 207Pb* 235U | ± 1σ (%) | 206Pb* 238U | ± 1σ (%) | error corr. | 206Pb* 238U | ± 1σ (Ma) | 207Pb* 235U | ± 1σ (Ma) | 206Pb* 207Pb* | ± 1σ (Ma) | Best Age (Ma) | ± 1σ (Ma) | % conc |
|---|---|---|---|---|---|---|---|---|---|---|---|---|---|---|---|---|---|---|---|
| **Sample 061218CH1: (Lat/Long: 46.860, -113.440)--NAD 1983 coordinate system** | | | | | | | | | | | | | | | | | | | |
| -061218CH1 Spot 15 | 573.61 | 52203.41 | 6.12 | 21.29 | 1.37 | 0.06 | 1.89 | 0.01 | 1.30 | 0.69 | 59.28 | 0.77 | 58.98 | 1.08 | 46.79 | 32.76 | 59.28 | 0.77 | NA |
| -061218CH1 Spot 7 | 84.98 | 2715.06 | 2.41 | 25.02 | 3.21 | 0.05 | 3.46 | 0.01 | 1.28 | 0.37 | 59.85 | 0.77 | 50.88 | 1.72 | NA | NA | 59.85 | 0.77 | NA |
| -061218CH1 Spot 1 | 76.54 | 1623.53 | 2.05 | 25.09 | 3.71 | 0.05 | 4.30 | 0.01 | 2.18 | 0.51 | 59.85 | 1.30 | 50.73 | 2.13 | NA | NA | 59.85 | 1.30 | NA |
| -061218CH1 Spot 14 | 1069.51 | 136270.91 | 22.35 | 20.84 | 0.96 | 0.06 | 1.44 | 0.01 | 1.08 | 0.75 | 59.94 | 0.64 | 60.87 | 0.85 | 97.43 | 22.60 | 59.94 | 0.64 | NA |
| -061218CH1 Spot 27 | 86.28 | 14839.99 | 2.45 | 22.03 | 2.99 | 0.06 | 3.33 | 0.01 | 1.45 | 0.44 | 60.17 | 0.87 | 57.89 | 1.87 | NA | NA | 60.17 | 0.87 | NA |
| -061218CH1 Spot 4 | 680.12 | 10422.29 | 6.44 | 21.76 | 1.15 | 0.06 | 1.66 | 0.01 | 1.20 | 0.72 | 60.31 | 0.72 | 58.71 | 0.95 | NA | NA | 60.31 | 0.72 | NA |
| -061218CH1 Spot 25 | 124.06 | 2942.85 | 1.70 | 25.10 | 2.70 | 0.05 | 2.90 | 0.01 | 1.07 | 0.37 | 60.61 | 0.64 | 51.34 | 1.45 | NA | NA | 60.61 | 0.64 | NA |
| -061218CH1 Spot 18 | 601.98 | 50699.30 | 20.82 | 20.80 | 1.27 | 0.06 | 1.78 | 0.01 | 1.24 | 0.70 | 61.07 | 0.76 | 62.09 | 1.07 | 101.59 | 30.08 | 61.07 | 0.76 | NA |
| -061218CH1 Spot 3 | 509.74 | 77358.74 | 5.29 | 21.27 | 1.14 | 0.06 | 1.55 | 0.01 | 1.05 | 0.68 | 61.37 | 0.64 | 61.07 | 0.92 | 49.18 | 27.18 | 61.37 | 0.64 | NA |
| -061218CH1 Spot 35 | 1364.35 | 39030.18 | 5.65 | 21.14 | 0.92 | 0.06 | 1.64 | 0.01 | 1.36 | 0.83 | 61.61 | 0.84 | 61.66 | 0.98 | 63.48 | 21.91 | 61.61 | 0.84 | NA |
| -061218CH1 Spot 13 | 583.74 | 69472.05 | 6.88 | 21.43 | 1.13 | 0.06 | 1.65 | 0.01 | 1.21 | 0.73 | 61.62 | 0.74 | 60.85 | 0.98 | 30.58 | 27.06 | 61.62 | 0.74 | NA |
| -061218CH1 Spot 17 | 223.80 | 9916.84 | 1.81 | 22.11 | 2.20 | 0.06 | 2.88 | 0.01 | 1.85 | 0.64 | 61.81 | 1.14 | 59.22 | 1.65 | NA | NA | 61.81 | 1.14 | NA |
| -061218CH1 Spot 24 | 48.99 | 2238.24 | 2.51 | 22.36 | 3.95 | 0.06 | 4.33 | 0.01 | 1.78 | 0.41 | 62.16 | 1.10 | 58.89 | 2.48 | NA | NA | 62.16 | 1.10 | NA |
| -061218CH1 Spot 23 | 938.89 | 41169.76 | 5.05 | 21.14 | 1.06 | 0.06 | 1.51 | 0.01 | 1.08 | 0.72 | 62.72 | 0.68 | 62.75 | 0.92 | 63.89 | 25.18 | 62.72 | 0.68 | NA |
| -061218CH1 Spot 16 | 447.59 | 12175.91 | 6.14 | 21.65 | 1.34 | 0.06 | 1.75 | 0.01 | 1.14 | 0.65 | 64.55 | 0.73 | 63.06 | 1.07 | 6.88 | 32.16 | 64.55 | 0.73 | NA |
| -061218CH1 Spot 22 | 826.60 | 16152.16 | 161.62 | 21.18 | 0.81 | 0.07 | 1.25 | 0.01 | 0.96 | 0.76 | 67.01 | 0.64 | 66.80 | 0.81 | 59.51 | 19.17 | 67.01 | 0.64 | NA |
| -061218CH1 Spot 20 | 348.48 | 36703.38 | 2.19 | 21.16 | 1.20 | 0.08 | 1.59 | 0.01 | 1.05 | 0.66 | 74.51 | 0.78 | 74.10 | 1.14 | 60.89 | 28.52 | 74.51 | 0.78 | NA |
| -061218CH1 Spot 8 | 1287.32 | 248545.12 | 47.89 | 12.95 | 1.51 | 0.23 | 5.32 | 0.02 | 5.10 | 0.96 | 139.10 | 7.02 | 211.96 | 10.17 | 1126.04 | 30.01 | 139.10 | 7.02 | NA |
| -061218CH1 Spot 11 | 1541.59 | 550168.92 | 6.78 | 11.28 | 1.13 | 0.38 | 1.60 | 0.03 | 1.13 | 0.71 | 198.92 | 2.22 | 329.16 | 4.50 | 1395.69 | 21.68 | 198.92 | 2.22 | NA |
| -061218CH1 Spot 30 | 738.24 | 545580.29 | 13.65 | 9.79 | 0.60 | 1.42 | 1.64 | 0.10 | 1.52 | 0.93 | 621.58 | 9.03 | 899.40 | 9.77 | 1662.47 | 11.07 | 1662.47 | 11.07 | 37.39 |
| -061218CH1 Spot 9 | 331.06 | 640452.72 | 2.40 | 9.30 | 0.73 | 4.07 | 2.16 | 0.27 | 2.03 | 0.94 | 1565.77 | 28.20 | 1648.87 | 17.59 | 1756.45 | 13.39 | 1756.45 | 13.39 | 89.14 |
| -061218CH1 Spot 19 | 510.93 | 595190.59 | 2.74 | 9.26 | 0.64 | 3.99 | 1.36 | 0.27 | 1.19 | 0.88 | 1531.86 | 16.29 | 1632.84 | 11.02 | 1765.46 | 11.74 | 1765.46 | 11.74 | 86.77 |
| -061218CH1 Spot 5 | 240.63 | 3973725.74 | 2.91 | 9.17 | 0.79 | 4.61 | 1.39 | 0.31 | 1.14 | 0.82 | 1724.65 | 17.21 | 1750.98 | 11.56 | 1782.53 | 14.43 | 1782.53 | 14.43 | 96.75 |
| -061218CH1 Spot 31 | 814.11 | 847504.18 | 3.25 | 9.09 | 0.73 | 4.08 | 1.39 | 0.27 | 1.19 | 0.85 | 1536.61 | 16.25 | 1650.39 | 11.38 | 1798.44 | 13.30 | 1798.44 | 13.30 | 85.44 |
| -061218CH1 Spot 21 | 997.66 | 1285484.55 | 2.46 | 9.09 | 0.96 | 3.94 | 1.54 | 0.26 | 1.21 | 0.78 | 1488.68 | 16.04 | 1621.84 | 12.48 | 1799.20 | 17.46 | 1799.20 | 17.46 | 82.74 |
| -061218CH1 Spot 6 | 99.36 | 88162.96 | 1.51 | 5.27 | 0.61 | 12.93 | 1.00 | 0.49 | 0.80 | 0.80 | 2589.72 | 17.07 | 2674.52 | 9.46 | 2739.25 | 9.97 | 2739.25 | 9.97 | 94.54 |
| **Sample 070518CH4: (Lat/Long: 45.824, -113.495)--NAD 1983 coordinate system** | | | | | | | | | | | | | | | | | | | |
| -070518CH4 Spot 19 | 326.78 | 25377.82 | 2.88 | 20.63 | 2.12 | 0.05 | 2.80 | 0.01 | 1.82 | 0.65 | 51.40 | 0.93 | 52.92 | 1.44 | 121.94 | 49.99 | 51.40 | 0.93 | NA |
| -070518CH4 Spot 29 | 278.97 | 130532.55 | 3.31 | 20.31 | 1.67 | 0.05 | 2.58 | 0.01 | 1.97 | 0.76 | 51.42 | 1.01 | 53.73 | 1.35 | 158.05 | 38.96 | 51.42 | 1.01 | NA |
| -070518CH4 Spot 7 | 413.56 | 62737.71 | 2.31 | 20.41 | 1.55 | 0.05 | 1.98 | 0.01 | 1.24 | 0.63 | 51.67 | 0.64 | 53.73 | 1.04 | 146.83 | 36.28 | 51.67 | 0.64 | NA |
| -070518CH4 Spot 14 | 228.44 | 18687.18 | 4.64 | 21.25 | 2.25 | 0.05 | 2.60 | 0.01 | 1.30 | 0.50 | 51.74 | 0.67 | 51.72 | 1.31 | 50.87 | 53.77 | 51.74 | 0.67 | NA |

# APPENDIX C

## ZIRCON (U-TH)/HE THERMOCHRONOLOGY RESULTS FROM THE ANACONDA METAMORPHIC CORE COMPLEX FOOTWALL

**(THIS DATA CAN BE FOUND IN SUPPLEMENTARY DATA ITEM 3)**

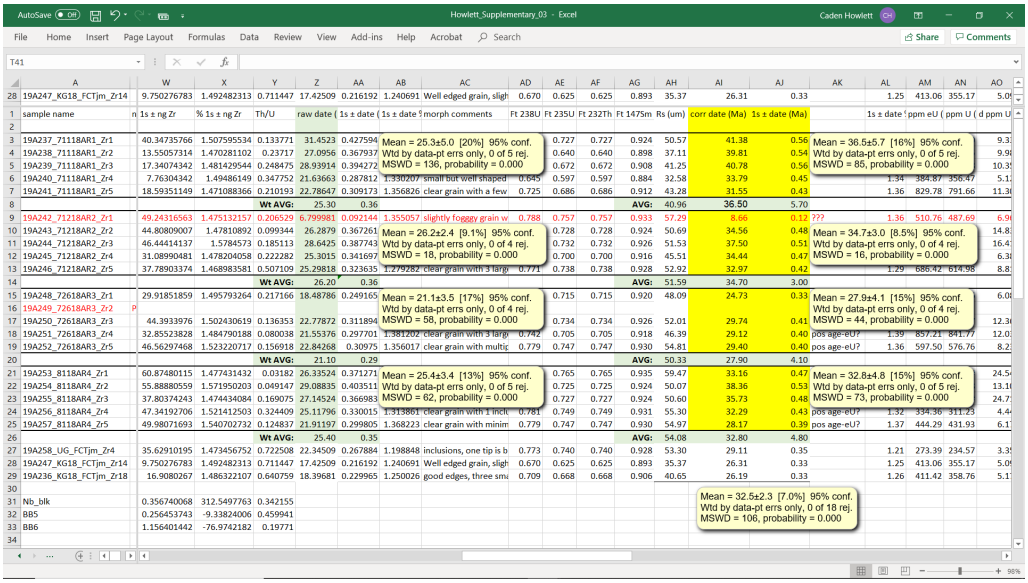

# APPENDIX D

GEOLOGIC MAP OF THE NORTHERN HALF OF THE PINTLER LAKE 7.5' QUADRANGLE AND THE SOUTHERN HALF OF THE WARREN PEAK 7.5' QUADRANGLE, SOUTHWESTERN MONTANA

**(MAP CAN BE FOUND IN SUPPLEMENTARY DATA ITEM 4)**